Effects of *SLC2A3* copy number variants on neurodevelopment and glucose metabolism in ADHD patient-specific neurons

Effekte der *SLC2A3* Kopienzahlvarianten auf Neuroentwicklung und Glukosemetabolismus in ADHS Patienten-spezifischen Neuronen

Doctoral thesis for a doctoral degree

at the Graduate School of Life Sciences,

Julius-Maximilians-Universität Würzburg,

Section Neuroscience

Submitted by

Charline Jansch

from

Neuss, Germany

Würzburg, 2019

Submitted on: ………………………………..……..

Members of the *Promotionskomitee*:

Chairperson: **Prof. Dr. Markus Sauer**

Primary Supervisor: **Prof. Dr. Klaus-Peter Lesch**

Supervisor (Second): **Prof. Dr. Frank Edenhofer**

Supervisor (Third): **Prof. Dr. Erhard Wischmeyer**

Date of Public Defence: …………………………….…………

Date of Receipt of Certificates: ………………………….……………

Table of Content

Abstract

Neuropsychiatric disorders, such as attention-deficit/hyperactivity disorder (ADHD), represent a burden which deeply impair the patient's life. Neurobiological research has therefore increasingly focused on the examination of brain neurotransmitter systems, such as the serotonin (5-HT) system, since a dysfunction has been repeatedly implicated in the pathology of these diseases. However, investigation of functional human neurons *in vitro* has been restricted by technical limitations for a long time until the discovery of human induced pluripotent stem cells (iPSCs) revolutionized the field of experimental disease models. Since the pathogenesis of neuropsychiatric disorders involves a complex genetic component, genome-wide association studies (GWAS) revealed numerous risk genes that are associated with an increased risk for ADHD. For instance, the novel ADHD candidate gene *SLC2A3* which encodes the glucose transporter-3 (GLUT3), facilitates the transport of glucose across plasma membranes and is essential for the high energy demand of several cell types, such as stem cells and neurons. Specifically, copy number variants (CNVs) of *SLC2A3* might therefore impact cerebral glucose metabolism as well as the assembly of synaptic proteins in human neurons which might contribute to the pathogenesis of ADHD.

We hypothesized that an altered *SLC2A3* gene dosage in human neurons can exert diverse protective or detrimental effects on neurodevelopmental processes as well as the coping of glucometabolic stress events, such as hypo- and hyperglycaemic conditions. The generation of specific iPSC lines from ADHD patients and healthy probands served as basis to efficiently differentiate stem cells into 5-HT specific neurons. Using this neuronal culture, we were able to examine effects of *SLC2A3* CNVs on the basal expression of *SCL2A3* and GLUT3 in human neurons. Furthermore, the focus was on potentially altered coping of the cells with glucose deprivation and the treatment with specific high- and low glycaemic media.

High-resolution fluorescence imaging in combination with electrophysiological and molecular biological techniques showed that:

1) The generated human iPSCs are fully reprogrammed human stem cells showing typical characteristics of embryonic stem cell-like morphology, growth behaviour, the ability to differentiate into different cell types of the human body and the expression of pluripotency-specific markers.
2) The neuronal subtype derived from our stem cells display typical characteristics of 5-HT specific median and dorsal neurons and forms synapses reflected by the expression of pre- and postsynaptic proteins.

3) Even if *SLC2A3* CNVs influence *SLC2A3* and GLUT3 basal expression, no significant alterations in gene and protein expression caused by hyper- and hypoglycaemic conditions, nor in the assembly of proteins associated with synapse formation could be observed in human iPSC-derived neurons.

Zusammenfassung

Neuropsychiatrische Erkrankungen, wie das Aufmerksamkeits-Defizit/Hyperaktivitäts-Syndrom (ADHS), stellen eine Belastung dar, die das Leben des Patienten schwerwiegend beeinträchtigen. Die neurobiologische Forschung hat sich deshalb zunehmend auf die Untersuchung der Neurotransmittersysteme des Gehirns, wie das serotonerge (5-HT) System fokussiert, da eine Dysfunktion wiederholt in Zusammenhang mit der Pathogenese solcher Erkrankungen gebracht wurde. Die *in vitro*-Untersuchung funktioneller humaner Neurone war jedoch lange Zeit durch technische Limitierungen eingeschränkt, bis die Entdeckung humaner induzierter pluripotenter Stammzellen (iPSCs) das Feld der experimentellen Krankheitsmodelle revolutionierte. Da die Pathogenese neuropsychiatrischer Erkrankungen eine komplexe genetische Komponente einschließt, haben genomweite Assoziationsstudien zahlreiche Risikogene aufgedeckt, die mit einem erhöhten Risiko für ADHS assoziiert werden. Das Kandidatengen *SLC2A3*, das den Glukosetransporter-3 (GLUT3) codiert, ermöglicht beispielsweise den Transport von Glukose über Plasmamembranen und ist somit essenziell für die hohe Energieanforderung verschiedenster Zelltypen, wie etwa Stammzellen und Neurone. Im Besonderen könnten die Kopienzahlvarianten (CNVs) des Gens *SLC2A3* daher den cerebralen Glukosemetabolismus, sowie die Ansammlung synaptischer Proteine beeinflussen und so zur Pathogenese des ADHS beitragen.

Wir nahmen an, dass eine veränderte *SLC2A3*-Gendosis in humanen Neuronen diverse protektive oder schädliche Effekte auf Neuroentwicklungsprozesse, sowie den Umgang mit glukometabolischen Stress-Ereignissen, wie etwa hypo- und hyperglykämische Bedingungen haben könnte. Die Generierung spezieller iPSC-Linien von ADHS-Patienten und gesunden Probanden diente als Basis, um Stammzellen effizient in 5-HT spezifische Neurone zu differenzieren. Diese neuronale Kultur ermöglichte uns die Untersuchung der Effekte der *SLC2A3* CNVs auf die Basalexpression von *SLC2A3* und GLUT3 in humanen Neuronen. Des Weiteren war der Focus auf einen potenziell veränderten Umgang der Zellen mit Glukoseentzug und der Behandlung mit speziellen hoch- und niederglykämischen Medien.

Hochauflösende Fluoreszenzaufnahmen in Kombination mit elektrophysiologischen und molekularbiologischen Techniken zeigten, dass:

1) Die generierten human iPSCs vollständig reprogrammierte humane Stammzellen sind, die die typischen Merkmale der embryonalen Stammzell-Morphologie, des Wachstumsverhaltes, der Fähigkeit in verschiedenste Zelltypen des menschlichen

Körpers zu differenzieren und der Expression Pluripotenz-assoziierter Marker aufweisen.

2) Der neuronale Subtyp, der aus unseren Stammzellen generiert wurde, die typischen Charakteristiken medianer und dorsaler 5-HT Neurone aufweist und Synapsen formt, verdeutlicht durch die Expression prä- und postsynaptischer Proteine.

3) Selbst wenn die *SLC2A3* CNVs einen Einfluss auf die basale Gen- und Proteinexpression haben, zeigte sich jedoch in humanen iPSC-erzeugten Neuronen keine signifikante Veränderung der Gen- und Proteinexpression aufgrund hyper- und hypoglykämischer Konditionen, noch der Ansammlung der Proteine, die mit der Formation der Synapsen assoziiert sind.

1. Introduction

1.1 Attention-deficit/hyperactivity disorder (ADHD) as an example of a neurodevelopmental and psychiatric disorder

Neuropsychiatric disorders are a huge burden on society by impairing multiple areas of life. The spectrum of these diseases includes, among others, schizophrenia, autism spectrum disorder (ASD) and attention-deficit/hyperactivity disorder (ADHD; MIM 143465). Nowadays, ADHD is conceptualized as a common but complex and clinically heterogeneous neurodevelopmental disorder characterized by developmentally inappropriate inattention, increased activity and impulsivity as well as emotional dysregulation (APA, 2000). ADHD has an onset at preschool age and strong persistence across the lifespan with a worldwide prevalence estimated at around 5-10% in children and 2-4% in adults (Fayyad et al 2007). However, ADHD has initially been considered as a disorder of childhood (cADHD) until several follow-up studies have revealed that even 72% of affected children show at least one-third of the symptoms required for the diagnosis of adult ADHD (aADHD) later in life (Faraone et al 2006). In addition, many studies have documented aADHD as associated with considerable risk for psychiatric co-morbidity, including as depression, anxiety, substance use disorders and failure in psychosocial adaptation (Bush 2010, Geissler & Lesch 2011, Jacob et al 2007). ADHD therapy includes pharmacological and non-pharmacological approaches. Stimulants and other drugs target the central monoaminergic systems, and particularly the neurotransmitters dopamine and norepinephrine as well as serotonin (Hannestad et al 2010). On the other hand, cognitive behavioural therapy or informing and training the patient's social environment in behaviour management are non-pharmacological approaches that can help patients and their families to cope better with their situation.

Insights into neuroanatomical correlates and functional aspects of ADHD gained via structural neuroimaging studies as well as neuropsychological approaches and functional imaging techniques, such as single photon emission computed tomography (SPECT), functional magnetic resonance imaging (fMRI), positron emission tomography (PET) or electroencephalography (EEG) revealed that ADHD patients show structural and functional alterations reflected by reduced cortical thickness and volume reduction of prefrontal cortex (PFC), striatum and cerebellum (Bush 2011, Carmona et al 2009, Castellanos 2009, Swanson et al 2011). These structures are involved in attention and cognition (Bush 2010). Furthermore, symptoms of ADHD were also found to be caused by altered prefrontal cortical top-down regulation of attention and behaviour (Arnsten 2011).

Many advances have been made in understanding the pathophysiological mechanism of this disorder. Several factors may contribute to, or exacerbate ADHD, including genetics and the social and physical environments. Environmental risk factors include substances, such as polychlorinated biphenyls (PCBs), foetal exposure to alcohol or maternal smoking, a low birth weight as well as psychosocial adversity, such as maltreatment and emotional trauma (Banerjee et al 2007). Twin, adoption, family and molecular genetic studies have proven ADHD to display a high heritability (up to 76%) (Biederman & Faraone 2005). Thus, it is generally accepted that the heritability of neuropsychiatric disorders like ADHD results from complex interaction between genetic and environmental factors (Burmeister et al 2008). As in other neuropsychiatric disorders, the genetic background of ADHD is complex and heterogeneous with a multitude of potential risk genes. Since individual variants of these risk genes can range from rare with strong impact to common with generally small effect size, it is difficult to find genes related to neuropsychiatric disorders (Lupski et al 2011, Sullivan & Psychiatric Genetics 2012). Therefore, extensive research was required to identify and validate genes which modulate the genetic vulnerability to psychiatric disorders. Genome-wide copy number variant (CNV) and single nucleotide polymorphism (SNP) association scans (GWAS) are beginning to reliably identify ADHD-associated genes (Elia et al 2012, Lesch et al 2011, Lesch et al 2008b, Williams et al 2012). Several risk genes have been shown to influence the liability to ADHD, such as *tryptophan hydroxylase-2* (*TPH2*) and *cadherin-13* (*CDH13*) (Lesch et al 2008, Lesch et al 2011, Elia et al 2012, Williams et al 2012).

A quite new candidate gene for ADHD is the gene *solute carrier family 2, facilitated glucose transporter member 3* (*SLC2A3*) that encodes for the glucose transporter-3 (GLUT3). In 2009, study in a three-generation Old Order Amish pedigree with focus on affective disorders (Yang et al 2009) first detected a duplication of *SLC2A3* on chromosome 12p13.31, which represents a common CNV in the general population. Conducting a CNV scan in a cohort of European ADHD patients, our working group replicated this finding of a *SLC2A3* duplication on chromosome 12p13.31 (Lesch et al 2011).

1.2 Cadherin-13 (CDH13): A protein involved in the pathophysiology of neuropsychiatric disorders

One of the most reproducible associations with ADHD (Lesch et al 2008b, Neale et al 2008, Neale et al 2010b, Rivero et al 2013, Salatino-Oliveira et al 2015) and ASD (Sanders et al 2011b) was found for *CDH13* which is a member of the cadherin superfamily, a gene family coding mainly for transmembrane glycoproteins (Ranscht & Dours-Zimmermann 1991). However, since Cdh13 lacks the common characteristic of a typical cell-cell adhesion glycoprotein, such as transmembrane and cytoplasmic domains, it seems to function as a

signalling molecule (Philippova et al 1998). During the development of the mouse brain, CDH13 is widely expressed in brain regions, such as amygdala, neocortex, hippocampus, thalamus, raphe nuclei, substantia nigra, striatum and cerebellum with a distribution outlining both the soma and the extending neurites (Forero et al 2017). Interestingly, CDH13 is involved in several neurodevelopmental processes, such as neurite outgrowth and axon guidance of motor neurons (Ciatto et al 2010, Rivero et al 2013), cell migration and cell survival under stress conditions in smooth muscle and vascular endothelial cells (Philippova et al 2009) and glutamatergic and GABAergic synapse development (Paradis et al 2007). In addition, *CDH13* overexpression influences migration and reorganization of the actin cytoskeleton and induces polymerization of actin stress fibers in SH-SY5Y neuroblastoma cells (unpublished data), whereas a down-regulation of *CDH13* decreases the number of actin stress fibers in HUVEC cells (Semina et al 2008). The specificity of CDH13 in the dorsal raphe (DR) has previously been reported (Forero et al 2017, Okaty et al 2015). Here, CDH13 is expressed at the contact points between serotonin (5-HT)-specific neurons and radial glia cells of the developing mouse DR, indicating an involvement in the radial glia-mediated migration of DR neurons (Forero et al 2017).

1.3 Glucose transport and metabolism

The monosaccharide glucose is one of the most important molecules in the energy metabolism and the primary energy source for most cells. For instance, it acts as a substrate for both catabolic and anabolic processes. However, plasma membranes are impermeable for hydrophilic molecules, and therefore, to transport this molecule from the extracellular fluid into the cell, particular transporter proteins are needed. In general, three families of solute carriers are distinguished that have been associated with glucose transport (Cesar-Razquin et al 2015, Feng & Frommer 2015, Thorens & Mueckler 2010b, Wright 2013). The first group includes the major facilitator superfamily (MFS) glucose facilitators GLUTs (SLC2) that enables the passive diffusion of glucose into the cell, while the sodium-driven glucose symporters SGLTs (SLC5) form the second group that mediates the secondary active co-transport of glucose (Wright et al 2011, Yan 2015). The recently characterized SWEET (SLC50) are the third and last group associated with glucose transport which are mainly responsible for efflux and intracellular trafficking of sugars in plants, however remains to be characterized in mammals (Chen et al 2010).

1.3.1 The *SLC2A* family of glucose transporters (GLUTs)

With respect of mammalian organisms, glucose uptake is mainly mediated by glucose transporters of the GLUT protein family that is part of the MFS of membrane transporters (Pao

et al 1998). As illustrated in Figure 1A, the GLUT protein family comprises fourteen isoforms, which each display distinct regulatory and/or kinetic properties that reflect their specific roles in cellular and whole-body glucose homeostasis and facilitate the bidirectional energy-independent transport of glucose and/or other hexoses (facilitative diffusion) (Kono et al 2005, Mueckler & Thorens 2013, Seki et al 2003, Thorens & Mueckler 2010a). They are comprised of ~500 amino acid residues, are characterised by 12 transmembrane spanning domains and an oligosaccharide side chain, which is either located on the first or on the fifth extracellular loop (Figure 1B) (Gibbs et al 1991, Wood et al 2003). Three subclasses of glucose transporters are distinguished according to similarities of the primary sequence (Thorens & Mueckler 2010a): class I includes the 'classical' isoforms GLUT1-4 and GLUT14 (Mueckler & Thorens 2013). The latter is known to be a paralog of GLUT3 (Wu & Freeze 2002). Class II comprises the transporters GLUT5, 7, 9 and 11, while class III involves the isoforms GLUT6, 8, 10 and 12. Interestingly, this class also includes the proton-dependent myoinositol transporter HMIT (GLUT13) (Mueckler & Thorens 2013, Thorens & Mueckler 2010a). Since their implication on several disorders, such as cancer (Barron et al 2016) and diabetes (Elsas & Longo 1992), GLUTs are important subjects for medical research and show great potential as drug targets for the treatment of a number of diseases.
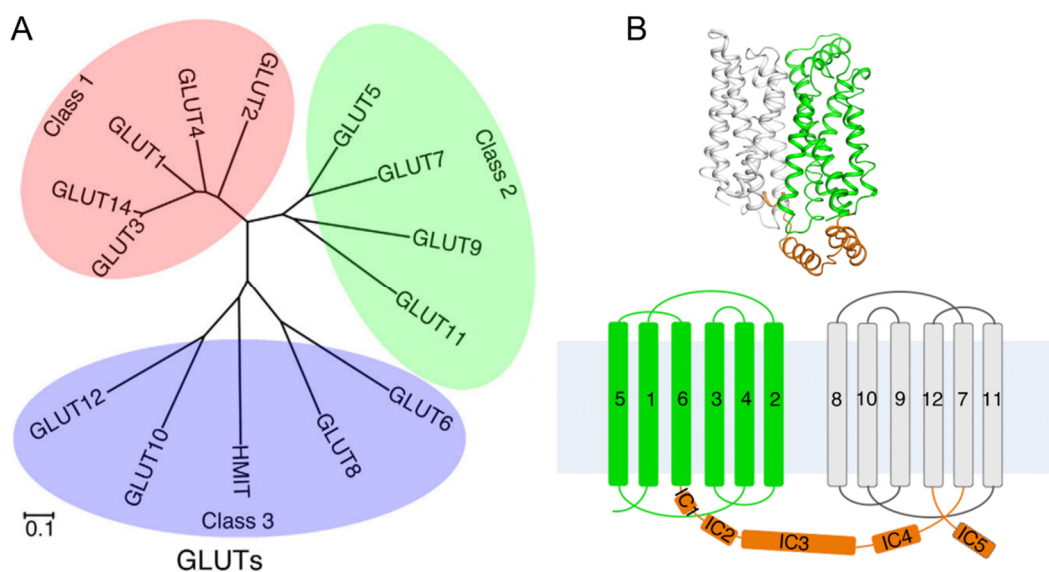
Figure 1: The phylogenetic tree of GLUTs in Homo sapiens.

(A) Multiple sequence alignment was performed with ClustalW and the results were presented with MEGA6. Fourteen members of GLUTs are illustrated. (B) The structural folds and overall structures of GLUTs show the 12 transmembrane helices divided into a N domain and a C domain, coloured in green and white, respectively. The intracellular helices domains (ICH) are coloured orange. Figure was adapted from Deng & Yan (2016).

1.3.2 *SLC2A3*: a novel candidate gene that may increase liability to neurodevelopmental disorders

The human gene is located at the short arm of chromosome 12, with a size of approximately 17 kb. While eleven human *SLC2A3* mRNA transcripts are listed, only two transcripts are described as protein-coding (www.ensembl.org), of which one comprises all 10 exons of the gene and is translated into a protein of 496 amino acids (54 kilodalton (kDa)), and in the contrary the other includes 4 exons, thus only part of the coding sequence and is translated into a 142 amino acid protein (15 kDa) (Simpson et al 2008). Besides its expression in the brain, *SLC2A3* is expressed in various peripheral tissues, such as placenta and kidney (Kayano et al 1988), in skeletal muscle (Stuart et al 1999), white blood cells (Mantych et al 1992) and testis (Haber et al 1993). The protein GLUT3 was the third glucose transporter isoform to be cloned (Kayano et al 1988) and due to its main expression in the brain it is known as the neuronal glucose transporter (Nagamatsu et al 1992). Here, it facilitates the transport of glucose across the plasma membranes and is therefore critically involved in the cerebral glucose metabolism by providing energy for neuronal activity (Nagamatsu et al 1993, Simpson and Davies 1994). GLUT3 consists of 12 transmembrane domains (TM), a long extracellular loop between TM1 and 2, including a glycosylation site and a regulated central hydrophilic pore and intracellular N, as well as C terminal ends (Dwyer, 2001). GLUT3 was shown to exhibit a quite low Michaelis constant (Km) for glucose implicating a strong affinity for this particular carbohydrate (Simpson et al 2008). Nevertheless, glucose is not the only molecule conveyed by GLUT3, as some other hexoses and closely related compounds, such as galactose, mannose or dehydroascorbic acid also serve as adequate substrates (Gould et al 1991, Rumsey et al 1997).

GLUT3 activity depends on the turnover number (k_{cat}) which is seven-fold higher for GLUT3 in neurons than GLUT1 in astrocytes (Lowe & Walmsley 1986, Simpson et al 2008). This fact combined with a half-life of 15 h (Khayat et al 1998a) serves as explanation why this glucose transporter is mainly found in neurons with their high energy demand. In humans, GLUT3 is expressed in both somata and neuronal extensions (Simpson et al 2018) and its expression is regulated by several factors, such as insulin (Maratou et al 2007), brain-derived neurotrophic factor (BDNF) (Burkhalter et al 2003), as well as glucose deprivation (Fladeby et al 2003). Additionally, the transcription factor cAMP response element (CRE)-binding protein (CREB) was shown to regulate the expression of human GLUT3 by binding to the promoter region (Jin et al 2013).

Since GLUT3 moderates the brain`s excitatory–inhibitory balance, it is impacting neurodevelopmental processes and activity-dependent neural plasticity (Ferreira et al 2011,

Merker et al 2017, Segarra-Mondejar et al 2018). GLUT3 dysfunction may therefore contribute to the pathophysiology of neuropsychiatric disorders. In 2008, Liu and colleagues (2008) associated decreased central levels of GLUT3 with hyperphosphorylation of tau protein in the human brain, a histopathological indication seen in patients with Alzheimer disease. One year later, a genome-wide expression analysis in schizophrenia revealed, amongst other genes, a significantly altered expression of *SLC2A3* in the patient group (Kuzman et al 2009), while a study conducted in 2011 revealed a two-marker haplotype associated with a particular neurophysiological endophenotype of dyslexia had a trans-regulatory impact on *SLC2A3* expression (Roeske et al 2011).

1.4 Stem cell research

1.4.1 Specific types of stem cells endure several states during development

Stem cells are characterized by the remarkable capacity of self-renewal due to infinite cell proliferation combined with the differentiation potential along different cell lineages in consequence of cell division (Evans & Kaufman 1981). In order to balance the number of stem cells and differentiated progeny, stem cells can adopt three different divisional strategies (Morrison & Kimble 2006): (1) Asymmetric cell division: hereby, two daughter cells rise of one mother cell being once an exact copy of the native stem cell and the other stem cell being destined to differentiate; (2) symmetric cell division: each stem cell divides symmetrically to generate either two daughter stem cells or two differentiating daughters; and (3) a combination of symmetric and asymmetric divisions. Which type of cell division is used by a stem cell depends on external (cell-extrinsic) environmental factors and/or internal (cell-autonomous or cell-intrinsic) regulatory mechanisms (Knoblich 2008). Those processes provide the classification into several groups underlying a distinct hierarchy which is based on the cell's differentiation potential. For instance, totipotent stem cells are able to differentiate into embryonic and extra-embryonic tissue or placental cells, and thus to generate a fully functional living organism (e. g. fertilized egg). Pluripotent stem cells (PSC), such as embryonic stem cells (ESCs) are formed by matured totipotent cells which maintain the ability of self-renewal, however contrary to their mother cell, their differentiation potential is limited to any of the three germ layers, namely ectoderm, endoderm and mesoderm (Stewart et al 2006). The next generation - multipotent stem cells - is committed to lineage specification of differentiation and reduced self-renewal frequency. Those cells show potential to only differentiate into a specific range of cell types which is dependent on the tissue (Mazurier et al 2004). Finally, oligopotent stem cells are even more limited to closely related cell types, while unipotent stem cells are the least potent and differentiate only into a single cell type.

1.4.2 Human induced pluripotent stem cells (iPSCs)

Most of the studies published on the biophysical characteristics of neurotransmitter systems have been conducted in experimental models involving mouse or rat. Even though they have greatly contributed to the understanding of neurotransmitter system function in the mammalian brain, the molecular and cellular specifications of this system in humans are still largely unknown. To study the specifics of human development in a more precise way, ESCs were conventionally used as an *in vitro* model. ESCs are highly regenerative and a powerful tool for drug development, disease modelling and cell-based therapies. However, the use of ESCs faces considerable ethical controversies and legal challenges (Ardhanareeswaran et al 2017, Brennand et al 2012, Kaiser & Feng 2015). To provide an alternative, Yamanaka and colleagues (2006) designed a strategy to reverse the cell fate program of mouse embryonic fibroblasts (MEFs) by the retroviral-mediated ectopic expression of four genes that had been previously associated with a cellular pluripotent state. In particular, the combined expression of the transcription factors octamer-binding transcription factor 4 (Oct4), SRY (Sex Determining Region Y)-box 2 (Sox2), kruppel-like factor 4 (Klf4) as well as avian myelocytomatosis viral oncogene homolog (c-Myc) lead to immune-matched ESC-like cells (Takahashi & Yamanaka 2006). Therefore, this specific set of transcription factors has been referred to as Yamanaka factors and those reprogrammed cells were called induced pluripotent stem cells (iPSCs). These artificially derived pluripotent cells exhibited similar characteristics as mammalian ESCs both *in vitro* and *in vivo*, such as ES-like morphology of compact, dense, roundly shaped colonies with sharp edges and typical ES-like growth behaviour, as well as their ability to differentiate into all cells of the human body. In 2007, the same group succeeded to reverse also the cell fate of human skin fibroblasts to a pluripotent state (Takahashi et al 2007). Although the first generation of iPSCs represented a viable alternative to obtain ESC-like stem cells, the clinical applicability of such a cell line would be limited due to the integrated transgenes implicating the risk of interference with gene transcription and insertional mutagenesis (Mikkers & Berns 2003) as well as tumour formation (Okita et al 2007). Based on these fundamental studies, numerous methods describing the reprogramming of somatic cells using different specific reprogramming setups were developed in order to facilitate the clinical application of iPSCs. Even though approaches using a lentiviral vector system to transduce Yamanaka factors yielded a higher efficiency than retroviral transduction (Ohmine et al 2011), the development of non-integrating reprogramming techniques was required to circumvent the potential risks caused by the integration of viral vectors. Reprogramming via messenger ribonucleic acid (mRNA)-based technology represents a safe, non-integrating and conserving method to deliver the pluripotent state to adult cells (Warren et al 2010) that can be performed in a S1-laboratory environment with lowered risk of harm for the researcher. Although synthetic

mRNAs are commercially available for cellular reprogramming, this method is highly labour intensive and requires daily attention by the addition of new mRNA for one week. Interestingly, the single-stranded Sendai virus (SeV) is an RNA-based virus that does not enter the nucleus. Therefore, it can be eliminated after several cell passages after the infection. Since SeV has a completely RNA-based reproductive cycle, it only occurs in the cytoplasm of infected cells and does not integrate into the cellular deoxyribonucleic acid (DNA). Moreover, the SeV vector system is more efficient for the introduction of the Yamanaka factors compared to retro- or lentiviral vector (Fusaki et al 2009) and can also be used for the reprogramming of other cell types, like blood cells.

These days, iPSCs are a common tool to generate patient-derived cell and tissue models. These models have emerged as fundamental approaches to reveal the molecular mechanisms underlying the pathogenesis of diseases, including neurodevelopmental disorders (Halevy et al 2015, Mariani et al 2015). For clinical application, such autologous cells could be used for transplantation events in cell replacement therapy in the future, while in basic research approaches, the generation of patient-specific affected cell types *in vitro* can help to understand the pathogenesis of several diseases. This promising field of research requires the expansion and refinement of established protocols describing the differentiation of human iPSCs into specific neuronal subtypes (Figure 2).
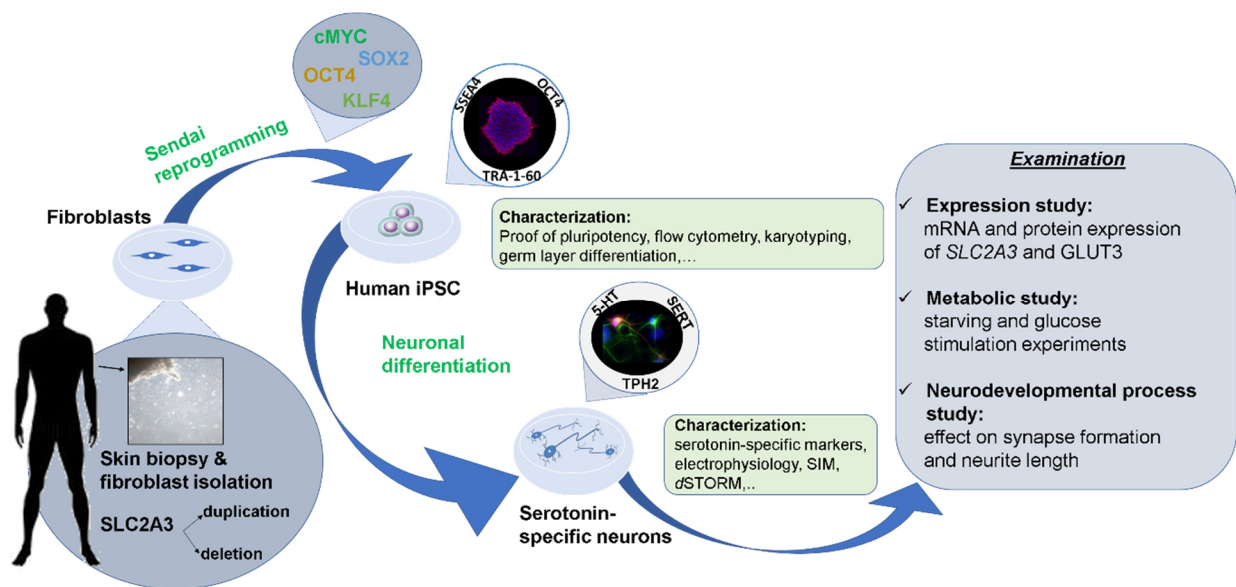
Figure 2: Generation of human iPSCs and iPSC-derived 5-HT specific neurons.

A scheme of the reprogramming technology that reverses the cell fate of adult cells and results in artificially created pluripotent stem cells. Here, the specific direct differentiation of iPSCs into 5-HT specific neurons and possibilities to study genetic variants of risk genes in a generated affected cell type are illustrated. Abbreviations: SIM: structured illumination microscopy; *d*STORM: *direct* stochastic optical reconstruction microscopy.

1.5 Specification of cellular subtypes along the neuronal lineage

As bilateral symmetric organisms' vertebrates develop two polarity axes which are determined by the location of the sperm entering the embryo on the animal pole as well as the gravitational force. During early embryogenesis, the anterior-posterior (A-P) axis divides the vertebrate central nervous system (CNS) into four specific regions, namely forebrain, midbrain, hindbrain and spinal cord, while the vertically dorso-ventral (D-V) axis divides from back to ventral side. The grey crescent is formed diagonally opposite to the sperms' entry point by cortical rotation and the blastopore develops during a process called gastrulation. The Spemann organizer is the upper edge of the blastopore and an important region coordinating cell fates by a complex interaction of several morphogens (Spemann and Mangold, 1924). The signalling molecules that are originated by the organizer are classified into several families, such as bone morphogenetic proteins (BMPs), the hedgehogs including sonic hedgehog (SHH), the fibroblast growth factors (FGFs), and the WNTs, arranging cell-cell communication for a directed differentiation. For instance, the process of cells becoming specialized towards the neural fate is triggered by the soluble BMP antagonists noggin, chordin, and follistatin secreted by the organizer (De Robertis 2009, Harland 2000, Weinstein & Hemmati-Brivanlou 1997). There have been many efforts to reproduce *in vitro* the conditions for the differentiation of iPSCs into specific neuronal types. In culture, treatment of iPSCs with serum-free medium induces the shift from self-renewal to differentiation with a favoured neural state (Zhang et al 2001). There are two specific ways to induced directed differentiation of iPSCs *in vitro*: neural differentiation requires either the formation of pluripotent stem cell aggregates, called embryoid bodies (EBs) or a monolayer culture method.

1.6 The monoaminergic neurotransmitter systems

1.6.1 The monoamine neurotransmitters: a general overview

A complex interplay of multiple genes and environmental factors causes abnormalities in brain development increasing the risk for neurodevelopmental and psychiatric disorders. Conditions of such diseases are associated with alterations at various brain structural and functional levels implicating significant interaction between the dopamine and 5-HT system. Basic physiological functions including sleep, motor control, food intake, sexual arousal, as well as influence mood and behavioural reinforcement are modulated by the monoamine neurotransmitters, namely noradrenalin (NA), dopamine, and 5-HT. For instance, dysfunction of the dopamine system has been associated with substance abuse, schizophrenia, ADHD and Parkinson's disease (PD). Imbalance in the 5-HT system has been linked to the aetiology of several conditions including anxiety, bipolar, impulsivity, depression and schizophrenia. Understanding

interactions between the monoamine systems is necessary to reduce side effects of pharmaceuticals that target these systems (Freitas-Ferrari et al 2010, Iqbal & van Praag 1995, Kapur & Remington 1996, Nieoullon 2002, Nieto Mendoza et al 2015). For instance, 5-HT specific neurons convert L-3,4-dihydroxyphenylalanine (L-DOPA) to dopamine via the L-amino acid decarboxylase (AADC) (Arai et al 1994, Ng et al 1970). Vesicular packaging of dopamine through the vesicular monoamine transporter (vMAT2) and activity-dependent release of dopamine is the consequence of 5-HT specific neurons' exposure to L-DOPA (Kannari et al 2000, Tanaka et al 1999). Gantz and colleagues (2015) showed that 5-HT specific terminals participate in D2 receptor-dependent dopamine signalling in the substantia nigra (SN) and reduce 5-HT$_{1A}$ receptor-dependent signalling in the DR following treatment with L-DOPA.

1.6.2 5-HT specific neurons in the brain

Even if there are only about 30x10^4 5-HT specific neurons in the human brain (Chen & Condron 2008), 5-HT is a key modulator in many physiological processes such as sleep regulation, food intake, sexual behaviour and is implicated in alcoholism, drug abuse, depression and anxiety (Alenina & Klempin 2015, Nichols & Nichols 2008, Walther & Bader 2003). Furthermore, 5-HT is an important regulator in early developmental processes such as cell proliferation, migration, differentiation, maturation and survival (Azmitia 2001, Lauder 1993, Lipton & Kater 1989, Migliarini et al 2013, Vitalis & Parnavelas 2003).

In rodent and human brain, projections of the 5-HT system ascend from the raphe nuclei, a cluster of nine nuclei (B1-B9) that extend along the midline of the brainstem (Dahlstroem & Fuxe 1964). These nuclei are commonly separated into a rostral group (B5-B9), responsible for the innervation of most brain regions, and a caudal group (B1-B3), which project towards the spinal cord and periphery (Alonso et al 2013, Kiyasova & Gaspar 2011, Muzerelle et al 2016). Neurons of the rostral subdivision can be further subdivided into the dorsal raphe (DR: B6+B7) and the median raphe (MR: B5+B8), which innervate forebrain and midbrain structures including the hippocampus, hypothalamus, striatum and the amygdala participating in regulating sensory or cognition processes along with emotional responses (Hensler 2006, Lesch & Waider 2012). The caudal section provides projections to the spinal cord and cerebellum regulating motor activity as well as the autonomic nervous system (Lidov & Molliver 1982). In addition to the differentiation of these nuclei along the rostral-caudal extension of the mid- and hindbrain, there is a high heterogeneity in the target specificity and function of the 5-HT specific neurons that constitute them (Okaty et al 2015). The DR is located right beneath the posterior part of cerebellar aqueduct and contains about half of all 5-HT specific neurons in the CNS, which can be further divided into six regions: rostral, caudal, dorsomedial, ventromedial, interfascicular, and lateral parts. The MR is located at the ventral expansion of

the DR or the midline of the pontine tegmentum where many 5-HT specific neurons are densely packed in the midline and some 5-HT specific neurons are scattered in the periphery. While DR 5-HT specific neurons innervate the prefrontal cortex, lateral septum, and ventral hippocampus, MR 5-HT specific neurons innervate the temporal cortex, medial septum, and dorsal hippocampus. Interestingly, 5-HT specific neurons between different raphe nuclei such as DR and MR communicate via 5-HT (Adell et al 2002, Lechin et al 2006, Muzerelle et al 2016).

Afferent projections to the raphe nuclei show diversity: acetylcholine (ACh) from the laterodorsal tegmental nucleus, dopamine from the substantia nigra and ventral tegmentum area, histamine from tuberomammillary hypothalamic nucleus and NA from the locus coeruleus. Additionally, excitatory glutamatergic inputs from the medial prefrontal cortex and lateral habenula nucleus and inhibitory GABAergic inputs have been reported (Aghajanian & Wang 1977, Bernard & Veh 2012, Celada et al 2001, Gervasoni et al 2000, for review see Maejima et al 2013, Varga et al 2009).

1.6.3 5-HT metabolism: the circle of life of a monoamine

Tryptophan hydroxylase (TPH) is the rate-limiting enzyme during the synthesis of 5-HT which is known to be a two-step process. While TPH1 controls most of peripheral 5-HT synthesis, TPH2 is exclusively expressed in brain 5-HT specific neurons (Gutknecht et al 2009, Walther et al 2003). Here, it catalyses the hydroxylation of the amino acid L-tryptophan to 5-hydroxy-L-tryptophan (5-HTP). During this process, Fe^{2+} acts as a co-factor and oxygen and tetrahydrobiopterin as co-substrates (Moran et al 2000, Pavon & Fitzpatrick 2006, Roberts & Fitzpatrick 2013, Walther & Bader 2003). 5-HT formed by the decarboxylation of 5-HTP is finally transported to the synaptic active zones of the neuron, packaged into vesicles by the vMAT2. At the active zones of a presynapse 5-HT is released into the extracellular space in response to a threshold action potential, binds to different pre- and postsynaptic receptors and therefore initiates signalling cascades at the synapse. Nowadays, a range of different 5-HT specific receptors are known and grouped in seven classes ($5-HT_{1-7}$) with at least 14 structural and pharmacologically distinct variants ($5-HT_{1A-F}$, $5-HT_{2A-C}$, $5-HT_3$, $5-HT_4$, $5-HT_{5A-B}$, $5-HT_6$ and $5-HT_7$) identified so far (Barnes & Sharp 1999, Hoyer et al 2002, Kroeze et al 2002, for review see McCorvy & Roth 2015, Yohn et al 2017). All of them belong to the G-protein coupled receptor (GPCR) superfamily, except of $5-HT_3$, which is a ligand-gated ion channel (Berger et al 2009, Engel et al 2013). For instance, the 5-HT receptors $5-HT_{1A}$, $5-HT_{1B}$ and $5-HT_2$ were shown to contribute to cell proliferation in the various subregions of the hippocampus (Banasr et al 2003), while in the prefrontal cortex, the $5-HT_{2A}$ receptor modulates 5-HT-induced neuronal activity during early postnatal stages of brain maturation (Zhang 2003). $5-HT_{1A}$, 5-

HT$_{1B}$, together with 5-HT$_{1D}$ receptors are located on somatodendritic and axonal region of 5-HT specific neurons (McDevitt & Neumaier 2011) and act as negative feedback effectors for 5-HT neuronal firing and 5-HT release (Andrade 1998, Andrade et al 2015, Araragi et al 2013). Here, activation of G protein-coupled inwardly rectifying potassium channels (GIRK) leads to membrane hyperpolarization and reduction or complete blocking of action potential firing (Blier et al 1989, Colino & Halliwell 1987, Hjorth & Sharp 1991, Penington et al 1993, Sprouse & Aghajanian 1987, Stamford et al 2000). 5-HT reuptake from the presynapse is performed by the serotonin transporter (SLC6A4, SERT) which terminates 5-HT action. 5-HT is either restored in vesicles by vMAT2 or enzymatically degraded by Monoamine oxidase A (MAO-A) which catalyses the oxidative deamination of 5-HT to 5-hydroxyindole acetaldehyde in the cytoplasm (for review see Maejima et al 2013, Torres et al 2003, Vergo et al 2007).

1.6.4 Modes of action of 5-HT: Synaptic versus extrasynaptic transmission

5-HT specific neurons act via two modes of secretion in a synaptic as well as non-synaptic manner: 1) 5-HT is released from a unidirectional chemical synapse (Fuchs et al 1982) from clear and dense core vesicles at active zones at presynaptic endings upon depolarization acting locally in "hard wired" circuits (Kuffler et al 1987). Synapses are formed near the cell bodies, which allows direct electrical recordings of pre- and postsynaptic events virtually at the synaptic sites. 2) In contrast, modulation of whole neuronal circuits requires the release of large amounts of signalling molecules from extrasynaptic sites that are located in the soma, dendrites and axons of the specific neuron. The mechanism how extrasynaptically released transmitters reach their distant targets is called "diffusion" (De-Miguel et al 2015). Molecules released in this way become ingredients of the extracellular environment of the nervous system and acts on extrasynaptic receptors, often located in large distances from the release sites (Borroto-Escuela et al 2015, Fuxe et al 2007, Trueta et al 2012).

1.7 Strategies to differentiate human iPSCs into 5-HT specific neurons: a preliminary study

To establish a reproducible and reliable differentiation procedure in order to obtain human iPSC-derived 5-HT specific neurons, I conducted a pre-study together with a master student, R. Kern, to reveal conceivable ways to generate this specific neuronal subtype. The human iPS cell line FSiPS reprogrammed by SeV from Normal Human Dermal Fibroblasts (NHDFs) that we used in this preliminary study was kindly provided by the working group of Prof. F. Edenhofer (Department of Genomics, Stem Cell Biology and Regenerative Medicine, Institute of Molecular Biology & CMBI, Leopold-Franzens-University Innsbruck). NHDFs are known to

be a cell type that can be easily reprogrammed and therefore serve as control cell line and for establishment purposes.

As a starting point, we based our work on two recently published protocols describing the generation of 5-HT specific neurons from human PSCs (Figure 3). Those methods either used a standard midbrain patterning protocol (Vadodaria et al 2015) or a hindbrain protocol (Lu et al 2015), respectively. The midbrain patterning procedure uses an EB formations system, followed by treatment with FGF8 to introduce the midbrain fate of the cells. In contrast, the hindbrain patterning procedure consists of an adherent culture system using a manipulation of signalling pathways by SHH and FGF4.

Generation of functional human serotonergic neurons from fibroblasts
Vadodaria et al 2015
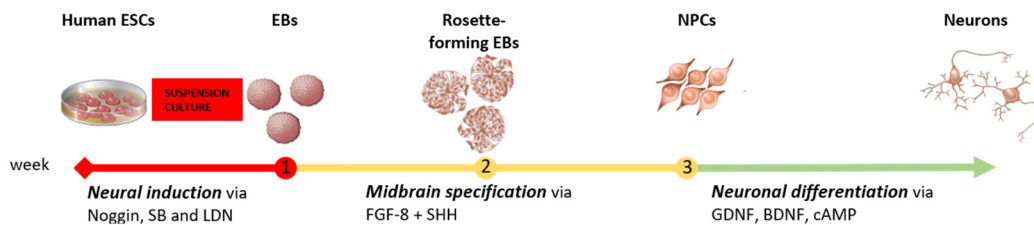
Generation of serotonin neurons from human pluripotent stem cells
Lu et al 2015
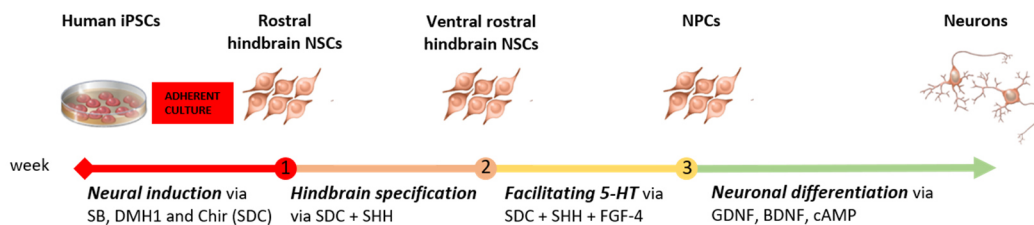
Figure 3: Overview of recent protocols describing the differentiation procedure of human PSCs into 5-HT specific neurons.

Two recently published methods describe the differentiation of human PSCs into 5-HT specific neurons by using an EB formation (Vadodaria et al 2015) or an adherent system (Lu et al 2015) and a manipulation of signalling pathways by specific molecules. Abbreviations: ESCs, embryonic stem cells; EBs=embryoid bodies; NPCs, neural progenitor cells; iPSC, induced pluripotent stem cells; NSCs, neural stem cells; SB=SB432543; LDN, LDN-193189; FGF, fibroblast growth factor; SHH, sonic hedgehog; GDNF, glial cell-derived neurotrophic factor; BDNF, brain-derived neurotrophic factor; cAMP, cyclic adenosine monophosphate; Chir, CHIR99021; SDC, Medium supplemented with SB+DMH-1+Chir. Adapted from Lu et al (2015) and Vadodaria et al (2015).

Since a midbrain patterning protocol primarily aims for a high percentage of catecholaminergic neurons, but only yields a low percentage of 5-HT specific neurons, we mainly focused on the use of a hindbrain patterning protocol. In 2015, Lu and colleagues (2015) developed a protocol for an efficient conversion of human iPSCs towards ventral hindbrain progenitors in adherent, and chemically defined conditions. Therefore, they achieved a great efficiency with the comprehensible selection of patterning factors: the concentration-dependent activation of WNT signalling by CHIR, which is an inhibitor of GSK3-beta and specifies caudal neural progenitor cells (Xi et al 2012). Furthermore, they used DMH1 as a highly selective small molecule BMP-inhibitor, known for its potential in the neuralization of human iPSCs (Neely et al 2012). The third factor, SB, inhibits the TGF-ß pathway and thus induces the differentiation of PSCs into several cell types, including neural cells (Chambers et al 2009). However, this described adherent neural induction step did not result in the desired amount of neural progenitor cells when applied to FSiPS cells. We obtained only a small number of neuronal cells in general and a rather mixed culture of neurons and non-neuronal cells. Numerous attempts to gain a pure neuronal culture failed in early steps of the differentiation process. The treatment of adherent cells with the corresponding patterning factors resulted in spontaneous differentiation or extraordinary cell morphology, both indicating the loss of the progenitor cell fate and further differentiation which caused massive cell death (Figure 4).
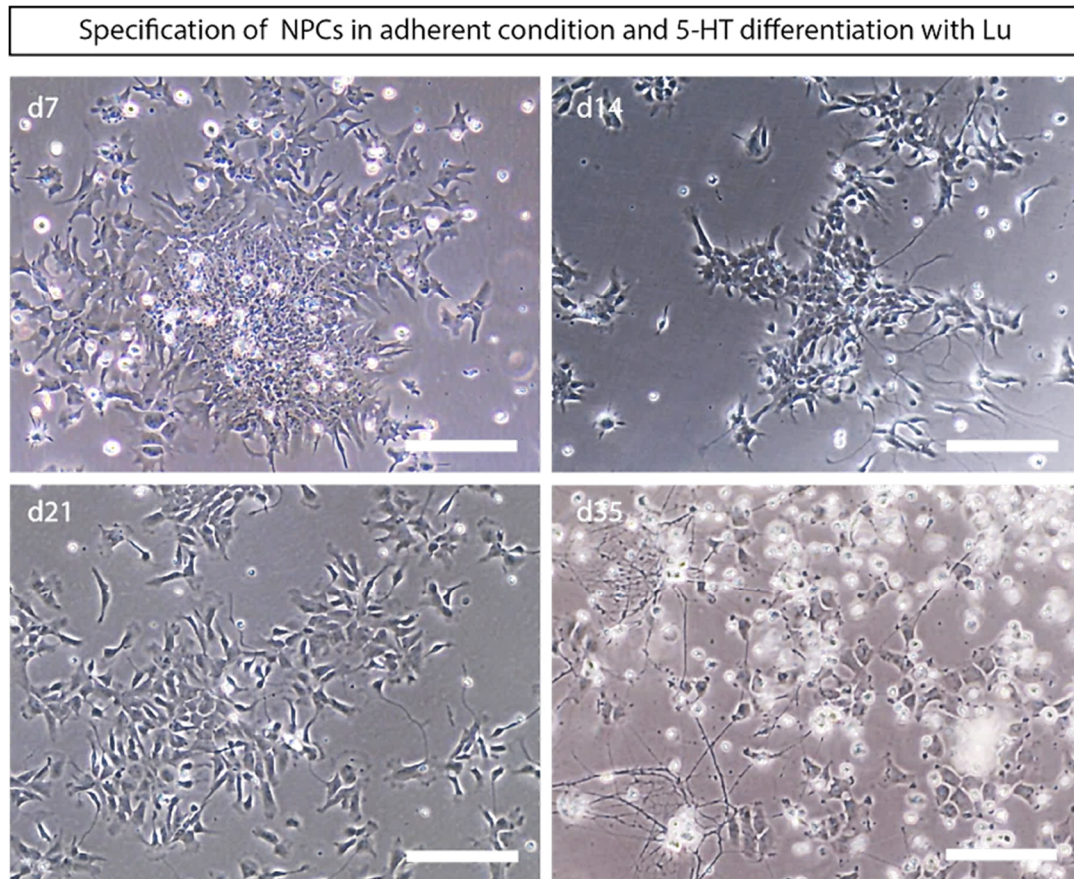
Figure 4: Performing a hindbrain protocol with an adherent neural induction step failed to deliver a high percentage of neuronal cells.

A hindbrain protocol was performed according to a previously published protocol (Lu et al 2015). Cells treated with a differentiation medium supplemented with SB, DMH1 and CHIR for 7 days did not display the morphology of human iPSC-derived neural progenitors (d7). Those cells gradually lost their morphological properties of progenitor cells over time and further specification via SHH (d14) and SHH + FGF4 (d21) caused spontaneous differentiations in those cultures. After 2 weeks of treatment with neural differentiation medium (d35), massive cell death and undirected differentiation were observed. Scale bar: 200 µm. Adapted from R. Kern's master thesis.

Therefore, we decided to use an EB system instead, as it formed reliable and robust aggregates of neural cells (Figure 5). Already the next day after cells were seeded in suspension culture, the typical assembly to spheroids could be observed. The emerging cell aggregates displayed sharp edges and strong variation in size and density and were treated with the combination of SB, DMH-1 and CHIR (SDC) as previously described. One week later, mid-sized EBs were plated on polyornithine (PO)- and laminin (LAM)-coated plates in SHH to induce ventralization of the generated rostral hindbrain progenitors. The cell clusters expanded as a monolayer with high density. A few days later, the first sign of neural differentiation emerged as typical neuroepithelial structures by the formation of rosettes in the centre of

colonies. FSiPS showed progenitor-like cells that were densely packed with no spontaneous differentiation in the core of the colony. From day 14, the rosettes were transferred to a freshly prepared PO/LAM-coated 6-well plate and were exposed to a combination of SHH and FGF4 for facilitating the 5-HT specific program of the ventral hindbrain progenitors. The cells were highly proliferative, which greatly increased the cell density over the one-week incubation period. Since a high density of neural progenitor cells is crucial to prevent spontaneous differentiation, cells had to be split every second to third day, however had to be seeded again in high density on PO/LAM. After three weeks of differentiation (d21), FSiPS-derived progenitors exhibited a typical neural progenitor cell morphology. The cells were tightly packed and showed small, delimited cell bodies.
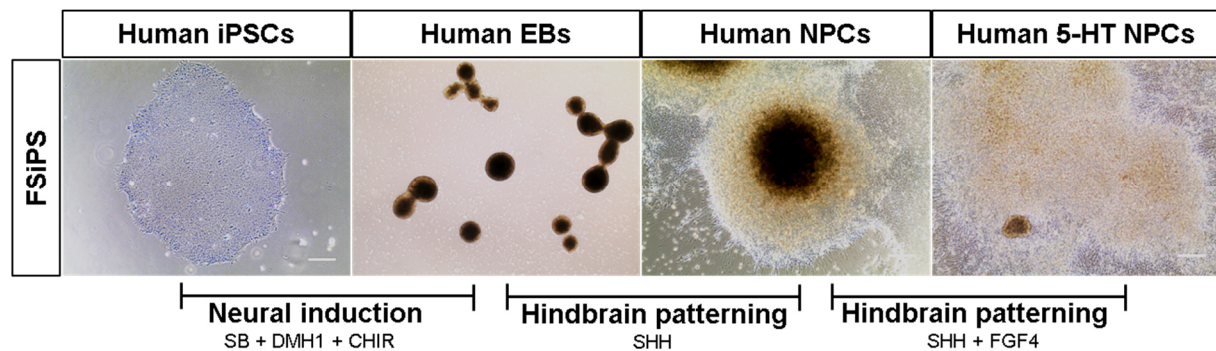
Figure 5: Optimized protocol for ventral hindbrain differentiation.

The combination of an EB system and the factors SHH and FGF4 allowed the establishment of a new approach for a directed ventral hindbrain differentiation. Scale bar: 200 µm. Adapted from R. Kern's master thesis.

In order to demonstrate that conversion of human iPSCs to neural progenitors with hindbrain identity was achieved, an immunofluorescence (IF) analysis of those cells was performed at day 7 and day 14 of the specification process (Figure 6A and B). After one week in neural induction medium, cells were stained with four well-established neural progenitor markers, namely SOX1, SOX2, nestin and paired box protein-6 (PAX6). The expression is a fundamental indicator of the identity of neural stem cells and is shown in Figure 6B. Nuclear localization of SOX1 and SOX2 was highly displayed at day 7 and the neural progenitors also showed cytoplasmatic localization of nestin. Homeobox protein Hox-A2 (HOXA2), a marker for a rostral hindbrain identity of neural progenitor cells, was also expressed by FSiPS cells.
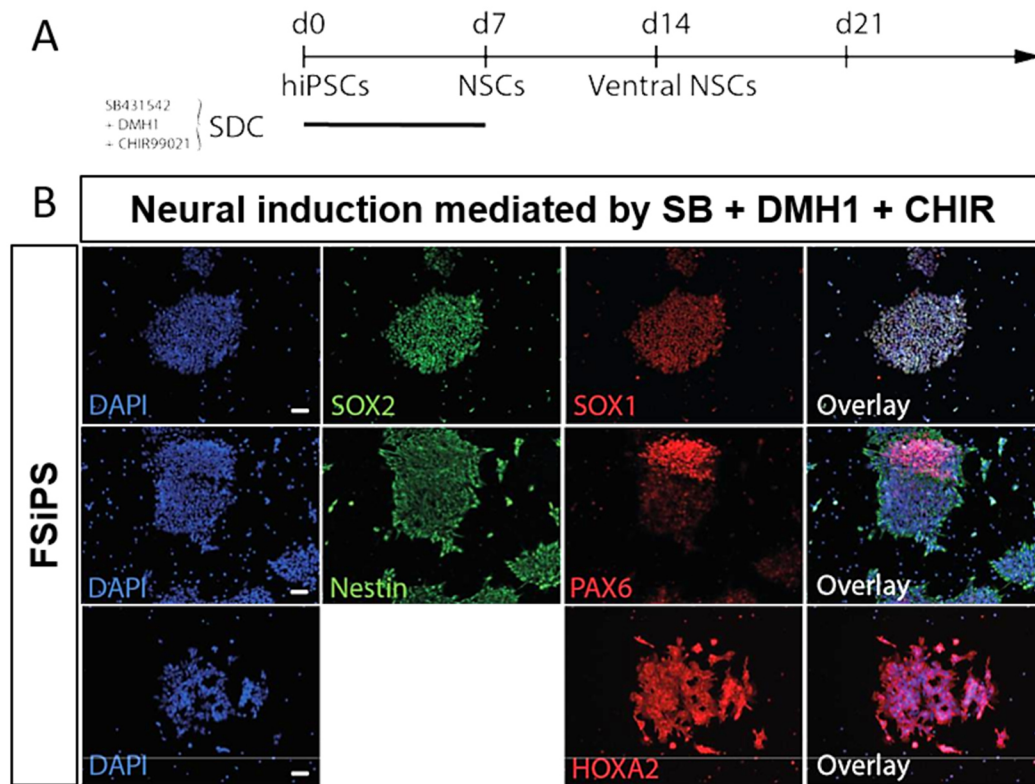
Figure 6: Generation of human iPSC-derived rostral hindbrain progenitors by neural induction with Ngg, LDN and SB.

(A) Schematic representation of 5-HT specific neuron generation process according to (Vadodaria et al 2015). (B) After one week of neural induction with NLS, cells were stained for typical neural markers, such as SOX2, Nestin, PAX6. High expression of HOXA2, a marker of rostral hindbrain progenitor cells, was also observed. Scale bar: 100 µm. Adapted from R. Kern's master thesis.

Several experiments demonstrate that the treatment of the differentiation cultures with a high concentration of SHH give rise to ventral progenitor cells (Chamberlain et al 2008, Ericson et al 1997). The absence of the dorsal marker PAX3/7 confirmed the ventralization effect of SHH, when applied to the cultures from day 7 onwards (Figure 7A and B). In contrast, the expression of the ventral hindbrain marker homeobox protein Nkx-6.1 (NKX6.1) was highly increased by the treatment of the cell cultures with SHH.
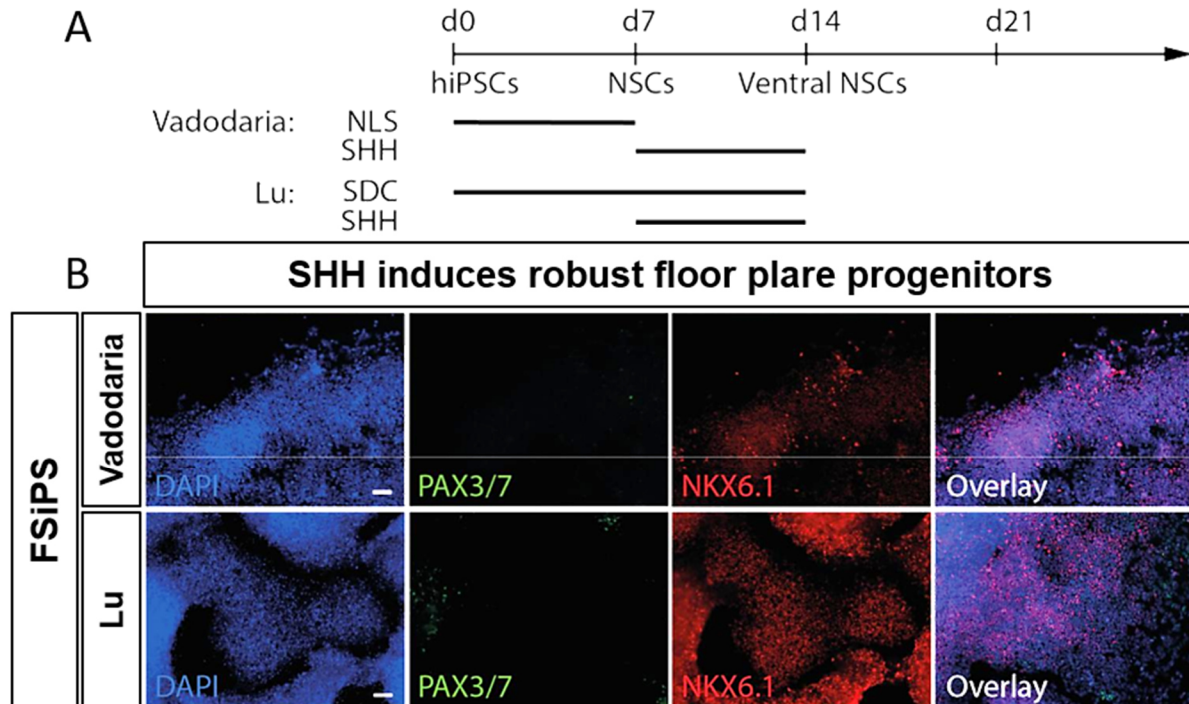
Figure 7: Ventralization of progenitor cells by the treatment of SHH from day 7 of specification.
(A) Schematic representation of 5-HT neuron generation process. (B) High concentration of SHH (1000 ng/mL) from d7 to d14, induced the expression of NKX6.1, a ventral hindbrain marker. No expression of dorsal hindbrain marker (PAX3/7) confirmed the effective ventralization via SHH. Scale bar: 100 μm. Adapted from R. Kern's master thesis.

Additionally, different concentrations of CHIR (0.8, 1.0, 1.4 μM) were used in SDC medium to assess the concentration-dependent effects of CHIR on A-P patterning of the progenitors (Figure 8). By analysing the expression of orthodenticle homeobox 2 (OTX2) a gradually decrease could be observed with an increased concentration of CHIR. The cells treated with a CHIR concentration of 0.8 μM showed strong OTX2 expression, while no OTX2 expression was found in cell cultures treated with CHIR 1.4 μM. HOXA2 is expressed by rostral progenitors and did not occur in cells treated with 0.8 μM. With increased CHIR concentration, HOXA2 gradually increased and was highly expressed by cells cultured with a CHIR concentration of 1.4 μM. HOXB1 is a marker for caudal hindbrain progenitors and was not expressed in cells cultured with 0.8 or 1.0 μM of CHIR. Cells treated with CHIR 1.4 μM displayed a few HOXB1+ cells, especially at the edge of cell colonies. In summary, no OTX2 expression was detected in cultures treated with 1.4 μM CHIR and most of the cells expressed HOXA2 but only a small fraction of HOXB1.
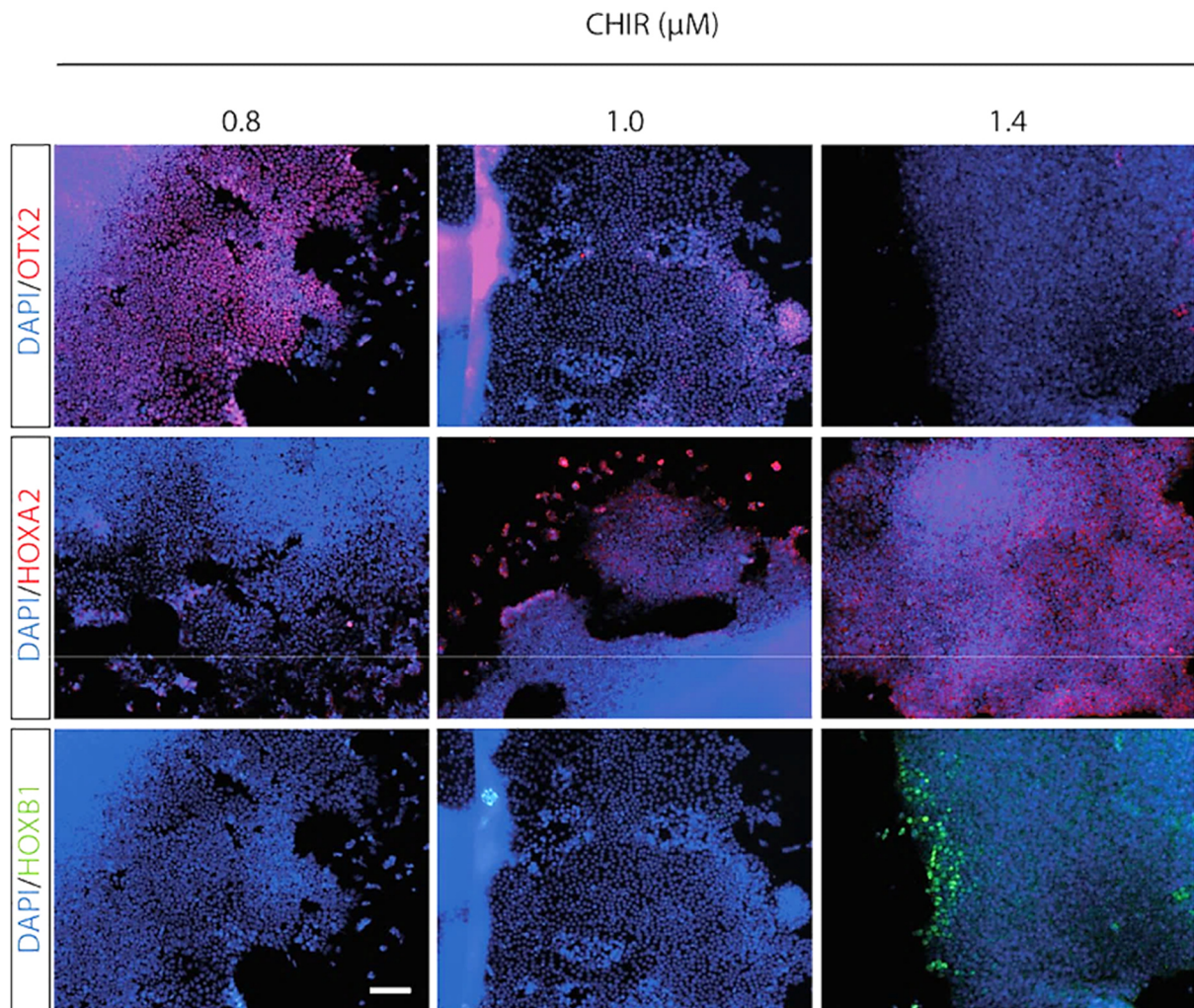
Figure 8: Cells stained for typical regional markers when treated with different concentrations of CHIR.

WNT activation by CHIR specifies caudal neural progenitors in a dose-dependent manner. With increasing concentrations of CHIR, the expression of the forebrain maker OTX2 gradually decreased. Cultures treated with 1.4 µM CHIR, most of the cells expressed HOXA2. HOXB1, a caudal hindbrain and spinal cord marker, was expressed by a few cells that were cultured with 1.4 µM CHIR. Scale bar: 100 µm. Adapted from R. Kern's master thesis.

However, after inducing neuronal fate of gained progenitors, we still yielded less 5-HT specific neurons than expected. Therefore, the goal of this thesis was to improve those first steps of our established differentiation procedure by enrichment of 5-HT specific progenitors.

1.8 Aim of the thesis

Since neuropsychiatric disorders involve a high burden to the social life of patients and their families, there is a demanding need to deepen our scientific knowledge of the neuronal mechanisms underlying the pathogenesis of neurodevelopmental disorders. The most

common neurodevelopmental disorder ADHD displays high heritability with complex genetics. Additionally, the cerebral glucose metabolism seems to be critical for neurodevelopmental processes, such as synaptogenesis and synaptic plasticity. Therefore, focussing on genetics that impact the neuronal energy demand in regard of the evolvement of neurodevelopmental diseases became more prominent over time. *SLC2A3* is essential for the cerebral energy supply, axonal transport and synaptic transmission (Mantych et al 1992) and a duplication of this gene has recently been associated with ADHD (Merker et al 2017a). We therefore claim that CNVs of the ADHD candidate gene *SLC2A3* encoding GLUT3 impacts glucose metabolism and the assembly of synaptic proteins in human neurons. To prove our hypothesis, we established a patient-derived neuronal cell culture model to examine the effects of *SLC2A3* CNVs on *SLC2A3* and GLUT3 basal expression, as well as on coping strategies of the neurons to fluctuating glucose availability and the synapse formation.

This thesis is composed of three specific objectives to achieve the main goal. In the first part, human iPSCs were generated from adult dermal fibroblasts from a 51-year-old female ADHD patient carrying a duplication of *SLC2A3*, a 48-year-old female ADHD patient carrying a deletion of *SLC2A3* and a 55-year-old female healthy donor serving as a control sample by transiently overexpressing OCT-3/4, SOX2, c-MYC and KLF4. Even though dysfunction of the 5-HT system is deeply involved in the pathogenesis of mental disorders, only little is known about the differentiation of iPSCs into 5-HT specific neurons. Therefore, the second objective was to establish a reliable procedure to generate this specific neuronal subtype from human iPSCs. Finally, basal expression levels of *SCL2A3* and GLUT3 were studied in human neurons, as well as the impact of glucose deprivation and the treatment with hyper- and hyperglycaemic conditions on GLUT3 expression. A super-resolution microscopy technique was used to visualize the synaptic compartments of generated human iPSC-derived neurons to reveal altered synaptic formation (if any) during the development of these cells.

2. Material and Methods

2.1 Material

2.1.1 Cell lines

Table 1: Cell lines used in this study

Cell line	Name	Detail
Fibroblast cell lines	CJ1	Control cell line
	CJ5	Patient cell line carrying a duplication of *SLC2A3*
	CJ7	Patient cell line carrying a deletion of *SLC2A3*
Human iPS cell lines	FSiPS CL2	Control cell line. Generated from NHDF and used to establish protocols
	CJ1 CL6	Control cell line
	CJ5 CL3	Patient cell line carrying a duplication of *SLC2A3*
	CJ7 CL6	Patient cell line carrying a deletion of *SLC2A3*
Mouse embryonic fibroblasts	CF-1 Mouse Embryonic Fibroblasts (MEF) feeder cells	Feeder cells for human iPSCs Amsbio, Abingdon, VA, USA (#GSC-6201G); irradiated, low density

2.1.2 Material and equipment for cell culture methods

Table 2: Cell culture media used in this study

Reagent	Manufacturer	Catalog #
DMEM/F12	Thermo Fisher Scientific, Waltham, MA, USA	11320-074
Neurobasal™ medium	Thermo Fisher Scientific	21103-049
Neurobasal™-A medium, no D-glucose, no sodium pyruvate	Thermo Fisher Scientific	A2477501
KnockOut™ DMEM/F-12	Thermo Fisher Scientific	12660-012
KnockOut™ DMEM	Thermo Fisher Scientific	10829-018
DMEM, high glucose, GlutaMAX™ supplement, pyruvate	Thermo Fisher Scientific	31966-021

Cell freezing medium-serum-free 1×	Sigma-Aldrich, St. Louis, MO, United States	C2639-50mL
DMEM, w: 4.5 g/L glucose, w: L-glutamine, w: sodium pyruvate, w: 3.7 g/L NaHCO3	PAN-Biotech, Aidenbach, Germany	P04-03590
StemMACS™ iPS-Brew XF, human	Miltenyi Biotech, Bergisch Gladbach, Germany	130-104-368
B-27™ plus neuronal culture system	Thermo Fisher Scientific	A3653401

Table 3: Cell culture reagents, supplements and kits used in this study

Reagent	Manufacturer	Catalog #
PluriSTEM™ dispase-II solution	Merck Millipore, Darmstadt, Germany	SCM133
Dispase-II solution	PAN Biotech, Aidenbach, Germany	P10-032100
Collagenase NB 4 standard grade	Amsbio, Abingdon, VA, USA	17454.01
Corning® Matrigel® hESC-qualified matrix, *LDEV-free, 5 mL	Corning, NY, USA	354277
Corning® Matrigel® growth factor reduced (GFR) basement membrane matrix, *LDEV-free, 10 mL	Corning	354230
TrypLE™ Express enzyme (1X), phenol red	Thermo Fisher Scientific, Waltham, MA, USA	12605-010
GlutaMAX™ supplement	Thermo Fisher Scientific	35050-038
MEM NEAA, non essential amino acid solution (100x) w/o: L-glutamine	PAN-Biotech, Aidenbach, Germany	P08-32100
2-mercaptoethanol (50 mM)	Thermo Fisher Scientific,	31350-010
Accutase cell detachment solution	Merck Millipore, Darmstadt, Germany	SCR005
Trypsin-EDTA (0.05%), phenol red	Thermo Fisher Scientific	25300062
N6,2′-O-Dibutyryladenosine 3′,5′-cyclic monophosphate sodium salt (cAMP)	Sigma-Aldrich, St. Louis, MO, United States	D0627-250MG
StemMACS™ Y27632 (rock inhibitor)	Miltenyi Biotech, Bergisch Gladbach, Germany	130-104-169
N-2 supplement (100X)	Thermo Fisher Scientific	17502-048 (5 mL), 17502001 (50 mL)
B-27™ supplement (50X), minus vitamin A	Thermo Fisher Scientific	12587-010
B-27™ supplement (50X), serum free	Thermo Fisher Scientific	17504-044
DPBS, no calcium, no magnesium	Thermo Fisher Scientific	14190169
CTS™ DPBS, calcium, magnesium	Thermo Fisher Scientific	A1285801
Human recombinant laminin-511	BioLamina, Sundbyberg, Sweden	LAMININ-511 (1mg)

Bovine serum albumin solution (7.5% in DPBS, sterile-filtered, BioXtra, suitable for cell culture)	Sigma-Aldrich	A8412-100ML
Fetal bovine serum, qualified, heat inactivated	Thermo Fisher Scientific	16140071
Poly-L-ornithine solution (mol wt 30,000-70,000, 0.01%, sterile-filtered, BioReagent, suitable for cell culture)	Sigma-Aldrich	P4957-50ML
L-ascorbic acid	Sigma-Aldrich	A4544-500G
KnockOut™ serum replacement	Thermo Fisher Scientific	10828028
Paraformaldehyde (PFA) solution 4% (Roti®-Histofix 4 %)	Carl Roth, Karlsruhe, Germany	P087.4
D-(+)-glucose solution	Sigma-Aldrich	G8769-100ML
Trypan blue solution	Sigma-Aldrich	T8154
Triton™ X-100	Sigma-Aldrich	T9284-100ML
Distilled water (cell culture grade, endotoxin-screened)	Thermo Fisher Scientific	15230071
Ibidi mounting medium	Ibidi, Martinsried, Germany	50001
StemMACS mRNA reprogramming kit	Miltenyi Biotech	130-107-581
CytoTune™-iPS 2.0 Sendai reprogramming kit	Thermo Fisher Scientific	A16517

Table 4: Small molecules and growth factors used in this study to manipulate signalling pathways

Reagent	Manufacturer	Catalog #
CHIR 99021	Axon Medchem, Groningen, Netherlands	Axon 1386 (2 mg)
StemMACS™ SB431542	Miltenyi Biotech, Bergisch Gladbach, Germany	130-106-543 (5 mg)
Recombinant human/murine/rat BDNF	Peprotech, Hamburg, Germany	450-02
Recombinant human GDNF	Peprotech	450-10
Recombinant mouse sonic hedgehog/Shh (C25II) N-terminus	R&D Systems, Minneapolis, MN, USA	464-SH-200
bFGF recombinant human protein	Thermo Fisher Scientific, München, Germany	13256-029
Recombinant human FGF-4	Peprotech	100-31
DMH-1	Tocris Bioscience, Bristol, United Kingdom	4126 (10 mg)

2.1.3 Antibodies and dyes

Table 5: List of primary antibodies and dyes used in this study

Name	Manufacturer	Cat#	Host	Dilution	Usage
Anti-OCT-3/4	Santa Cruz Biotechnology Inc, Santa Cruz, CA, USA	sc5279	Mouse (monoclonal)	1:50	Epifluorescence
Anti TRA-1-60	Santa Cruz Biotechnology Inc	sc21705	Mouse (monoclonal)	1:50	Epifluorescence
Anti-SSEA-4	Thermo Fisher Scientific, Waltham, MA, United States	MA1-021	Mouse (monoclonal)	1:200	Epifluorescence
Anti-AFP	Dako, Santa Clara, CA, USA	A0008	Rabbit (polyclonal)	1:400	Epifluorescence
Anti-TRA-1-60-Vio488 Live Cell Stain	Miltenyi Biotech, Bergisch Gladbach, Germany	130-106-872	Human (monoclonal)	1:100	Epifluorescence
Anti-SMA	Abcam, Cambridge, United Kingdom	ab7817	Mouse (monoclonal)	1:200	Epifluorescence
Anti-TRA-1-60-PE	Miltenyi Biotech	130-100-347	Human (monoclonal)	1:11	Flow cytometry
Anti-SSEA-4-APC	Miltenyi Biotech	130-098-347	Human (monoclonal)	1:11	Flow cytometry
Human/mouse /rat SOX1 antibody	R&D Systems, Minneapolis, MN, USA	AF3369	Goat (polyclonal)	1:150	Epifluorescence
HNF-3β antibody (H-4)	Santa Cruz Biotechnology Inc	sc-374376	Mouse (monoclonal)	1:50	Epifluorescence
Purified anti-Pax-6 antibody	BioLegend, San Diego, CA, USA	901301	Rabbit (polyclonal)	1:100	Epifluorescence
Human nestin antibody	R&D Systems	MAB1259	Mouse (monoclonal)	1:100	Epifluorescence
Human/mouse /rat SOX2 antibody	R&D Systems	MAB2018	Mouse (monoclonal)	1:500	Epifluorescence
NKX2.2	DSHB Hybridoma Bank, Lowa City, IA, USA	74.5A5	Mouse (monoclonal)	1:50	Epifluorescence

Anti-NKX6-1 antibody	Sigma-Aldrich, St. Louis, MO, USA	HPA036 774	Rabbit (polyclonal)	1:500	Epifluorescence
Anti-GATA2 antibody	Sigma-Aldrich, St. Louis	HPA005 633	Rabbit (polyclonal)	1:500	Epifluorescence
Anti-HOXA2 antibody	Sigma-Aldrich	HPA029 774	Rabbit (polyclonal)	1:200	Epifluorescence
Pax-3/7 antibody (B-5)	Santa Cruz Biotechnology Inc	sc-365843	Mouse (monoclonal)	1:50	Epifluorescence
Anti-βIII Tubulin mAb	Promega, Madison, WI, USA	G7121	Mouse (monoclonal)	1:1000	Epifluorescence; SIM
Glial Fibrillary Acidic Protein (GFAP)	Agilent Technologies, Santa Clara, CA, USA	Z0344	Rabbit (polyclonal)	1:5000	Epifluorescence
Tryptophan hydroxylase-2 antibody	Novus Biologicals, Nordenstadt, Germany	NB100-74555	Rabbit (polyclonal)	1:2000	Confocal; SIM
Tryptophan hydroxylase-2 antibody	Novus Biologicals	NB100-2447	Goat (polyclonal)	1:100	Confocal
5-HT (serotonin) antibody	Immunostar, Hudson, NY, USA	20080	Rabbit (polyclonal)	1:500	Confocal
5-HT (serotonin) transporter antibody	Immunostar	24330	Rabbit (polyclonal)	1:5000	Confocal
Anti-GABA antibody	Sigma-Aldrich, St. Louis	A2052	Rabbit (polyclonal)	1:1000	Confocal
Anti-Tyrosine hydroxylase antibody	Abcam	ab112	Rabbit (polyclonal)	1:1000	Confocal
MAP2	Synaptic Systems GmbH, Göttingen, Germany	188 004	Guinea pig (polyclonal)	1:1000	Epifluorescence
Tau	Synaptic Systems GmbH	314004	Guinea pig (polyclonal)	1:500	Epifluorescence
Anti-NeuN antibody, clone A60	Merck Millipore, Darmstadt, Germany	MAB377	Mouse (monoclonal)	1:100	Epifluorescence
Human Cadherin-13 antibody	R&D Systems	AF3264	Goat (polyclonal)	1:200	SIM

Bassoon	Synaptic Systems GmbH	114004	Guinea pig (polyclonal)	1:300	*d*STORM
Homer	Synaptic Systems GmbH	160 011	Mouse (monoclonal)	1:300	*d*STORM
Anti-Glucose Transporter GLUT3 antibody [EPR10508(N)] - N-terminal	Abcam	ab191071	Rabbit (monoclonal)	1:100	Epifluorescence SIM *d*STORM
Anti-Glucose Transporter GLUT3 antibody	Abcam	ab15311	Rabbit (polyclonal)	1:100	Epifluorescence
4',6-diamidino-2-phenylindole (DAPI)	Thermo Fisher Scientific	D1306		300 nM	Epifluorescence Confocal SIM *d*STORM

Table 6: List of secondary antibodies used in this study

Name	Manufacturer	Catalog#	Specificity	Dilution	Usage
Donkey anti-mouse IgG (H+L) ReadyProbes™ secondary antibody, Alexa Fluor 488	Thermo Fisher Scientific, Waltham, MA, USA	R37114	IgG (H&L)	1:400	Epifluorescence; Confocal; SIM
Donkey anti-rabbit IgG (H+L) highly cross-adsorbed secondary antibody, Alexa Fluor 488	Thermo Fisher Scientific	A21206	IgG (H&L)	1:400	Epifluorescence;
Donkey anti-rabbit IgG (H+L) highly cross-adsorbed secondary antibody, Alexa Fluor 555	Thermo Fisher Scientific	A31572	IgG (H&L)	1:400	Epifluorescence; Confocal; SIM
Donkey anti-goat IgG (H+L) cross-adsorbed secondary antibody, Alexa Fluor 555	Thermo Fisher Scientific	A21432	IgG (H&L)	1:400	Epifluorescence

Donkey anti-mouse IgG (H+L) highly cross-adsorbed secondary antibody, Alexa Fluor Plus 555	Thermo Fisher Scientific	A32773	IgG (H&L)	1:400	Epifluorescence
Goat anti-mouse IgG (H+L) cross-adsorbed secondary antibody, Alexa Fluor 532	Thermo Fisher Scientific	A-11002	IgG (H&L)	1:400	*d*STORM
Goat anti-rabbit IgG (H+L) cross-adsorbed secondary antibody, Alexa Fluor 532	Thermo Fisher Scientific	A-11009	IgG (H&L)	1:400	*d*STORM
Donkey anti-goat IgG (H+L) cross-adsorbed secondary antibody, Alexa Fluor 647	Thermo Fisher Scientific	A-21447	IgG (H&L)	1:400	SIM; *d*STORM
Alexa Fluor® 647 AffiniPure donkey anti-guinea pig IgG (H+L)	Jackson ImmunoResearch, West Grove, PA, USA	IR706-605-148	IgG (H&L)	1:400	*d*STORM
Goat anti-rabbit IgG-HRP	Santa Cruz Biotechnology Inc, Santa Cruz, CA, USA	sc-2054	IgG-HRP	1:7500	Western blot
HRP goat anti-mouse Ig	BD Biosciences, Franklin Lakes, NJ, USA	554002	IgG-HRP	1:1000	Western blot
IRDye® 680RD goat anti-rabbit IgG (H + L), 0.5 mg	LI-COR®, Bad Homburg, Germany	P/N 926-68071	IgG (H&L)	1:5000	Western blot
IRDye® 800CW goat anti-mouse IgG (H + L), 0.5 mg	LI-COR®	P/N 926-32210	IgG (H&L)	1:5000	Western blot

2.1.4 Material for molecular biology methods

Table 7: Material and equipment for RNA analysis

Materials and reagents	Components	Manufacturer
Lysis buffer (RNA isolation)	- RNA Protect Cell Reagent - DMEM/F12 1:1	Qiagen GmbH, Hilden, Germany Thermo Fisher Scientific, Waltham, MA, USA
Cell scrapers		Sarstedt, Nürnbrecht, Germany
Safe-lock tubes (1.5 mL)		Eppendorf, Hamburg, Germany
RNAprotect cell reagent		Qiagen GmbH
RNeasy plus mini kit	- gDNA Eliminator Mini Spin Columns - RNeasy Mini Spin Columns - Collection Tubes (1.5 mL and 2 mL) - Buffer RLT Plus - Buffer RW1 Buffer RPE (mixed with 4 volumes of ethanol 96–100%) - RNase-Free Water	Qiagen GmbH
Ethanol (70% and 96–100%)		AppliChem, Darmstadt, Germany
14.3 M β-mercaptoethanol (β-ME)		Sigma-Aldrich, St. Louis, MO, USA
Dnase I solution	70 µL RDD buffer + 10 µL DNase I	Qiagen GmbH
TissueLyser		Peqlab Biotechnologie GmbH, Erlangen, Germany
NanoDrop ND-1000		Peqlab Biotechnologie GmbH
5x iScript reaction mix		Bio-Rad Laboratories, München, Germany
iScript reverse transcriptase		Bio-Rad Laboratories
Nuclease-free water		Bio-Rad Laboratories
iQ™ SYBR® Green supermix		Bio-Rad Laboratories
ddH$_2$O		Merck Millipore, Darmstadt, Germany
thermal cycler CFX384		Bio-Rad Laboratories

Table 8: Material and equipment for protein analysis

Materials and reagents	Components	Manufacturer
Lysis buffer for Western blot analysis	- Radio-immunoprecipitation assay (RIPA) buffer	Sigma-Aldrich, St. Louis, MO, USA
	- Complete mini protease inhibitor cocktail – EDTA free tablets	Roche, Grenzach-Wyhlen, Germany
	- Phosphatase inhibitor cocktail tablets	Roche
Cell scrapers		Sarstedt, Nürnbrecht, Germany
Safe-lock tubes (2 mL)		Eppendorf, Hamburg, Germany
Precision Red advanced protein assay reagent		Biomol GmbH, Hamburg, Germany
96-well plate		Sarstedt
Spectrophotometer		Thermo Fisher Scientific, Waltham, MA, USA
Multiskan Spectrum software		Thermo Fisher Scientific
External chamber electrophoresis buffer (1x)	MOPS SDS buffer (20x) diluted with ddH$_2$O	Thermo Fisher Scientific
Inner chamber electrophoresis buffer	External chamber buffer with 0.25% antioxidant	Thermo Fisher Scientific
Transfer buffer (1x)	Transfer buffer (20x) - 10% methanol - 0.1% antioxidant - in ddH$_2$O	Thermo Fisher Scientific Sigma-Aldrich
1 x PBS	- 10x PBS diluted with distilled water	Lonza, Köln, Germany
PBS-T	- 1x PBS - 0.1% Tween-20	Sigma-Aldrich
Odyssey blocking solution	Odyssey blocking buffer: PBS-T 1:1	LI-COR®, Bad Homburg, Germany
NuPAGE 4-12% Bis-Tris gel		Thermo Fisher Scientific
NuPAGE LDS sample buffer 4x		Thermo Fisher Scientific
NuPAGE reducing agent 10x		Thermo Fisher Scientific
ddH$_2$O		Merck Millipore, Darmstadt, Germany
XCell sure lock electrophoresis chamber		Thermo Fisher Scientific
Thermomixer		Eppendorf
Vortexer		Eppendorf
Chameleon® duo pre-stained protein ladder		LI-COR®
Electrophoresis power supply (400V-400mA)		Consort, Turnhout, Belgium
Sponge pads		Thermo Fisher Scientific

Nitrocellulose membrane with filter papers		Thermo Fisher Scientific
Tween-20		Sigma-Aldrich

2.1.5 Oligonucleotides for RT-PCR and qRT-PCR

Table 9:The CytoTune™ 2.0 reprogramming vectors

CytoTune™ Sendai vector	Factor	GenBank ID
CytoTune™ 2.0 KOS	Human Klf4 Human Oct3/4 Human Sox2	BC029923.1 NM_002701.4 NM_003106.2
CytoTune™ 2.0 hc-Myc	Human c-Myc	K02276.1
CytoTune™ 2.0 hKlf4	Human Klf4	BC029923.1

Table 10: Primer SeV detection

Target	Sequence (5´→3)	Product size	Manufacturer
SeV	Forward: GGATCACTAGGTGATATCGAGC Reverse: ACCAGACAAGAGTTTAAGAGATATGTATC	181 bp	Sigma-Aldrich, St. Louis, MO, USA
KOS	Forward: ATGCACCGCTACGACGTGAGCGC Reverse: ACCTTGACAATCCTGATGTGG	528 bp	Sigma-Aldrich
Klf4	Forward: TTCCTGCATGCCAGAGGAGCCC Reverse: AATGTATCGAAGGTGCTCAA	410 bp	Sigma-Aldrich
c-Myc	Forward: TAACTGACTAGCAGGCTTGTCG Reverse: TCCACATACAGTCCTGGATGATGATG	532 bp	Sigma-Aldrich

Table 11: Oligonucleotides for qRT-PCR

Target	Sequence (5´→3)	Manufacturer
CDH13	Forward: AGAGATGTTGGCAAGGTAGTCGA Reverse: GAACTTGGACCTTTCTGGCCT	Sigma-Aldrich, St. Louis, MO, USA
TPH2	Forward: ACGGAGAGGGTTTTCCCTG Reverse: TGCCAAGTAGCTGATGCTCT	Sigma-Aldrich
GAD1	Forward: CAAACATTTATCAACATGCGCTTC Reverse: CTATGACACTGGAGACAAGGC	Sigma-Aldrich
TH	Forward: CCTGGTTCCCAAGAAAAGTGTCAGA Reverse: CCCTTCAGCGTGGTGTAGACCTC	Sigma-Aldrich
SLC2A3	Forward: GGGTATGATCGGCTCCTTTT Reverse: GCATTTCAACCGACTTAGCTACT	Sigma-Aldrich
GAPDH	N/A	Qiagen, Hilden, Germany (Hs_GAPDH_1_SG QuantiTect Primer Assay)
ACTB	N/A	Qiagen (Hs_ACTB_1_SG QuantiTect Primer Assay (QT00095431))
UBC	N/A	Qiagen (Hs_UBC_1_SG QuantiTect Primer Assay)

2.1.6 Cell culture Equipment

Table 12: Cell culture equipment in a stem cell laboratory

Product	Manufacturer	Cat#
B Braun™ CUTFIX disposable scalpels (B Braun™ 5518016)	Thermo Fisher Scientific, Waltham, MA, USA	10242611
Insulin syringe, BD Micro-Fine™	BD Bioscience, Franklin Lakes, NJ, USA	324824
Parafilm® M all-purpose laboratory film	Bemis, Neenah, WI, USA	Parafilm® M PM996
Disposable tweezers	Fuhrmann GmbH, Much, Germany	36279-3
Disposable tweezers, ratiomed sterile/ transparent 12.5 cm	Megro GmbH, Wesel, Germany	MEG 126300.1

Round coverslips,12 mm,1x100 items	Hartenstein GmbH, Würzburg, Germany	DKR1
Nunc™ Thermanox™ coverglass, round (13mm diameter)	Thermo Fisher Scientific	174950
Cell culture multiwell plate, 48 well, PS, clear, Cellstar®, TC, lid with condensation rings, sterile, single packed	Greiner Bio-one, Kremsmünster, Austria	677180
Cell culture multiwell plate, 24 well, PS, clear, Cellstar®, TC, lid with condensation rings, sterile, single packed	Greiner Bio-one	662160
Cell culture multiwell plate, 12 well, PS, clear, Cellstar®, TC, lid with condensation rings, sterile, single packed	Greiner Bio-one	665180
Cell culture multiwell plate, 6 well, PS, clear, Cellstar®, TC, lid with condensation rings, sterile, single packed	Greiner Bio-one	657160
Costar® 6-well clear flat bottom ultra-low attachment multiple well plates, individually wrapped, sterile	Corning, NY, USA	3471
TC Flask T25, Cell+, vented cap	Sarstedt, Nürnbrecht, Germany	83.3910.302
TC Flask T75, Cell+, vented cap	Sarstedt, Nürnbrecht	83.3911.302
TC Dish 100, standard	Sarstedt, Nürnbrecht	83.3902
TC Dish 100, Cell+	Sarstedt, Nürnbrecht	83.3902.300
Biosphere® tip 200µL	Sarstedt, Nürnbrecht	70.760.202
Aspiration pipette 2mL	Sarstedt, Nürnbrecht	86.1252.011
5 mL serological pipet, sterile, individually wrapped	Sarstedt, Nürnbrecht	86.1253.001
10 mL serological pipet, sterile, individually wrapped	Sarstedt, Nürnbrecht	86.1254.001
25 mL serological pipet, sterile, individually wrapped	Sarstedt, Nürnbrecht	86.1685.001
50 mL serological pipet, sterile, individually wrapped	Sarstedt, Nürnbrecht	86.1256.001
Corning® BioCoat™ poly-D-lysine/laminin 8-well culture slide, 4/pack, 12/case	Corning	354688
Nunc™ Lab-Tek™ II: 8-well chambered coverglass w/ non-removable wells	Thermo Fisher Scientific	155409
µ-Dish 35 mm, high glass bottom	IBIDI, Martinsried, Germany	81158
15 mL cellstar centrifuge tube, sterile, DNAse/RNase free (case of 1000 tubes)	Greiner Bio-one	188271
Tube 50mL, 114x28mm, PP	Sarstedt	62.547.254
Disposal bag 600x780mm	Sarstedt	86.1200
Disposal bag 200x300mm	Hartenstein GmbH	VB20
Foliodress® mask comfort	Hartmann, Wiener Neudorf, Austria	9925372
Disposable arm protection	Hygostar, Franz Mensch GmbH, Buchloe, Germany	28301

Cell scraper 16cm 2-pos.-blade	Sarstedt	83.1832
Filtropur V25, 250mL, 0.2µm	Sarstedt	83.3940.001
Steriflip™ sterile disposable vacuum filter units	Merck Millipore, Darmstadt, Germany	SCGP00525
Stericup™ sterile vacuum filter units	Merck Millipore	SCVPU02RE
4-well Nunc™ cell culture vessel	Thermo Fisher Scientific	176740
Cellometer disposable counting chambers: SD100 Slides (2 counting chambers per slide)	Nexcelom Biosciences via Peqlab Biotechnologie, Erlangen, Germany	CHT4-SD100-002
CryoPure vessel 1.0mL white	Sarstedt	72.377
Eppendorf safe-lock tubes, 1.5 mL, Eppendorf Quality™, transparent, 1000 tubes	Eppendorf, Hamburg, Germany	0030120086
Eppendorf safe-lock tubes, 2 mL, Eppendorf Quality™, transparent, 1000 tubes	Eppendorf	0030120094

Table 13: Technical equipment in a stem cell laboratory

Equipment	Manufacturer
Laboklav Eco	Panasonic, Kadoma, Zimbabwe
Cell culture hood (ClassII Biological Safety Cabin)	NuAire, Eurasburg, Germany
Cellometer auto T4 bright field cell counter	Nexcelom Biosciences via Peqlab Biotechnologie, Erlangen, Germany
Centrifuge (Rotofix 32 A)	Hettich Zentrifugen, Tuttlingen, Germany
CO_2 incubator (C 200)	Labotect, Göttingen, Germany
MCO-170AIC-PE IncuSafe CO2 incubator	Panasonic
Motorized inverted system microscope IX81 X-Cite fluorescence illuminator XM10 camera	Olympus, Hamburg, Germany
EVOS™ XL core configured microscope with mechanical stage	Novus Biologicals, Nordenstadt, Germany
FluoView FV1000 confocal microscope	Olympus
Inverted structured illumination microscope (SIM)	Zeiss ELYRA, Oberkochen, Germany
Direct stochastic optical reconstruction microscope *(dSTORM):* wide-field setup for localization microscopy Diode laser with a wavelength of 640 nm (iBeam smart) Diode-pumped solid-state laser with a wavelength of 532 nm (gem, maximum power of 500 mW) Bandpass filters High numerical oil-immersion objective (alpha Plan-Apochromat 100x/1,46 Oil DIC)	 TOPTICA Photonics, Gräfelfing, Germany Carl Zeiss Microscopy, Jena, Germany Laser Quantum, Stockport, United Kingdom Semrock, Rochester, NY, USA Carl Zeiss Microscopy

Inverted fluorescence microscope (Zeiss Axio Observer.Z1) Autofocus system (Definite Focus) Dichroic beam splitter Dichroic mirror EMCCD cameras (iXon Ultra 897) detection filters	Carl Zeiss Microscopy Semrock Chroma, Bellows Falls, VT, USA Andor Technology, Belfast, United Kingdom Semrock
Water bath (JB Aqua 12)	Grant Instruments, Cambridge, United Kingdom
Vacuum pumpVacusafe	Integra Biosciences, Biebertal, Germany
Flow cytometer BD FACSCanto™ II	BD Biosciences, San Jose, CA, USA

2.1.7 Software

Table 14: Software used in this thesis

Software	Usage	Manufacturer
Microsoft Excel 2016	Quantifications and analyses	Microsoft Corporation, Redmond, WA, USA
GraphPad Prism 8	Statistical analysis and data illustration	GraphPad Software, San Diego, CA, USA
Image Studio™ Lite 5.2	Western blot quantification	LI-COR®, Bad Homburg, Germany
BIO-1D analysis software	Western Blot detection and analysis	Vilber Lourmat Eberhardzell, Germany
ImageJ 1.52e	Neuronal subtype specification	National Institutes of Health (NIH), Bethesda, MD, USA (Wayne Rasband)
LinReg 11.1	RNA analyses	Jan Ruijter (Academic Medical Center Amsterdam, Netherlands)
qBase+ 3.0	RNA analyses	Biogazelle (Prof. Jo Vandesompele, Dr. Jan Hellemans, Zwijnaarde, Belgium)
NanoDrop ND-1000 3.7	RNA analyses	Peqlab Biotechnologie GmbH, Erlangen, Germany
CFX-Manager 3.0	RNA analyses	Bio-Rad Laboratories, München, Germany
CellSens V2.3	Immunofluorescence analyses	Olympus, Leinfelden-Echterdingen, Germany

Fluoview, version 4.1.a	Confocal microscopy	Olympus
Imaris 9.3	SIM	Bitplane, Zurich, Switzerland
ZEN imaging software 3.0	SIM	Zeiss ELYRA, Oberkochen, Germany
ThunderSTORM (ImageJ plug-in)	*d*STORM	National Institutes of Health (NIH)
ChAS 4.0	Karyotypical analysis	Thermo Fisher Scientific, Waltham, MA, USA
BD software for BD FACSCanto™ II flow cytometer	Flow cytometry	BD Biosciences, San Jose, CA, USA

2.2 Methods

2.2.1 Cells

A written consent was signed by all study participants and the study was approved by the scientific ethical committee (96/11). Primary human fibroblasts and human iPSCs were used as cell culture models. For this purpose, dermal fibroblasts isolated from healthy persons as well as ADHD patients were reprogrammed into induced stem cells as described in Section 2.2.2.2 and Section 2.2.2.3. Stocks of the original virus-induced stem cells ("mother plates") and of mother plate-derived and established iPSC lines are stored in the liquid nitrogen storage tanks of the Laboratory of Translational Neuroscience in the Center of Mental Health for future studies.

One human control iPSC line was kindly provided by Prof. F. Edenhofer (Department of Genomics, Stem Cell Biology and Regenerative Medicine, Institute of Molecular Biology & CMBI, Leopold Franzens-University Innsbruck) at the beginning of our study. Displaying a high reprogramming efficiency, NHDFs serve as control group and tool to establish protocols. Also reprogrammed by a SeV, this cell line is comparable to our home-made cell lines.

2.2.2 Cell culture methods

2.2.2.1 Cell culture laboratory

All experiments involving handling of the cells were performed under sterile conditions in a structurally separated cell culture laboratory (biosecurity category S2). Inside this laboratory, a high degree of attentive working routine was essential, and the operative needed to wear a dedicated S2 laboratory coat, a face mask and protective sleeves. All reagents and materials were regularly cleaned with ethanol (70%), and the laboratory equipment, such as the inverted light microscope was wiped with Mycoplasma-Off™ Wipes before and after every use. Cells

were cultured in an incubator at 37°C in 5% CO_2 and handled under a specific cell culture laminar flow hood to guarantee aseptic work. Before and after use, the hood was cleaned with 70% ethanol and surfaces were irradiated with ultraviolet (UV) light. Biological contaminations were avoided by using this cell-biological equipment and by following good aseptic technique.

2.2.2.2 Isolation of fibroblasts from a healthy person and ADHD patients

Dermal fibroblasts were isolated from a skin biopsy of a clinically diagnosed 51-year-old female ADHD patient carrying a duplication (*SLC2A3* copy number state (CN)=3) and a 48-year-old female ADHD patient carrying a deletion of *SLC2A3* (*SLC2A3* CN=1). Additionally, skin fibroblasts of a 55-year-old female healthy person displaying a normal genotype (*SLC2A3* CN=2) served as a control cell line. For this purpose, human dermal skin obtained by punch biopsy was transferred to an Eppendorf safe-lock tube (1.5 mL) in CTS™ phosphate-buffered saline with calcium and magnesium (DPBS+; Thermo Fisher Scientific) plus gentamicin (1μL/mL). Stored at 4°C for up to 36 h, the skin was transferred to a well of a 4-well Nunc™ cell culture vessel for mechanical disaggregation. Washed with 500 μL DPBS+, the fat part was removed using a scalpel (Thermo Fisher Scientific). Washed with DPBS+ twice, the samples were additionally washed with phosphate-buffered saline without calcium and magnesium (DPBS; Thermo Fisher Scientific) and incubated at 4°C for 16-18 h in 2 mL dispase-II solution (2.4 U/mL) (PAN Biotech). The samples were washed with DPBS+ once. After removing epidermal tissue, each sample was washed with DPBS+ once, transferred to a 15 mL falcon tube and treated with 5 mL of a collagenase NB 4 standard grade solution (500 U/mL) (Amsbio) at 37°C for 45 min. The samples were centrifuged twice at 1200 rpm for 5 min, the supernatant was removed and the samples were resuspended and transferred into a T25 adherent tissue flask (Sarstedt) in fibroblast growth medium composed of Dulbecco's modified eagle's medium (DMEM; PAN-Biotech), 10% fetal bovine serum (FBS; Thermo Fisher Scientific), 1 μg/mL gentamicin (Thermo Fisher Scientific), 1% MEM non-essential amino acid solution (100x) (NEAA; PAN-Biotech), 100 μM β-mercaptoethanol (Gibco) and cultured at 37°C in 5% CO_2. Cells were fed every 3 days and after monolayer formation, primary fibroblasts were passaged using accutase cell detachment solution (accutase, Merk Millipore) every 3-4 days in a ratio of 1:8 and cultured in a T75 adherent tissue flask (Sarstedt). Accutase is known as a cell detachment solution of proteolytic and collagenolytic enzymes.

2.2.2.3 Reprogramming of primary fibroblasts into human iPSCs using the CytoTune-iPS Reprogramming Kit 2.0

Primary fibroblasts (passage 3) of a healthy donor with a single copy of *SLC2A3* as well as of two ADHD patients carrying either a duplication or a deletion of *SLC2A3* were reprogrammed

into human iPSCs using the CytoTune-iPS Reprogramming Kit 2.0 (Thermo Fisher Scientific) as previously described (Jansch et al 2018). For this purpose, 75,000 fibroblasts of each genotype were seeded in fibroblast growth medium into 12-well plates. The next day, cells were transduced with the non-integrative SeV to transiently overexpress OCT3/4, SOX2, cMYC and KLF4. 24 h later, the virus was removed by changing the medium and cells were fed every other day using fresh fibroblast growth medium. A few days after infection, a change in the cell morphology of adult dermal fibroblasts was observed, which persisted until stem cell-like colonies formed. On day 6, irradiated MEFs (Ambio) were thawed, centrifuged at 1000 rpm for 3 min, resuspended in fibroblast growth medium and seeded in a 6-well plate (400,000 MEFs/well). The next day, transduced fibroblasts were detached using 300 µL/well accutase and incubated for 3-5 min at 37°C. 2 mL/12-well of DMEM/F12 were added to stop the activity of this cell detachment reagent, the cells were transferred to a falcon tube with 2 mL DMEM/F12 and centrifuged at 800 rpm for 3 min, the supernatant was discarded, and 1 mL of fresh fibroblast growth medium was added to the cells. Finally, each well full of reprogrammed cells was seeded in one well of a 6-well plate covered with MEFs in fibroblast growth medium with 10 µM ROCK inhibitor (RI; Miltenyi Biotech). The next day, the medium was switched to reprogramming medium (KnockOut™ DMEM/F12 (Thermo Fisher Scientific), 20% KnockOut™ serum replacement (Thermo Fisher Scientific), 1 mM L-glutamine (Thermo Fisher Scientific), 1% NEAA, 100 µM 2-mercaptoethanol, 10 ng/mL bFGF recombinant human protein (Thermo Fisher Scientific) and 200 µM L-ascorbic acid (Sigma-Aldrich). From then on, the culture medium was replaced every day and the culture vessels were monitored daily for the emergence of human iPSC colonies. Since the appearing colonies grew too dense on the cell culture vessel, the cells had to be passaged in a ratio 1:3. For this purpose, cells were washed with 500 µL DPBS once and 500 µL accutase were added and incubated for 3-5 min at 37°C. 2 mL of DMEM/F12 were added to the well to stop the accutase activity, the solution was transferred to a 15 mL falcon tube and centrifuged at 800 rpm for 3 min. The supernatant was removed, the cell pellet was resuspended in 1 mL fibroblast growth medium and 333 µL of the cell suspension was transferred to a fresh MEF-coated 6-well plate. The remaining cell solution was centrifuged, and cells were frozen using KnockOut™ serum replacement supplemented with 10% DMSO (Sigma-Aldrich). Colonies with hESC-like appearance appeared in a range of 26 to 47 days post infection and each colony was then manually transferred to a well of a Matrigel (Corning)-coated 48-well plate in StemMACS™ iPS-Brew XF (Miltenyi Biotec) supplemented with 10 µM RI. For this purpose, reprogrammed colonies were labelled with a pluripotency-associated marker according to the life staining protocol described in Section 2.2.4.1. Colonies that had to be picked were marked on the bottom of the culture dish and at least 10 distinct colonies were picked and expended in separate 48-, 24-,12- or 6-well Matrigel-

coated culture plates. Single colonies were lifted using a 25 gauge 1½ inch needle (BD Bioscience) by carefully surrounding the colony and lifting it up. The swimming colony was then transferred to the Matrigel-coated 48-well using a 200 μL pipette. 48 h later, the medium was replaced by with fresh reprogramming medium to allow the colonies to attach to the culture plate. After that, the medium was changed every day. Additionally, the remaining cells of the original reprogramming plate were frozen and stored in the liquid nitrogen storage tanks. Once the cells in the 48-well were fully confluent, the reprogrammed cells were detached using accutase as described before, centrifuged at 800 rpm for 3 min, and transferred to a 12-well and finally to a 6-well of a respective Matrigel-coated plate in StemMACS™ iPS-Brew XF supplemented with 10 μM RI. The reprogrammed colonies were treated like normal human ESC colonies and passaged, expanded and maintained using standard culture procedures until frozen cells from two 60-mm plates were obtained and characterization tests proved the generated cells to be fully reprogrammed human iPSCs. For long-term culturing human reprogrammed colonies as well as established iPSCs were kept in StemMACS™ iPS-Brew XF in a 6-well format with a daily change of StemMACS™ iPS-Brew XF. Cells were split every 3 to 4 days using accutase and frozen using KnockOut™ serum replacement supplemented with 10% DMSO to create a stock of cells with early passages. The time needed to derive vector-free iPSCs varies depending on culture and passage conditions and takes about 1–2 months after gene transduction.
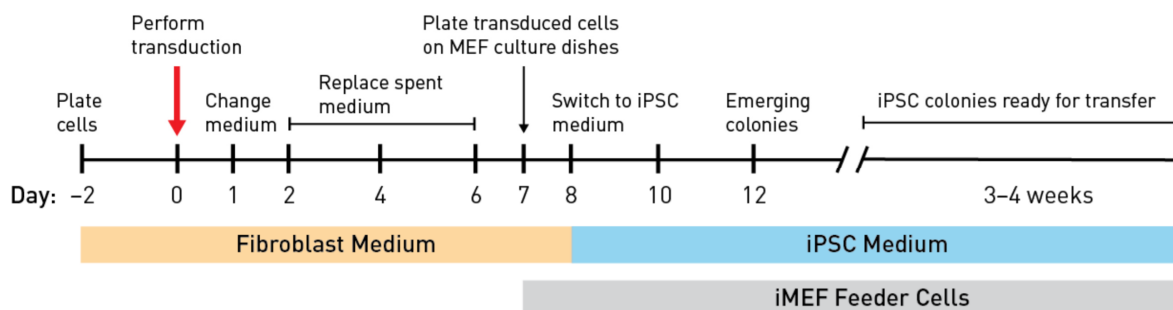

Figure 9: Timeline for reprogramming technology via SeV.

Adult dermal fibroblasts were reprogrammed using the CytoTune-iPS Reprogramming Kit 2.0 (Thermo Fisher Scientific) according to the manufacturer's instructions. Figure was adapted from Thermo Fisher Scientific: https://assets.thermofisher.com/TFS-Assets/LSG/manuals/cytotune_ips_2_0_sendai_reprog_kit_man.pdf.

2.2.2.4 Culture and passaging of human induced pluripotent stem cells

Frozen iPSCs were taken from the -196°C liquid nitrogen storage tank to be thawed at 37°C. Still containing small pieces of ice, the sample was transferred into a falcon tube (Sarstedt)

with fresh DMEM/F12. After centrifugation at 800 rpm for 3 min, the supernatant was discarded, and 1.5 mL of fresh StemMACS™ iPS-Brew XF was carefully pipetted to the cell pellet without separating the stem cell clumps and therefore avoiding the separation into single cells. The whole cell suspension was then transferred into a Matrigel-coated well of a 6-well plate in StemMACS™ iPS-Brew XF supplemented with 10 µM RI and the cells were kept at 37°C, 5% CO_2 in an incubator. Routinely, the stem cell culture medium was changed every day and cell densities were checked under an inverted light microscope (EVOS). Once human iPSC colonies reached 70-80% confluency, they were split in a ratio of 1:10 according to the following protocol. After washing the human iPSCs with 1 mL 1x PBS, 500 µL accutase were added to the cells and incubated for 3-5 min at 37°C. PBS was used to wash away any rest of Mg^{2+} from the medium to avoid interference with the accutase. In this case, accutase was used to detach the cells from the well-surface where they adhere via cell adhesion molecules and integrins. After 3-5 min of incubation, human iPSCs detached from the surface and the cell culture plate was carefully transferred to the bench to avoid breaking up the cell colony fragments. Since longer incubation in accutase would compromise the cellular integrity, 2 mL of DMEM/F12 were added to the well to stop the activity of this cell detachment reagent. Using a 5 mL pipette, cells were transferred to a falcon tube with 2 mL DMEM/F12 and centrifuged at 800 rpm for 3 min, the supernatant was discarded, and 1 mL of fresh StemMACS™ iPS-Brew XF was added to the cells. Human iPSCs were usually split at a 1:10 ratio, therefore 100 µL of the cell suspension were transferred into a well of a Matrigel-coated 6-well plate that had been washed once with 1x PBS (1 mL) and contained 1.5 mL of fresh StemMACS™ iPS-Brew XF supplemented with 1 µL/mL RI. From this time, cells needed approximately 3-4 days to reach confluency again.

2.2.2.5 Coating strategies for human iPSC cultures

Corning Matrigel is a widely used coating strategy for human iPSC cultures. Extracted from the Engelbreth-Holm-Swarm (EHS) mouse sarcoma, a tumour rich in extracellular matrix proteins, Matrigel is a reconstituted basement membrane preparation. Once isolated, it is approximately 60% laminin, 30% collagen IV and 8% entactin. Heparan sulfate proteoglycan (perlecan), TGF-β, epidermal growth factor, insulin-like growth factor, FGF, tissue plasminogen activator, metalloproteinases and other growth factors naturally occur in the EHS tumour and are therefore components of the Matrigel matrix. Each Matrigel vial is delivered with a specific dilution factor which indicates the amount of Matrigel that should be diluted in 25 mL of DMEM/F12 to coat cell culture vessels. The Matrigel solution is then pipetted to the respective vessel and incubated for 1 h at room temperature (RT). After the incubation period, the vessels were sealed using Parafilm (Bemis GmbH) and stored at 4°C for up to 4 weeks. Before use,

the Matrigel solution was removed and the culture vessel was washed once with DPBS. In case of a well plate, wells that were not needed right away were filled with DPBS for later use.

For differentiation, PO (Sigma-Aldrich) and LAM (BioLamina)-coated plates were prepared. Here, PO was diluted in DBPS in a ratio 1:5 overnight at RT. The next day, the cell culture vessel was washed 3 times for 5 min using DPBS. Finally, a LAM solution in DBPS (1:100) was applied to the vessel and incubated for 2 h at 37°C. After incubation time, the vessels were washed 3 times for 5 min using DPBS, then either immediately used or sealed with Parafilm and stored at 4°C for up to 4 weeks.

For all coating strategies conducted in this study, the necessary amounts of coating solution can be seen in Table 15.

Table 15: Coating strategies

Cell culture vessel	Coating solution (µL)
24-well Plate	250*
12-well Plate	500*
6-well Plate	1000*
10 cm dish	5000

*necessary volume / well

2.2.2.6 Generation of 5-HT specific and catecholaminergic neurons using a specific neuronal differentiation protocol

To differentiate human iPSCs into a mixed neuronal culture of 5-HT specific and catecholaminergic neurons, iPSC colonies maintained on Matrigel-coated 6-well plates in StemMACS™ iPS-Brew XF supplemented with 10 µM RI were neuralized according to a hindbrain differentiation protocol established in this doctoral thesis.

For this purpose, human iPSCs were washed with 1 mL PBS and incubated using 500 µL accutase for 3-5 min at 37°C. The accutase activity was stopped using 4 mL DMEM/F12 and the cell suspension was centrifuged at 800 rpm for 3 min. The cell pellet was carefully resuspended in neural induction medium (NIM: DMEM/F12:Neurobasal (1:1), 1× N2 supplement (Thermo Fisher Scientific), 1× B27 supplement (Thermo Fisher Scientific), 1.4 µM CHIR99021 (Axon Medchem), 2 µM DMH1 (Tocris Bioscience) and 2 µM SB431542 (Miltenyi Biotec) and the cell suspension was transferred to one 6-well of a Costar® 6-well clear flat bottom ultra-low attachment multiple well plate (Corning) to generate EBs which contain rostral hindbrain progenitors. Neural induction medium was changed every other day and 5-7 days later mid-sized, free-floating EBs were transferred to PO/LAM-coated plates in neural

progenitor cell (NPC) medium, namely NIM supplemented with SHH C25II (1000 ng/mL; R&D) for ventralization of rostral hindbrain progenitors. After 1 week, rosette-forming EBs were manually isolated and plated on PO/LAM-coated plates in NPC medium containing SHH C25II (1000 ng/mL) and FGF4 (10 ng/mL; Peprotech) to specify the serotonergic fate of those progenitors for one further week. Meanwhile, the medium was changed every other day. After 3 weeks of differentiation, NPCs showing the morphology of 5-HT specific progenitors were manually removed using a 1000 µL pipette, dissociated using accutase for 3 min and finally plated at lower densities for neuronal differentiation (for 4 to 8 weeks) in neuronal maturation medium (NMM) containing brain-derived neurotrophic factor (20 ng/mL, Peprotech), glial cell–derived neurotrophic factor (20ng/mL, Peprotech), dibutyrl-cyclicAMP (1 mM, Sigma-Aldrich), L-ascorbic acid (200nM, Sigma-Aldrich) and LAM (1 µg/mL) in DMEM-F12/Neurobasal+N2+B27.

2.2.3 Molecular biology methods: RNA analyses

2.2.3.1 Cell lysis for RNA isolation

RNAprotect cell reagent was added directly to cells in culture medium, to provide instantaneous RNA stabilization. For this purpose, the cell medium was removed, and a specific amount of the lysis solution (consisting of 5 volumes of RNAprotect cell reagent and 1 volume of cold proliferation culture medium) was added to each cell culture vessel as listed in Table 16. After an incubation time of 2 min, cells were scraped and transferred into a 1.5 mL safe-lock tube (Eppendorf). After stabilization in RNAprotect cell reagent, cells could be stored at -20°C with the cellular RNA remaining intact and undegraded.

Table 16: Amount of RNAprotect cell reagent used in this study

Cell culture vessel	RNAprotect cell reagent (µL)
24-well Plate	100*
12-well Plate	250*
6-well Plate	500*
10 cm dish	1500

*necessary volume / well

2.2.3.2 RNA extraction using RNeasy® Protect Cell Mini Kit

Total RNA was purified using the RNeasy® Protect Cell Mini Kit. For this purpose, cells stabilized in RNAprotect cell reagent were thawed and centrifuged for 5 min at 7600 rpm. The Buffer RLT Plus inactivates RNases to avoid RNA degradation and was used to lyse and homogenize the pellet as described in the following. After centrifugation, the supernatant was removed, 600 µL of the Buffer RLT plus supplemented with ß-ME (10 µL per 1 mL buffer) was

added to reduce RNA degradation during RNA purification. Complete disruption of plasma membranes of cells and organelles was achieved by vortexing and homogenization using the TissueLyser at 20 hz for 30 s. All spin column centrifugation steps, described in the following, were performed at 20–25°C at 10000 rpm in a standard microcentrifuge. The homogenized lysate was transferred to a gDNA eliminator spin column and centrifuged for 30 s. After centrifugation, 1 volume of 70% ethanol was added to the flow-through that contained the RNA, and the solution was applied to a RNeasy spin column and centrifuged again at 10000 rpm for 15 s. This step was repeated twice. Then, 700 µL of the washing buffer RW1 were added to the RNeasy spin column, centrifuged for 15 s and the flow-through was discarded. To remove any rests of genomic DNA, 80 µL of the DNase I solution were pipetted to each tube and incubated for 15 min. Afterwards, 350 µL of the RW1 buffer were added and samples were centrifuged for 30 s. 500 µl of Buffer RPE were added twice to the RNeasy spin column and the samples were first centrifuged for 15 s and then for 2 min to wash the spin column membrane. High-quality RNA was then eluted in 40 µL of RNase-free water. For this purpose, the RNeasy spin column was placed in a new 1.5 mL collection tube, the respective amount of RNase-free water was added directly to the spin column membrane and the samples were centrifuged again for 1 min.

2.2.3.3 Quantification quality control of isolated RNA

The spectrophotometer NanoDrop ND1000 was used to quantify the isolated RNA by measuring the optical density (OD) at 260 nm, considering a concentration of 40 ng/µL at an OD_{260} of 1. Furthermore, contamination through proteins and the presence of other impurities could be detected by the OD_{260}/OD_{280} and OD_{260}/OD_{230} ratios. A ratio of approximately 2.0 was considered as highly pure for RNA.

2.2.3.4 Complementary desoxyribonucleic acid (cDNA) synthesis

The complementary DNA (cDNA) synthesis was conducted using the iScript™ cDNA synthesis kit. This kit consists of a 5x iScript reaction mix, nuclease-free water and an iScript Moloney Murine Leukemia Virus (MMLV)-derived modified reverse transcriptase (RT), an RNA-dependent DNA polymerase with ribonuclease (RNase) H+ activity which catalyses the reaction in which cDNA will be synthesized from a mRNA template. 1000 ng of isolated total RNA were used for the cDNA synthesis. The reaction mix was set up to a final volume of 20 µL. Next to the samples, controls without RT (RT-controls), as well as negative controls without RNA, were used to reveal contaminations. The cDNA synthesis reaction was performed in 3 steps (5 min: 25 °C, 30 min: 42 °C, 3 min: 85 °C) using an automated thermocycler. The obtained cDNA was diluted 1:5 in 1x Tris-EDTA (TE) buffer and aliquoted for storage at -20°C.

2.2.3.5 Reverse transcription polymerase chain reaction (RT-PCR)

To prove that the CytoTune™ 2.0 reprogramming vectors and transgenes (Table 11) had been eliminated from the cells, reverse transcription polymerase chain reaction (RT-PCR) was performed. RT-PCR was carried out using 10 µL of cDNA from the reverse transcription reaction (Section 2.2.3.4) to detect the SeV genome and transgenes in cells reprogrammed using the CytoTune™ 2.0 Sendai reprogramming vectors. RT-PCR primer sequences and the expected product sizes are listed in Table 12. PCR products were analysed using 2% agarose gel electrophoresis.

2.2.3.6 Quantitative real-time polymerase chain reaction (qRT-PCR)

In this study, qRT-PCR was conducted to analyse and compare the expression level of *SLC2A3* in control and patient fibroblasts, iPSCs as well as iPSC-derived neurons. Furthermore, to analyse the expression of specific markers of the different neuronal subtypes gained by the established protocol described in section 2.2.2.6, mRNA expression levels of *TPH2*, *TH* and *GAD1* were compared in control and patient human iPSC-derived neurons. The iQ™ SYBR® Green Supermix from BioRad was used, containing the fluorescence stain SYBR, i*Taq*™ DNA polymerase, reaction buffer with dNTPs, magnesium chloride and stabilizers. SYBR green, an asymmetrical cyanine dye used as a nucleic acid stain, bound to the new synthesized DNA strands, and in every cycle the fluorescence increased proportional to the amount of new synthesized DNA. The number of cycles needed to reach the fluorescence threshold is presented by the quantification cycle (C_q) value. For all conducted qRT-PCRs, samples were tested in triplicates using 384-well plates. All PCRs were run in the thermal cycler CFX384 controlled by the software CFX manager 3.0. For each qRT-PCR experiment, *GAPDH*, *ACTB* and *UBC* were used as reference genes for normalization of the data and qRT-PCR data analysis was done using the programs CFX-Manager 3.0, Microsoft Excel 2016, LinReg and qBase+. C_q values from CFX manager 3.0 imported into Microsoft Excel 2016 were formatted for further analyses via LinReg and QBase. The software LinReg allows the calculation of the amplification efficiency per well from a slope of the amplification curve in the exponential phase. A PCR efficiency of 100% illustrates a duplication of the amount of amplicon in each cycle (E=2), whereas a value of 1 means no amplification. Finally, an average amplification efficiency for each amplicon was calculated. Subsequently, the software qBase+ was used to process the data output and to calculate normalized gene expression values, considering the efficiency values provided by LinReg software as well as using the most stably expressed reference genes to normalize the data.

2.2.4 Molecular biology methods: Protein analyses

2.2.4.1 Cell-staining via immunofluorescence

In this thesis, IF staining of markers against neuronal progenitors and neuronal subtypes facilitated the characterization of the neuronal cell culture models that had been developed during the establishment of a differentiation process of human iPSCs into specific neuronal subtypes. Furthermore, this method helped to assess the distribution of GLUT3 in human iPSCs as well as in iPSC-derived neurons and with the use of synaptic markers, such as Bassoon and Homer, enabled the identification of pre- and postsynaptic structures in neurons.

For this purpose, half of the culture medium was removed and an equal amount of 4% PFA was applied to the cells for pre-fixation for 10 min at RT. In the following, the solution was removed from the cells completely and a specific amount of 4% PFA according to Table 17 was added to the cells and incubated for 15 min at RT. This step was necessary to retain cell morphology and the location of all cellular proteins. After washing with DPBS 1x, wells were incubated in a blocking solution for 45 min at RT to prevent unspecific binding of the antibodies. Permeabilization and blocking was done in one step using 0.1% Triton X-100, 10% FBS, and 1% BSA in DPBS. However, in case of the visualization of the surface markers TRA-1-60 and SSEA4 and the transporter SERT as well as of the labelling of the extracellular domain of GLUT3, no permeabilization was performed and thus the blocking solution was prepared without using 0.1% Triton X-100. Samples were incubated with primary antibodies overnight at 4°C according to the antibody dilutions listed in Table 7. The following day, cells were washed with DPBS 1X and incubated in secondary antibody for 1 h in darkness. Secondary antibodies used in this study can be seen in Table 8. To visualise the cell nuclei, a counterstaining with 4', 6-diamidino-2-phenylindole (DAPI) was made. Finally, cells were covered with mounting medium to preserve the fluorescence of the fluorochromes and to prevent photobleaching of stained cells. Immunofluorescence signal was then examined with specific microscopy methods, such as high-end fluorescence imaging including super-resolution microscopy.

Table 17: Amounts of 4% PFA used to fix cells

Cell culture vessel	Volume per vessel (µL)
24-well plate	200*
12-well plate	400*
6-well plate	1000*
IBIDI *d*STORM slide	1000*
Thermo Fisher *d*STORM slide	200*

*necessary volume / well

The visualization of CDH13 in human iPSC-derived neurons required a protein labelling in pre-fixed living cells. This procedure was performed together with A. Forero (Division of Molecular Psychiatry, Center of Mental Health, University of Würzburg). For this purpose, living cells were first incubated with the primary antibody against CDH13 on ice for 1 h, then fixed and incubated with further primary antibodies overnight at 4°C. Following steps were performed according to the standard procedure described before.

2.2.4.2 Cell lysis for protein analyses

In order to analyse GLUT3 expression levels by Western blot, cells were cultured on 100 mm dishes for adherent cells (Sarstedt) and lysed at 80–90% confluency to release the cellular proteins. After the cells were washed using 1 x DPBS, 600 µL ice-cold lysis buffer was added and each dish was incubated for 2 min on ice. Finally, cells were scraped and transferred to ice-cold microcentrifuge tubes, sonicated to disrupt cell membranes and to release cellular contents and centrifuged for 2 min at 10000 rpm and 4°C. The supernatant containing the protein was then transferred to a fresh tube and stored at -80°C for later protein quantification using the Precision Red advanced protein assay reagent.

2.2.4.3 Protein quantification using Precision Red advanced protein assay reagent

Protein concentration was calculated in duplicates for each sample using the Precision Red advanced protein assay reagent which accurately measures protein concentrations ranging from 0.25 to 50 mg/mL. For this purpose, 10 µL per sample were added to the respective well of a 96-well plate and mixed with 300 µL Precision Red reagent. Additionally, 300 µL of the reagent were added in two wells being the blank. After an incubation at RT for 1 min, the absorbance at 600 nm was quantified with a spectrophotometer. Protein concentration was calculated based on 1.00 OD_{600nm}=125 µg protein per mL reagent per cm and multiplied by 30 to achieve the protein concentration in µg/mL of the original protein solution.

2.2.4.4 Western blot procedure

In this study, levels of GLUT3 in human fibroblasts, iPSCs and iPSC-derived neurons were examined by Western blot. Additionally, GAPDH as common housekeeping proteins were used in all experiments as reference proteins and loading controls to normalize expression values and quantification of the proteins of interest. Membranes were analysed using the Fusion imaging system (Vilber Lourmat).

For a more detailed description, Western blotting was performed as follows. Cell lysates (30 µg of total protein content) were mixed with reducing agent and a lithium dodecyl sulfate loading (LDS) buffer which facilitated the loading and visualization of samples during the

sodium dodecyl sulfate (SDS) polyacrylamide gel electrophoresis (SDS-PAGE). After subsequently denaturing the samples by incubation at 70°C for 10 min, 25 μL of each denatured sample were loaded into the gel together with 4 μL of the protein ladder, chambers were filled with electrophoresis buffer and a run with 200 V was started lasting approximately 1 h. Afterwards, the gel was carefully assembled together with pre-soaked sponges, filter papers and the membrane in the chamber and transfer buffer was added to the blot module. Finally, the chamber was placed in ice and a current of 30 V was applied for 1 h. Coloured bands of the protein ladder as first evidence of a successful transfer appeared on the nitrocellulose membrane after the run was finished. Membrane was washed for 2 min in 1 x PBS on a shaking platform. Before incubating the membrane in the antibody solutions, unspecific binding sites had to be blocked by a blocking solution for 1 h in agitation at RT. Blocked membranes were incubated in the corresponding primary antibody solutions (working dilutions are listed in Table 5) overnight at 4°C on a rocking platform. The next day, membrane was washed in PBS-T 4x for 5 min to remove rests of non-bound primary antibody. The membrane fragments were incubated in the secondary antibody solutions (listed in Table 6) for 1 h at RT under agitation in darkness then. After 1 h, membranes were washed using PBS-T 4x for 5 min and once using 1 x PBS. After detection of the proteins, the Image Studio™ Lite 5.2 was used to quantify obtained images.

2.2.4.5 Flow cytometry

Flow cytometry using conjugated antibodies directed against surface pluripotency markers was performed together with C. K. Kwok (Department of Stem Cell and Regenerative Medicine, Institute of Anatomy and Cell Biology II, University of Würzburg) as described before (Jansch et al 2018). Isotype and unstained controls were included as controls and dead cells labelled by Viobility 405/452 Fixable Dye were excluded from the analysis. 1×10^6 cells per sample were harvested enzymatically using accutase and centrifuged at 1200 rpm for 5 min at 4°C. Cell pellets were resuspended in a staining buffer containing 5 % FCS in DPBS, centrifuged at 300 × g for 3 min at 4 °C and incubated for 15 min at 4°C using TRA-1-60-PE and 10 μL SSEA-4-APC antibodies diluted in staining buffer. Cells were washed and carefully singularized in DPBS for analysis. Data was acquired using BD FACSCanto™ II flow cytometer and the BD software.

2.2.5 Microscopy techniques

Cells were cultured on poly-D-lysine (PDL)/LAM-coated 8-chamber slides (20,000 cells/well; Corning) for epifluorescence and confocal microscopy, on PO/LAM-coated 24-well plates (Greiner Bio-One; 30,000 cells/well) for structured illumination microscopy (SIM) and on

PO/LAM-coated glass bottom dishes (ibidi; 200,000 cells/slide) as well as on PO/LAM-coated 8-well chambered coverglass slides (Thermo Fisher Scientific; Nunc™ Lab-Tek™ II coverglass; 30,000 cells/well) for *direct* stochastic optical reconstruction microscopy (*d*STORM). Image acquisition and processing of SIM and *d*STORM was done together with S. Wäldchen (Department of Biotechnology and Biophysics, Biocenter, University of Würzburg) and A. Forero (Division of Molecular Psychiatry, Center of Mental Health, University of Würzburg). Microscopy techniques were performed as described before (Forero et al 2017, Jansch et al 2018).

2.2.5.1 Epifluorescence

Images were obtained using an Olympus motorized inverted system microscope IX81, an X-Cite fluorescence illuminator, and an XM10 camera. Pictures were taken at 10x, 20x, and/or 40x magnifications through the exposure channels for Alexa Fluor 488, Alexa Fluor 555, Alexa Fluor 647 and DAPI. Images were then processed using software CellSense (Olympus), and corrected for contrast and brightness using ImageJ (Schneider et al 2012).

2.2.5.2 Confocal Microscopy

Images were generated using a FluoView FV1000 confocal microscope (Olympus) with 20X UPlanSAPO, NA 0.75 (air) and 40X UPlanFLN, NA 1.30(oil) objectives. Stack images were taken by laser illumination at 561 nm (Alexa Fluor 555), 488 nm (Alexa Fluor 488), and 405 nm (DAPI). 12-bit raw images were processed with the imaging software Fluoview, version 4.1.a (Olympus).

2.2.5.3 Structured illumination microscopy (SIM)

Images were captured with a commercial SIM microscope (Zeiss ELYRA, Oberkochen, Germany) using an oil-immersion objective (Plan-Apochromat 63 × /1.4 Oil Dic M27) (Gustafsson 2000, Wegel et al 2016). Excitation of the fluorophores was performed by laser illumination at 642 nm (Alexa Fluor 647), 561 nm (Alexa Fluor 555), 488 nm (Alexa Fluor 488), and 405 nm (DAPI) and fluorescence light was filtered by appropriate detection filters: LP 655 (Alexa Fluor 647), BP 570–620 + LP 750 (Alexa Fluor 555), BP 495–550 + LP 750 (Alexa Fluor 488), and BP 420–480 + LP 750 (DAPI). Images were recorded with five rotations and five phase steps of the illumination pattern. Recorded data were processed with the ZEN imaging software (Zeiss). They were processed under standard ELYRA settings of the manual mode, selecting the Raw Scale option to keep the original dynamic range and therefore ensure a reliable comparison of the actual sample and the control samples. Following the structured illumination processing, the four channels were aligned (ZEN imaging software).

2.2.5.4 3D reconstruction

Movies illustrating 3D reconstruction were done using Imaris (Bitplane). The images used were taken with SIM at intervals of 125 nm. The fluorescence images were represented by surface visualization and the animation was conducted by rotation and zooming. The final product was exported as an .avi file.

2.2.5.5 *Direct* stochastic optical reconstruction microscopy (*d*STORM)

For fluorophore photo switching, a buffer containing 1% glucose and 100 mM β-mercaptoethylamine (Sigma-Aldrich) in DPBS adjusted to a pH 8.0 was used. To reveal synaptic structures and GLUT3 expression in neurons *d*STORM was performed on a wide-field setup for localization microscopy (van de Linde et al 2011). A diode laser with a wavelength of 640 nm (iBeam smart, TOPTICA Photonics, maximum power of 200 mW) and a diode-pumped solid-state laser with a wavelength of 532 nm (gem, Laser Quantum, maximum power of 500 mW) were used for excitation of Alexa Fluor 647 and Alexa Fluor 532 respectively. Laser beams were cleaned-up by bandpass filters (Semrock) and combined by appropriate dichroic mirrors (LaserMUX filters, Semrock). Afterwards they were focused onto the back focal plane of the high numerical oil-immersion objective (alpha Plan-Apochromat 100x/1,46 Oil DIC, Carl Zeiss Microscopy), which is part of an inverted fluorescence microscope (Zeiss Axio Observer.Z1, Carl Zeiss Microscopy) equipped with an autofocus system (Definite Focus, Carl Zeiss Microscopy). To separate the excitation light from the fluorescence light, a suitable dichroic beam splitter (Semrock) was placed into the light path before the laser beams enter the objective. Fluorescence light of Alexa Fluor 647 and Alexa Fluor 532 was collected by the objective and splitted by a dichroic mirror (Chroma) to two separate EMCCD cameras (iXon Ultra 897, Andor Technology). Before entering the cameras, it was filtered by appropriate detection filters (Semrock/Chroma).

For every image, 15 000 frames were taken with an integration time of 10 ms per frame. Data analysis was performed using ThunderSTORM (Ovesný et al 2014). Gold beads were used for drift correction.

2.2.6 Electrophysiological recording of human iPSC-derived neurons

Electrophysiological examination of human iPSC-derived neurons was done together with Prof. E. Wischmeyer and Dr. S. Kollert (Institute of Physiology, Molecular Electrophysiology, University of Würzburg). For electrophysiological assessment, human iPSC-derived 5-HT progenitors were seeded in a cell density of 30,000 cells/well on PO/LAM-coated coverslips placed in a 24-well plate. To follow the maturation of 5-HT specific neurons over a specific time

frame, whole-cell recordings (Hamill et al 1981) of at least 10 neurons per independent experiment (n=3) were performed weekly over a period of 6 weeks at RT in a bath solution consisting of 135 mM NaCl, 5.4 mM KCl, 1.8 mM $CaCl_2$, 1 mM $MgCl_2$, 10 mM glucose, 5 mM HEPES, pH 7.4. Patch pipettes were pulled from borosilicate glass capillaries (Kimble Products, England), and heat-polished to give input resistances of 2-5 MΩ (whole-cell). The pipette recording solution contained 120 mM potassium methansulfonate (CH_3KO_3S), 4 mM NaCl, 1 mM $MgCl_2$, 0.5 mM $CaCl_2$, 10 mM ethylene-bis(oxyethylenenitrilo) tetraacetate (EGTA), 3 mM ATP-Mg, 0.3 mM GTP-TRIS and 10 mM HEPES (pH 7.2). Properties of 5-HT specific neurons were analysed according to existing electrophysiological criteria (de Kock et al 2006, Li et al 2001, Vandermaelen & Aghajanian 1983), such as amplitude, half-height width (HHW) and action potential frequency. Our main criteria for 5-HT specific neuron identity were action potential HHW of >1.5 ms and maximal sustained firing rate of <12 Hz (Mlinar et al 2015). Currents were recorded with an EPC9 (HEKA) patch-clamp amplifier and low pass-filtered at 2 kHz. Stimulation and data acquisition were controlled by the PULSE/PULSEFIT software package (HEKA) and data analysis was performed with IGOR software (WaveMetrics, Lake Oswego, OR, USA).

2.2.7 Cell counting to evaluate efficiency of neuronal subtype generation

To determine the particular potential of human iPSCs to differentiate into specific neuronal subtypes using the established differentiation protocol described in section 2.2.2.6, the ratio of TPH2-, TH- and GABA-positive cells to ßTubIII-positive cells was calculated. Therefore, mature neurons were stained with appropriate markers according to the IF protocol described in section 2.2.4.1 and five areas per independent experiment (n=3) were randomly selected.

2.2.8 Cytogenetical techniques

2.2.8.1 Karyotype analysis

Karyotypes were verified by Giemsa banding (GTG-banding) as published (Jansch et al 2018). Karyotypical examination was done together with A. Maierhofer and J. Flunkert (Institute of Human Genetics, University of Würzburg). GTG-banding is a cytogenetical technique used to produce a visible karyotype by staining condensed chromosomes – a useful method for identifying genetic alterations during the reprogramming process of adult cells into pluripotent stem cells. For this purpose, human iPSCs were cultured in MACS iPS-Brew medium in T-25 flasks. Reaching confluency around 70%, cells were incubated for 1 h with 10 µg/mL KaryoMAX™ colcemid™ solution in PBS (Thermo Fisher), centrifuged at 1400 rpm for 8 min and the pellet was resuspended in 10 mL of a 0.075 M KCl solution. After an incubation period of 13 min at 37°C, the solution was centrifuged at 1400 rpm for 8 min, the pellet was

resuspended in an ice-cold fixative composed of methanol and glacial acetic acid (3:1 dilution) and the solution was incubated overnight at 4°C. The next day, the suspension was centrifuged at 1400 rpm for 8 min, the pellet resuspended in fresh fixative and the solution was transferred dropwise on a microscope slide. After "flame-drying" of the slide over a Bunsen burner, a quality check of the material was performed using phase-contrast microscopy. For GTG-banding, slides were exposed to a temperature of 90°C for 90 min, incubated using 200 µL Trypsin/100 mL 1 x DPBS for 50-60 s, washed and stained using a 5% Giemsa solution for 4 min. After a final washing step using distilled water, slides were ready for cytogenetic examination. Specifically, 10 metaphases per sample were examined with a resolution of 450-500 bands using Axioskop (Zeiss).

2.2.8.2 Molecular Karyotyping: Affymetrix CytoScanHD

In this study, the Affymetrix CytoScanHD Service provided by the company ATLAS Biolabs GmbH (Berlin, Germany) was used to analyse *SLC2A3* CNVs in the generated human iPSC lines. We found the "ThermoFisher CytoScan HD Full Service" to present the most comprehensive and relevant coverage of this specific type of structural variation of *SLC2A3*. Affymetrix' GeneChip™ technology applies a combination of photolithography and combinatorial chemistry to directly synthesise 25mer oligonucleotides on a glass surface. Here, up to 6.5 million different oligonucleotides are synthesised on a 1.7 cm² surface. Row data obtained by the company ATLAS Biolabs GmbH was finally analysed using the software Chromosome Analysis Suite (ChAS; NetAffx 33.2, hg19).

2.2.9 Statistical evaluation

All experiments described in this study which include human iPSC-derived neurons have been conducted in a total of 3 independent differentiations per cell line (n=3). Measurement of neuronal subtype efficiency was calculated by five randomly chosen areas per differentiation and cell line. Statistical examination and graphical presentation were done using GraphPad Prism 8. All values were referred to a control sample of the respective experiment that was given the arbitrary value 1. One-way ANOVA, Kolmogorov–Smirnov, Shapiro-Wilk test and Bonferroni's Multiple Comparison Test or Kruskal-Wallis test, Kolmogorov–Smirnov and Dunn's multiple comparisons test were used. Differences were considered to be significant when P≤0.05 (* p=0.01 to 0.05; ** p=0.001 to 0.01; *** p<0.001).

3. Results

3.1 Generation of human iPSCs from adult dermal fibroblasts

An initial genome-wide screening approach for CNVs in ADHD revealed a significant excess of *SLC2A3* duplication carriers in a subsequent analysis of a German population sample: 251 childhood and 675 adult ADHD cases vs. 767 controls. 2.6% of subjects in the control group and 4.9% of cases displayed this CNV (Merker et al 2017a). Based on these findings, primary fibroblasts of a healthy donor with a single copy of *SLC2A3* as well as of two ADHD patients carrying either a duplication or a deletion of *SLC2A3* were reprogrammed into human iPSCs using SeV technology (Figure 10). The generation of the patient-specific duplication carrier cell line was recently published (Jansch et al 2018).
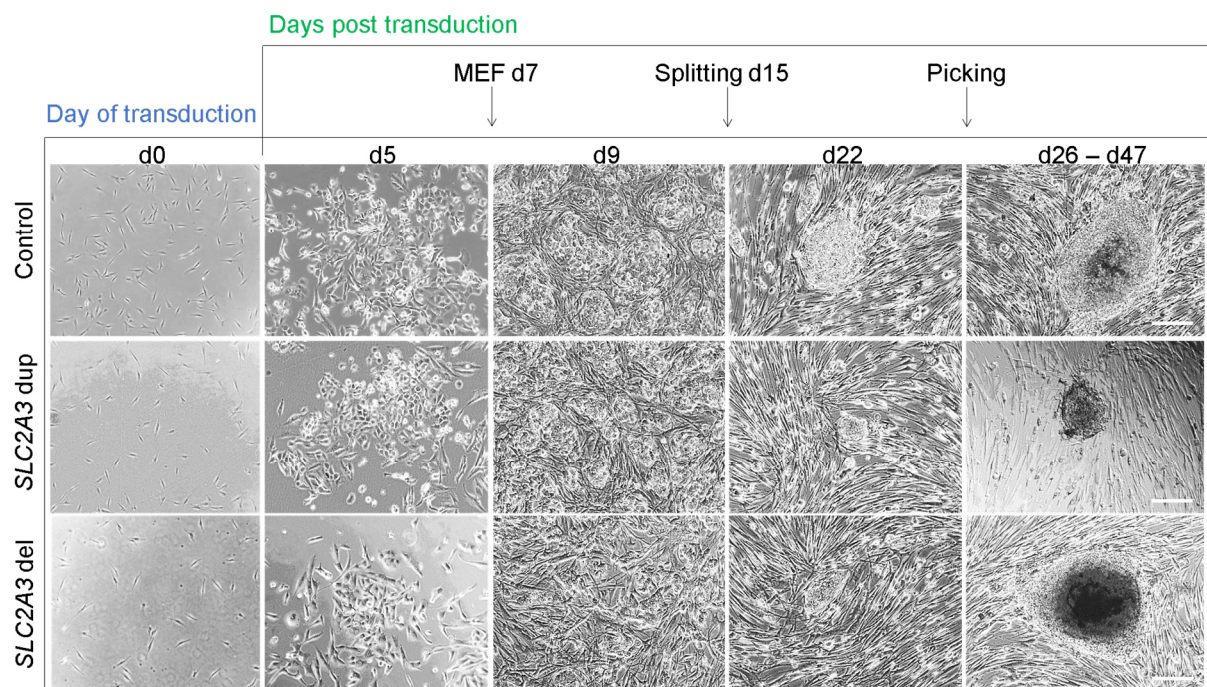
Figure 10: SeV reprogramming of adult cells into human iPSCs.

Human dermal fibroblasts were reprogrammed into iPSCs using the technique of SeV reprogramming. A few days after infection, stem cell-like colonies appeared. Those ESC-like structures were picked on day 26-47, depending on the cell colonies' morphology. Dup, Duplication cell line; del=Deletion cell line. Scale bar: 100 µm. Figure was adapted from Jansch et al. (2018).

Human iPSC colonies cultured on Matrigel displayed the typical human ESC-like morphology of compact, dense, roundly shaped colonies with sharp edges as well as the typical human ESC-like growth behaviour of highly proliferating stem cells (Figure 11A). For all three generated cell lines, karyotypical analysis by standard G-banding was performed together with A. Maierhofer and J. Flunkert (both from the Institute of Human Genetics, University of Würzburg) which revealed a normal female karyotype without numerical or structural chromosome abnormalities of human iPSCs (46, XX) (Figure 11B).
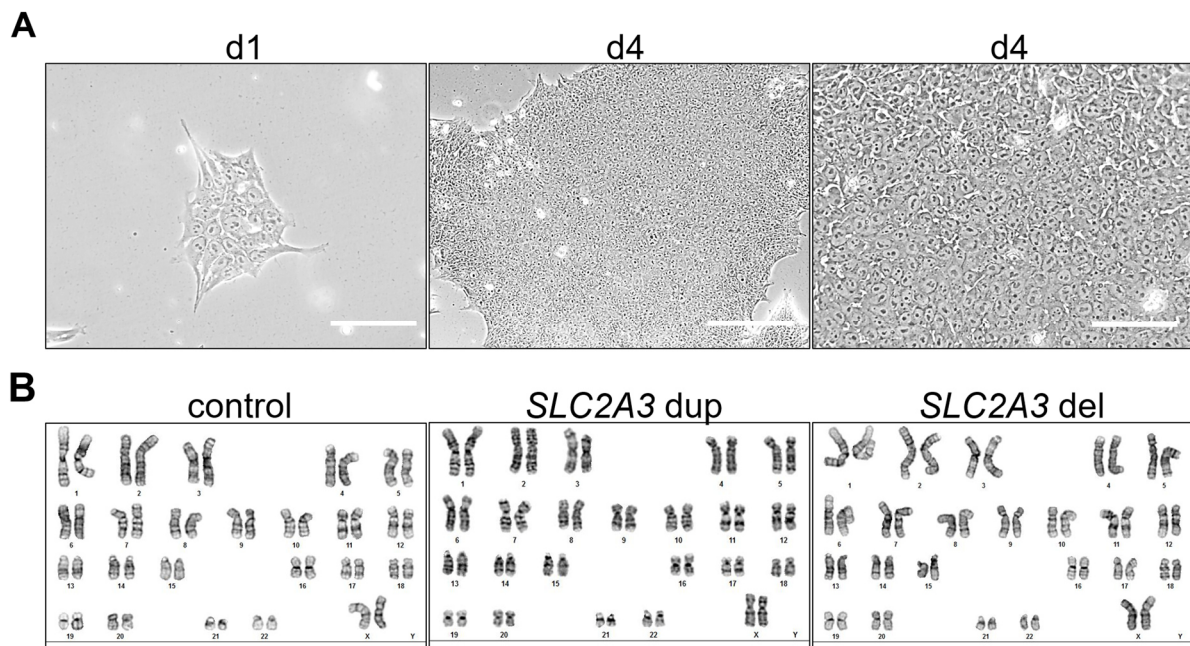
Figure 11: Reprogramming of fibroblasts results in human iPSCs which display typical stem cell morphology, but no karyotypical alterations.

(A) Exemplary picture of human iPSCs. Generated stem cells display a typical human ESC-like morphology. One day after splitting, human iPSCs already show stem cell colony formation. Four days after splitting, human iPSCs form typical human ESC-like colonies of dense, round cells. Scale bar: 100 µm; close-up picture d4: 200 µm. (B) All three generated human iPSC lines have a normal female karyogram without numerical or structural chromosome abnormalities (46, XX). Figure was adapted from Jansch et al. (2018).

The Affymetrix CytoScan HD Array confirmed that two of the generated human iPSC lines carry hemizygous CNVs of *SLC2A3*, while one cell line shows a normal CN of 2.00 and therefore serves form there on as control cell line in this study (Figure 12). Illustrated in Figure 12A, examination of chromosome 12 confirmed that two of the generated human iPSC lines (referred to as *SLC2A3* dup and *SLC2A3* del) carry either a duplication or a deletion of the *SLC2A3* gene locus, compared to the control iPSC line. The CN state of the iPSC line carrying the duplications is 1.00, while the cell line carrying a deletion has a CN state of 3.00. ChAS

software enables the illustration of a Karyoview of chromosome 12 (Figure 12B). Result tables illustrated in Figure 12C show that human iPSCs carry a gain or a loss of the *SLC2A3* gene locus with a size of 120 kilobase pair (kbp) (chr12: 8,004,411-8,124,048; hg19). The duplicated chromosomal region comprises the complete gene locus of *SLC2A3* and the initial exons of *SLC2A14*, a paralog of *SLC2A3*.
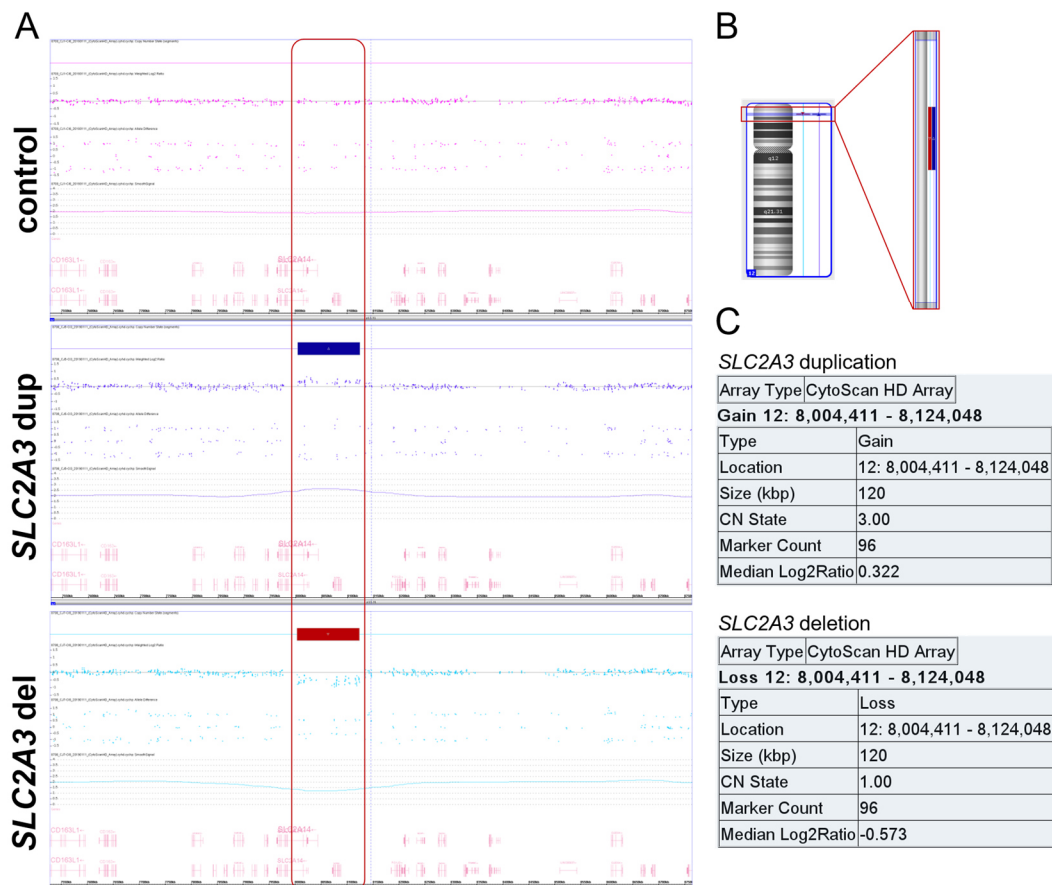
Figure 12: Generated human iPSC lines carry a duplication and a deletion of the gene *SLC2A3*.
(A) Row data gained by the Affymetrix CytoScan HD Array was analysed using the software Chromosome Analysis Suite (ChAS; NetAffx 33.2, hg19). Examination of chromosome 12 confirmed that two of the generated human iPSC lines (*SLC2A3* dup; *SLC2A3* del) carry either a duplication or a deletion of the *SLC2A3* gene locus, compared to the control iPSC line. (B) Karyoview of chromosome 12 showing the duplicated and deleted region in p13.31 with a close-up picture focusing on the altered area (red box). (C) Human iPSCs carry a gain or a loss of the *SLC2A3* gene locus with a size of 120 kbp (chr12: 8,004,411-8,124,048; hg19). The duplicated chromosomal region comprises the complete gene locus of the *SLC2A3* paralog *SLC2A14*.

The absence of SeV specific transcripts in human iPSCs was ratified by reverse transcriptase (RT)-PCR after 20 passages (Figure 13A) and stem cells were repeatedly confirmed as mycoplasma-free before conducting experiments (Figure 13B). Moreover, flow cytometric

analysis additionally confirmed the pluripotent identity of the cell lines through homogeneous expression of pluripotency specific markers TRA-1-60 and SSEA-4 (double-positive cells: 97.5%) (Figure 13C).
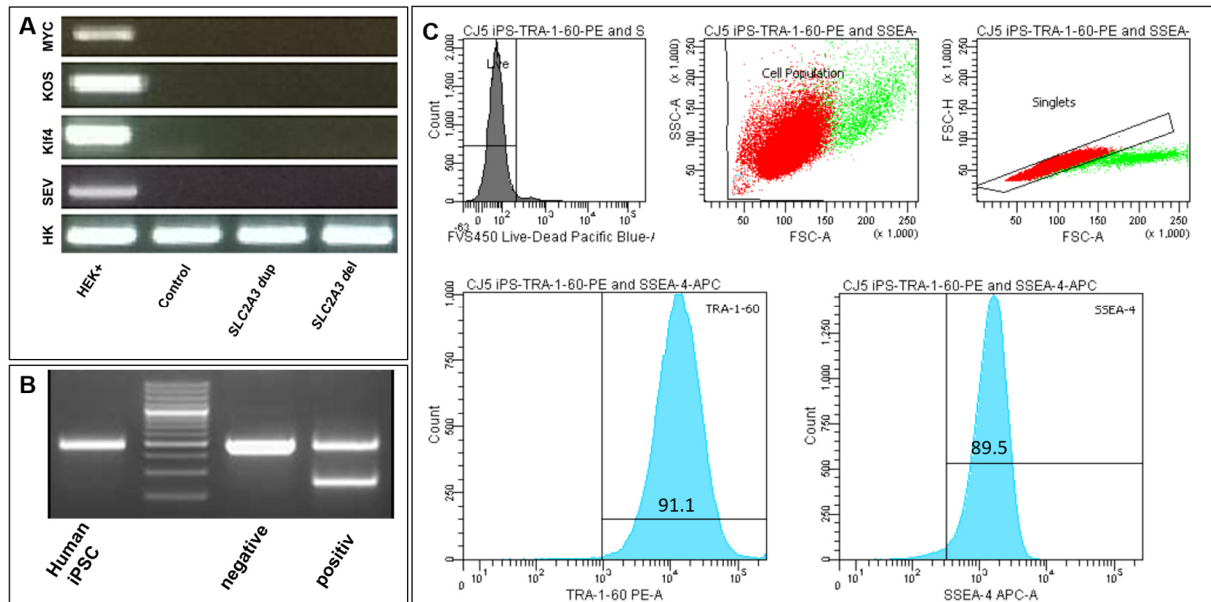
Figure 13: Human iPSCs display typical stem cell characteristics.

(A) RT-PCR gene expression analysis shows elimination of the non-integrating viral genome in all three iPS cell lines. (B) Exemplary result of a mycoplasma test showing that iPSCs carrying a *SLC2A3* duplication are free of mycoplasma contamination. (C) Exemplary result of a flow cytometry analysis of TRA-1-60 and SSEA4 that revealed high expression of pluripotency associated markers in generated iPSCs carrying a duplication of *SLC2A3*. Figure was adapted from Jansch et al. (2018).

Additionally, IF analysis proved the expression of the pluripotency-associated surface markers TRA-1-60 and SSEA-4 and the transcription factor OCT-3/4, which confirms the pluripotent character of those cell lines (Figure 14).
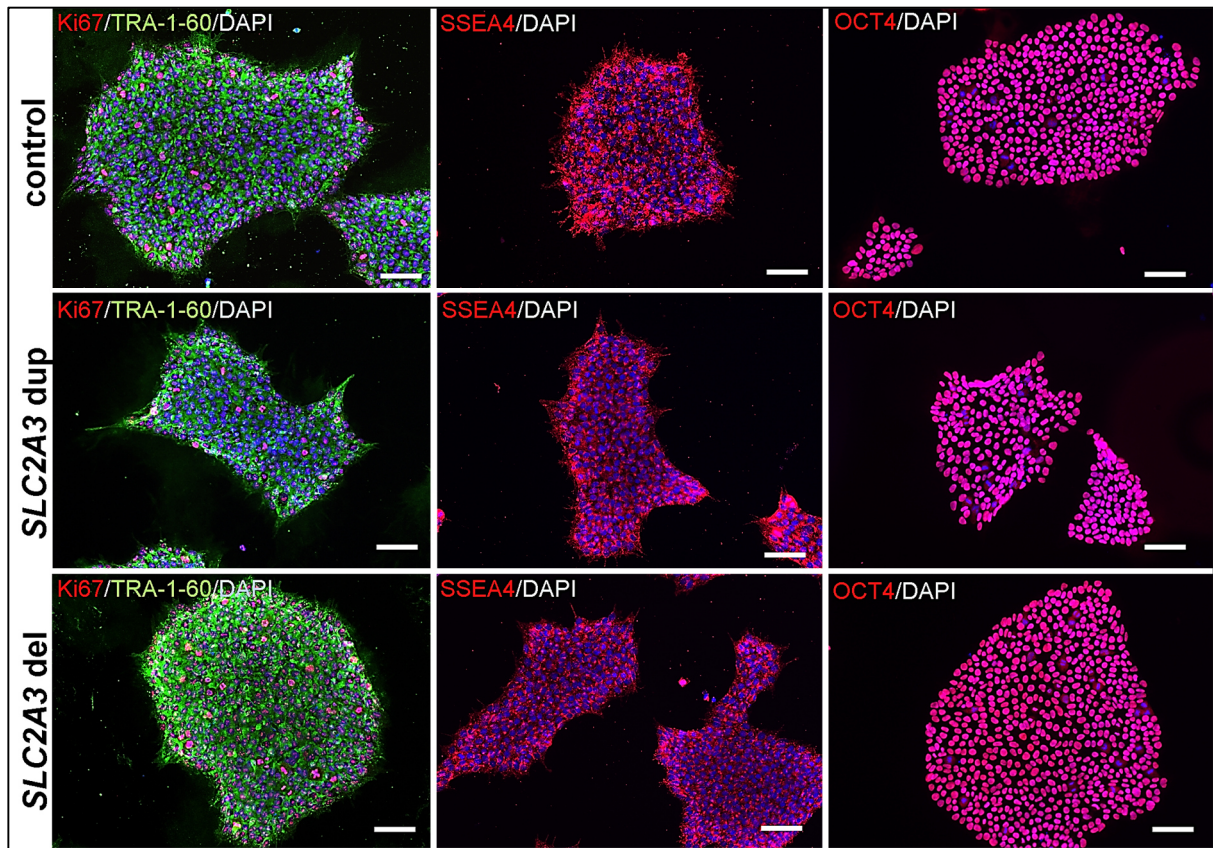
Figure 14: Human iPSCs display the typical human ESC-like pluripotent features.

All three generated human iPSC lines express pluripotency-associated markers Ki67, TRA-1-60, SSEA and OCT4 analysed via epifluorescence. Cell nuclei were counterstained with DAPI. Scale bar: 100 μm. Figure was adapted from Jansch et al. (2018).

Germ layer differentiation demonstrated the default differentiation capacity of obtained human iPSCs into EBs when cultured in serum containing medium (Figure 15). Human iPSCs differentiated towards mesodermal, endodermal and ectodermal layer specific cells as observed by positive IF staining against alpha-smooth muscle actin (SMA), alpha-1-fetoprotein (AFP) and beta-Tubulin III (ßTubIII), respectively.
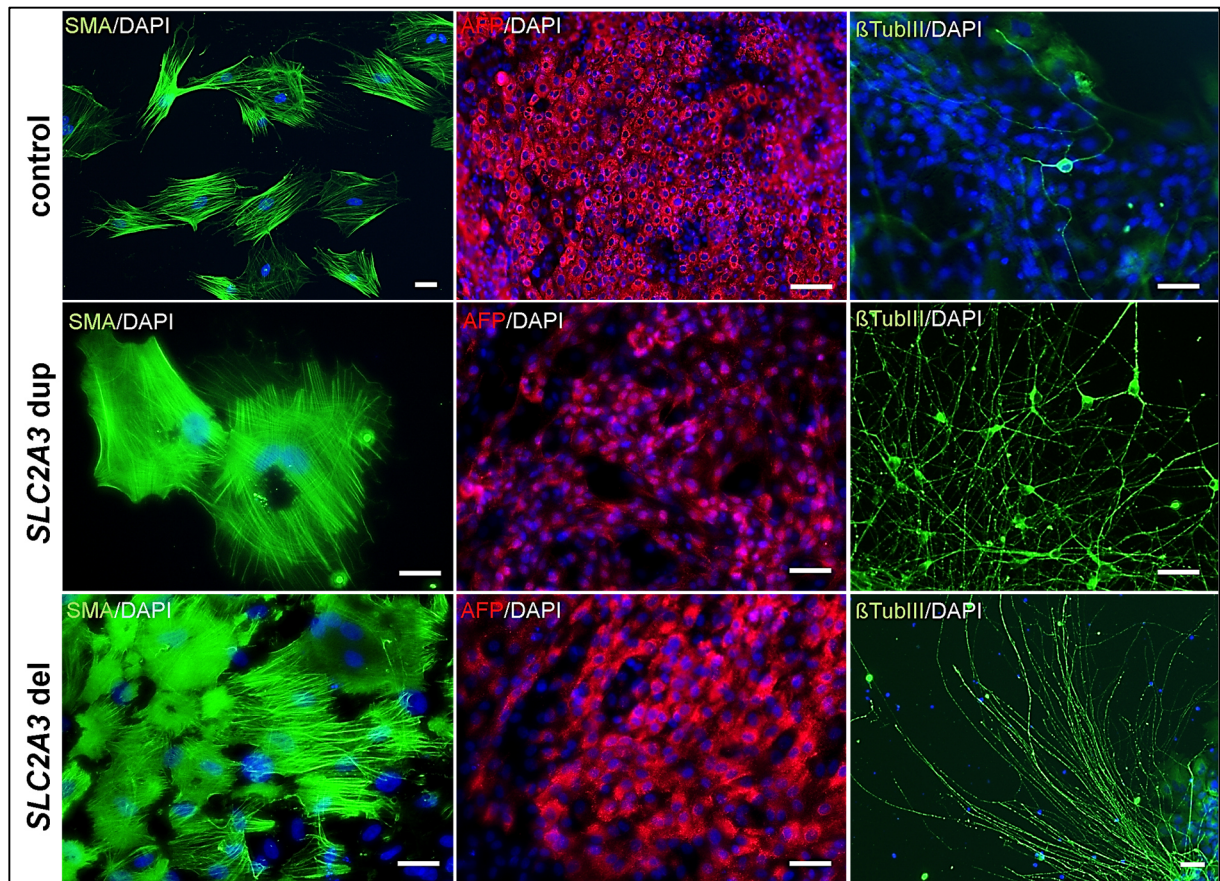
Figure 15: Human iPSCs are able to differentiate into cells of all three germ layers.

Default differentiation of human iPSCs resulted in cells of all three germ layers (mesoderm: alpha-smooth muscle actin (SMA); endoderm: alpha-1- fetoprotein (AFP); ectoderm: beta-Tubulin III (ßTubIII). Cell nuclei were counterstained with DAPI. Scale bar: 50 µm. Figure was adapted from Jansch et al. (2018).

3.2 Generation of monoaminergic neurons from human iPSCs

A challenging topic of this thesis was to establish a protocol for a reliable differentiation of human iPSCs into 5-HT specific mature neurons that form synaptic connections and show the characteristic features of functional neurons of this subtype. As mentioned before, a preliminary study conducted by R. Kern under my supervision served as basis to develop this differentiation strategy. Finally, during my PhD program I generated 5-HT specific neurons from human iPSC by combining specific differentiation strategies and manipulation of signalling pathways. Given that the use of an adherent culture system did not result in the generation of a pure neuronal cell culture, but in a loss of neural progenitor cells, I adjusted the recent protocol published (Lu et al 2015) for our needs.

3.2.1 Establishment of a reproducible differentiation protocol from human iPSCs into 5-HT specific cells

Generation of human iPSC-derived 5-HT specific neurons was facilitated by the combination of an EB formation system, manipulation of signalling pathways and specific selection steps (Figure 16). Based on a previously published method neural differentiation was induced by inhibition of TGF-β, GSK-3 signalling, as well as the inhibition of the BMP pathway (Lu et al 2015). A combination of the factors SB, CHIR and DMH-1 resulted in rostral hindbrain progenitors (NPC medium) which were further treated with a specific, time-dependent combination of SHH and FGF4 to specify their 5-HT fate, before neuronal maturation was induced.
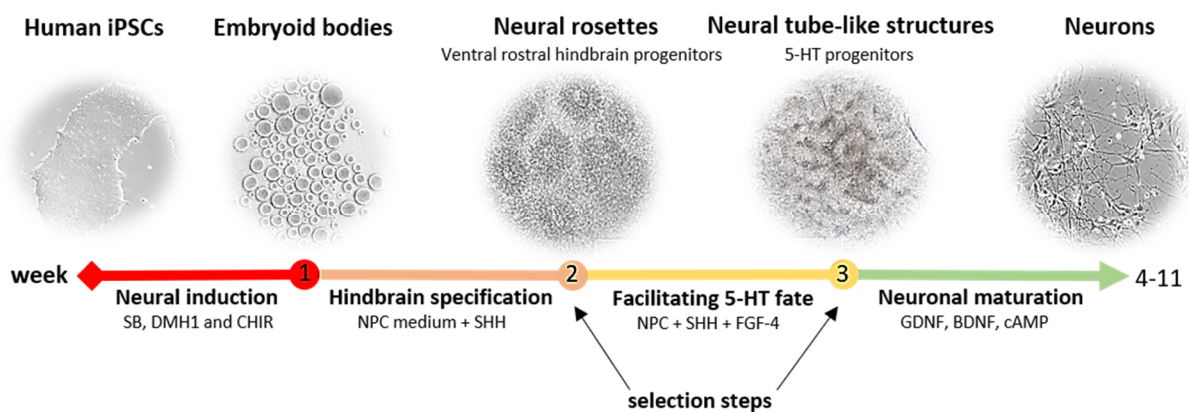
Figure 16: Differentiation procedure to generate human iPSC-derived 5-HT specific neurons.
Scheme of the differentiation protocol describing the generation of human iPSCs-derived 5-HT specific neurons by inhibition of TGF-β (SB) and GSK-3 (CHIR) signalling, as well as the inhibition of the BMP pathway (DMH-1). Here, specific selection steps combined with a time-dependent treatment of rostral hindbrain progenitors with SHH and FGF4 resulted in the generation of 5-HT specific neurons.

As illustrated in Figure 17, the developmental fate of ventralized rostral hindbrain progenitors was confirmed by IF. Rostral hindbrain progenitors were positively stained for neural markers Nestin, SOX1 and SOX2 and the rostral hindbrain marker HOXA2 (Figure 17A-B). Rostral hindbrain NPCs were ventralized by SHH illustrated by an increased expression of ventral rostral hindbrain markers NKX2.2 and NKX6.1 and a decreased expression of the dorsal marker PAX3/7 (Figure 17C-D). Furthermore, after treatment with a combination of SHH and FGF4 NPCs showed expression of 5-HT neuron-specific markers GATA-binding factor 2 (GATA2) and forkhead box A2 (FOXA2) revealing the 5-HT specific fate of the cells (Figure 17E).
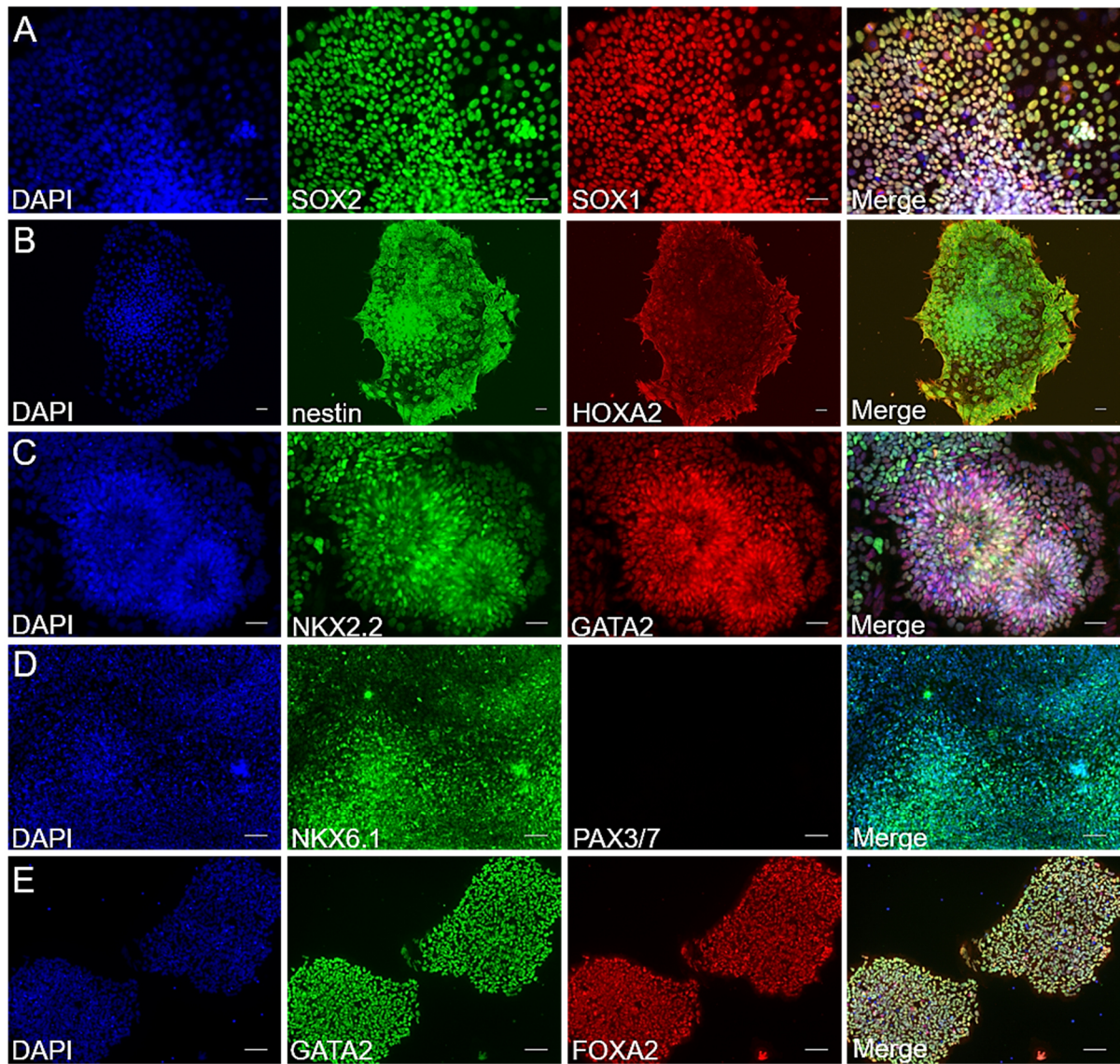
Figure 17: Differentiation of human iPSCs into 5-HT specific progenitors.

Generation of 5-HT specific progenitors illustrated by epifluorescence microscopy. (A-B) Specification of rostral hindbrain progenitors. After one week of neural induction cells were stained for typical neural markers, such as Nestin, SOX2 and SOX1. High expression level of HOXA2, a marker for hindbrain progenitors, was additionally found at this time point in these cells. (C-D) Ventralization of cells was shown by positive IF staining of NKX2.2, NKX6.1, GATA2 and negative staining of PAX3/7, when treated with 1,000 ng/mL SHH for one week. (E) Ventralized rostral progenitors were treated with FGF4 for one further week to generate 5-HT specific progenitors. Scale bar: 50 µm (A-C), 100 µm (D-E). Cell nuclei were counterstained with DAPI.

3.2.2 Hindbrain progenitors differentiate into a mixed culture of specific neuronal subtypes

After five weeks of neuronal maturation, most of the cells developed into ßTubIII+ neurons (>70%) and only a very low percentage of glial fibrillary acidic protein positive (GFAP+) astrocytes (Figure 18A). Additionally, neurons have been proven to be mature by positive staining of the dendritic marker microtubule-associated protein 2 (MAP2), the axonal marker Tau protein and the neuronal nuclear protein (NeuN), a marker for mature neurons (Figure 18B and C).

ßTubIII/GFAP/DAPI   MAP2/GFAP/NeuN   Tau/GFAP/NeuN
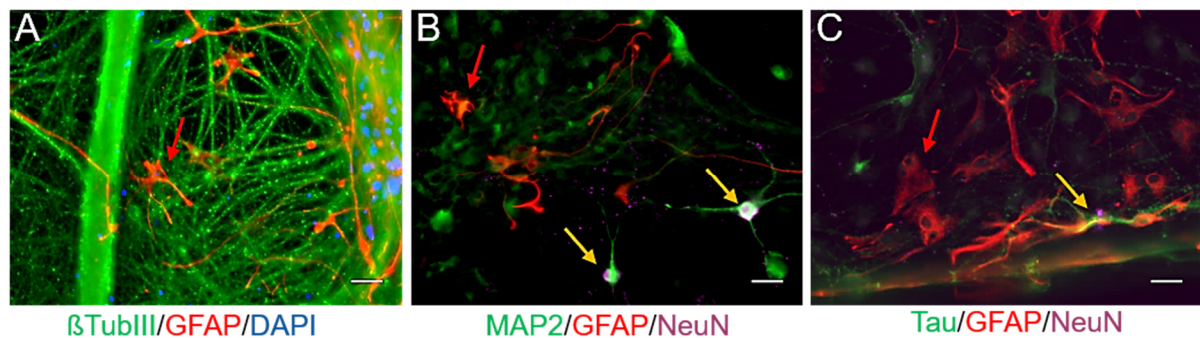
Figure 18: Generation of mature neurons from human iPSC-derived 5-HT specific progenitors.
Our differentiation protocol generates (A) ßTubIII+ neurons (green) and (A-C) GFAP+ astrocytes (red, examples marked by red arrows) following 5 weeks of neuronal maturation. Maturity of those 5-weeks old neurons was confirmed by positive staining of (B) MAP2 (green)/NeuN (magenta) and (C) Tau (green)/NeuN (magenta). Mature neurons are marked by yellow arrows. All pictures were taken by epifluorescence microscopy. Scale bar: 50 µm. Cell nuclei were counterstained with DAPI.

Among the ßTubIII+ cells, a high percentage of the neurons in our culture system displayed a 5-HT specific phenotype illustrated by a positive TPH2 staining. IF analyses of 5-HT specific markers, such as 5-HT, 5-HTT and TPH2 additionally proved the 5-HT specific fate of those cells (Figure 19).
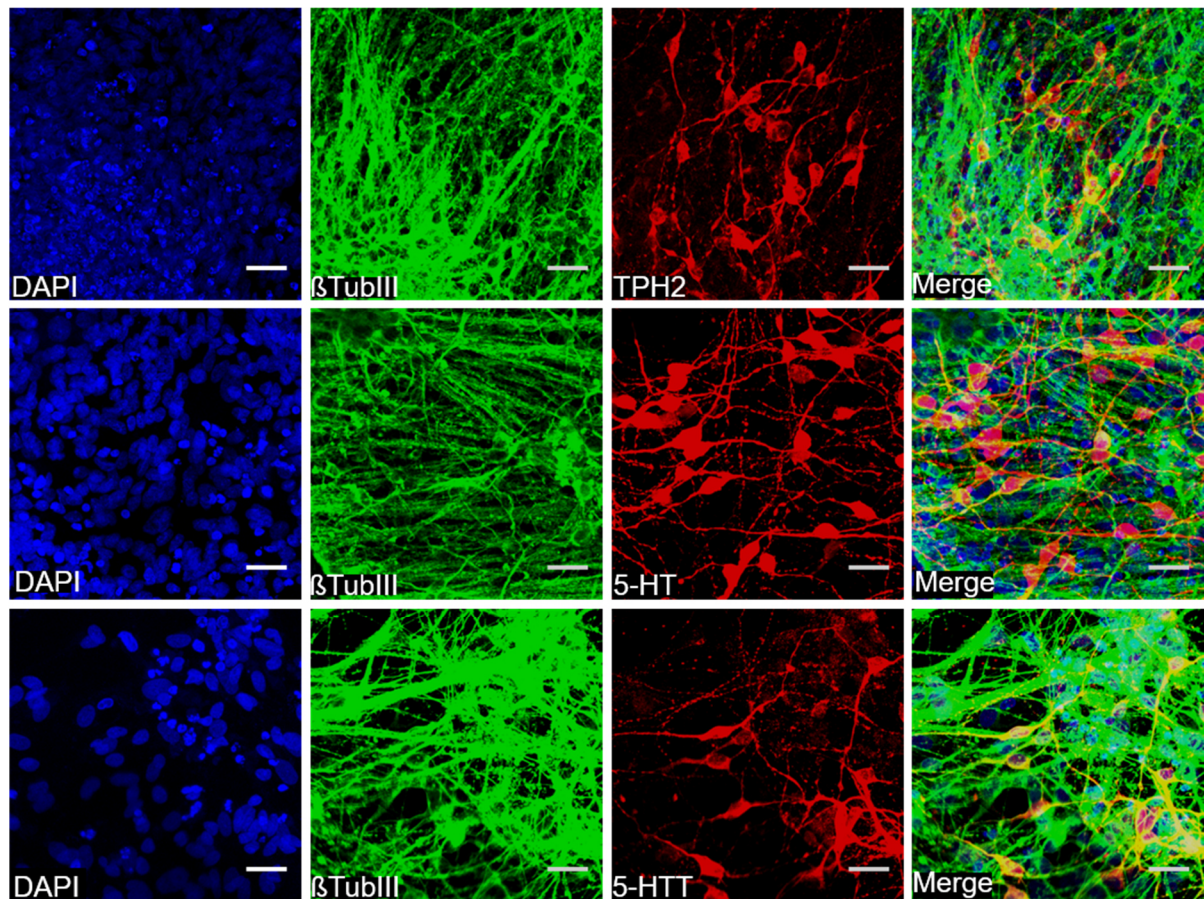
Figure 19: Generation of 5-HT specific neurons from human iPSC-derived 5-HT specific progenitors.

All neurons were co-stained for an antibody against ßTubIII and TPH2, 5-HT and 5-HTT after 4-5 weeks of neuronal maturation (differentiation week 7-8). Pictures were taken using confocal microscopy. Scale bar: 50 µm. Cell nuclei were counterstained with DAPI.

The determination of specific neuronal subtypes in our cell culture system via IF of neuronal subtype marker (Figure 20A and B) showed that besides the 42 % of 5-HT specific neurons, 40% showed a catecholaminergic and 12% a GABAergic phenotype. The mRNA expression of *TPH2*, *tyrosine hydroxylase* (*TH*) and *glutamate decarboxylase 1* (*GAD1*) genes supports the dominant presence of 5-HT specific neurons revealed by the cell counting analysis (Figure 20C).
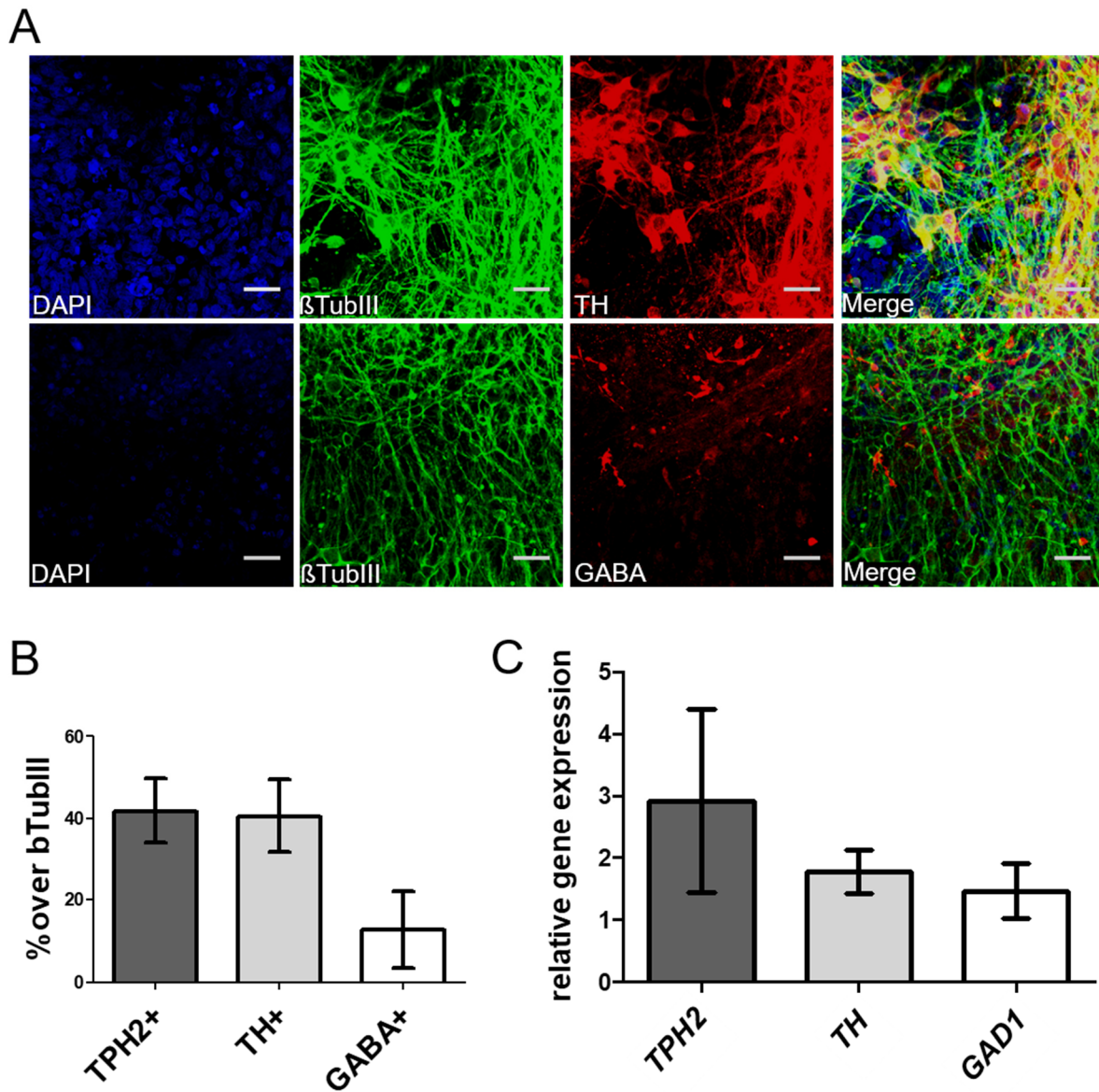
Figure 20: Specification of different neuronal subtypes.

(A) Representative IF staining of specific neuronal markers after 4-5 weeks of neuronal maturation (differentiation week 7-8). Pictures were taken using confocal microscopy. Scale bar: 50 µm. Cell nuclei were counterstained with DAPI. (B) Quantification of the amount of 5-HT specific (TPH2+), catecholaminergic (TH+) and GABAergic (GABA+) neurons within the neuronal culture (n=3 independent differentiations). (C) Relative gene expression levels of human iPSC-derived 5-HT specific (*TPH2*), catecholaminergic (*TH*) and GABAergic (*GAD1*) neurons (n=2 independent differentiations). Data is expressed as mean ± SEM.

3.2.3 Human iPSC-derived 5-HT specific neurons display phenotypes of median as well as dorsal raphe 5-HT specific neurons

Due to the specificity of CDH13 expression and its clinical implications, the expression of this protein was analysed in human iPSC-derived 5-HT specific neurons using SIM. Image acquisition and processing was done together with S. Wäldchen (Department of Biotechnology and Biophysics, Biocenter, University of Würzburg) and A. Forero (Division of Molecular Psychiatry, Center of Mental Health, University of Würzburg). Our results indicate that CDH13 is highly expressed in a subset of the TPH2+ neurons (Figure 21A) but is lacking from the majority of 5-HT specific neurons identified in our culture (Figure 21B). Additionally, CDH13 was expressed in TPH2-negative (TPH2-) neurons (Figure 21B). The high specificity of CDH13 was used as a marker for dorsal raphe cells in our human iPSC-derived neuronal culture. We observed the same expression pattern as previously detected in murine 5-HT specific neurons (Forero et al 2017), with CDH13 outlining both the soma and extending neurites (Figure 21A, C, D).
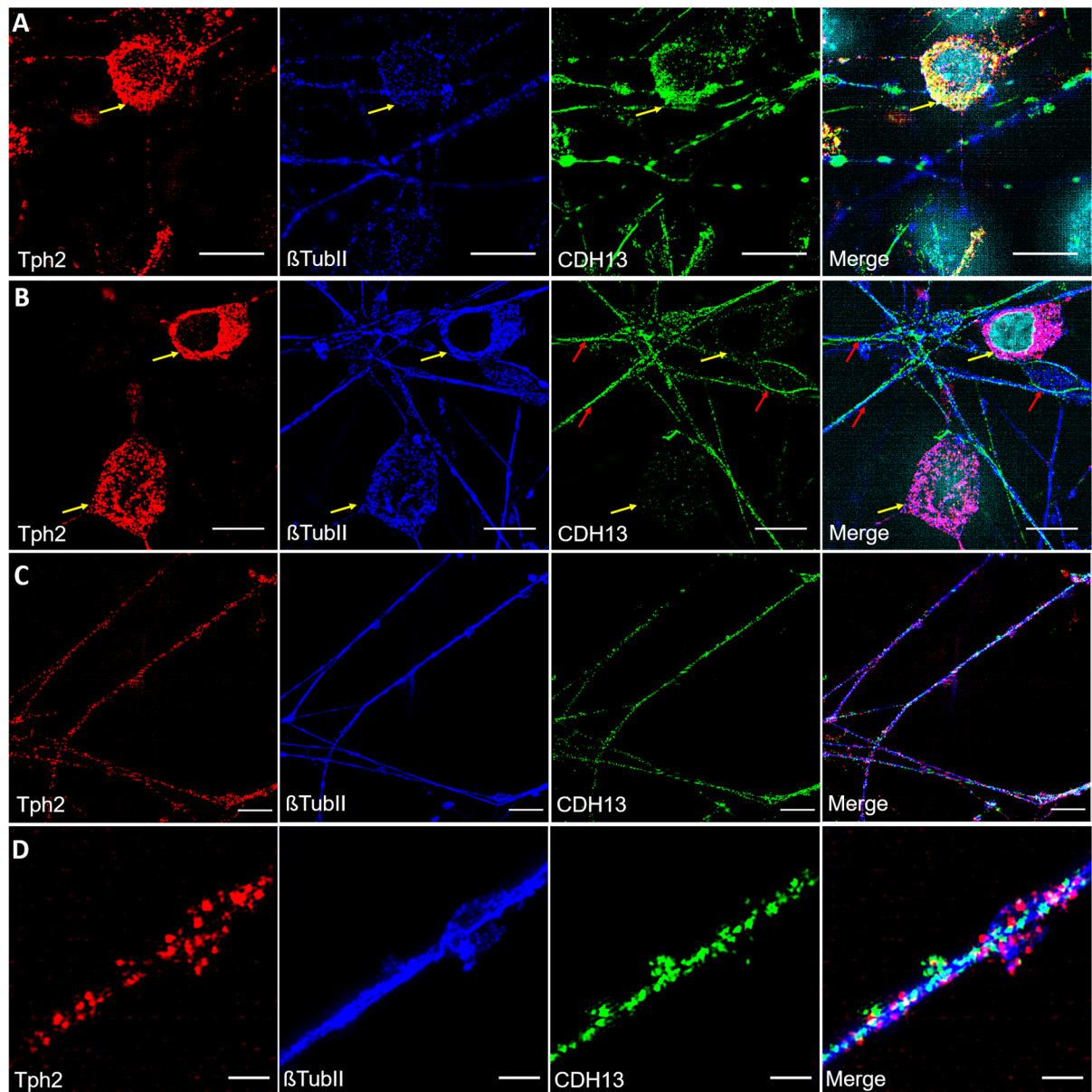
Figure 21: CDH13 expression in TPH2+ neurons using SIM.

(A) IF staining of a TPH2+ neuron which is positive for CDH13 (yellow arrows). (B) IF staining of TPH2+ neurons which are negative for CDH13 (yellow arrows). Additionally, ßtubIII+ fibers that are negative for TPH2 are immunoreactive for CDH13 and marked by a red arrow. (C) IF staining of a TPH2+ fibers being positive for CDH13. (D) Close-up image of (C). Scale bar: (A, B, C) 10 μm; (D) 2 μm.

A three-dimensional reconstruction of these CDH13+ 5-HT specific neurons shows two TPH2+ neurons in very close proximity with CDH13 expression at the contact region between them (Figure 22A; A`). This suggests a potential role in cell-cell interaction.
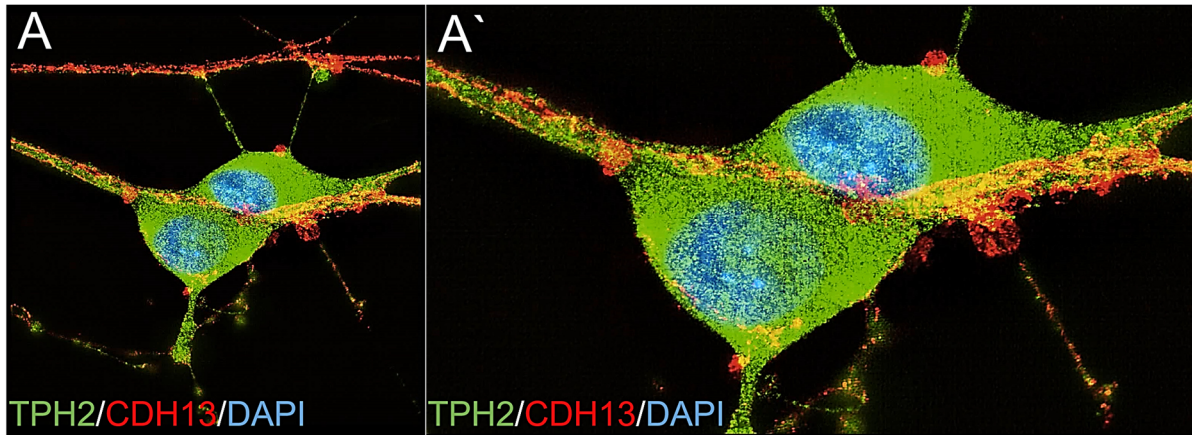
Figure 22: Three-dimensional reconstruction of CDH13+ 5-HT specific neurons.

(A) CDH13 is found in the membrane of TPH2+ neurons displaying a punctate pattern which suggests a potential role in cell-cell interaction. (A`) Close-up image of (A) reveals the distribution of CDH13 along soma and neurites of TPH2+ neurons. CDH13 is strongly expressed at the contact region between them.

3.2.4 Use of confocal and super-resolution imaging to reveal synaptic connectivity of 5-HT specific neurons

To further evaluate adequate synapse formation and connectivity among the differentiated 5-HT specific neurons, we performed confocal microscopy and *d*STORM, a super-resolution microscopy technique that would allow the visualization of synaptic structures (Figure 23). *d*STORM measurements were conducted at the Department of Biotechnology and Biophysics, together with S. Wäldchen and A. Forero. Here, neurons specifically stained for TPH2 were additionally analysed for the expression of synaptic proteins. To reveal the pre- and postsynaptic structure, we selected Bassoon, a marker for the presynaptic active zone; PSD-95, the major scaffolding protein in the excitatory postsynaptic density (PSD), and Homer, a PSD scaffolding protein. As shown in Figure 23A and B, Bassoon is not only expressed in axon terminals, but also evenly along the soma and processes of TPH2+ 5-HT specific neurons. Interestingly, these neurons show Bassoon expression in Map2+ dendrites (Figure 23A) and in close proximity to PDS-95 (Figure 23B). We next searched for the presence of synaptic structures by looking for areas where Bassoon and Homer were in close proximity. We found Alexa Fluor 647 for Bassoon and Alexa Fluor 532 for the labeling of Homer to be a suitable combination for the two-color *d*STORM analysis (Figure 23C). TPH2+ neurons were

targeted that express the presynaptic Bassoon, as well as the postsynaptically expressed Homer, with an overall more pronounced expression of Bassoon compared to Homer (Figure 23C-C´´). However, even if close proximity of contact points between Homer and Bassoon could be seen (Figure 23C´´), no typical bar structures illustrating synaptic transmission were found. The schematic illustration depicts the neuron's 5-HT release via an extrasynaptic somatodendritic (Figure 23D) and synaptic transmission (Figure 23E).
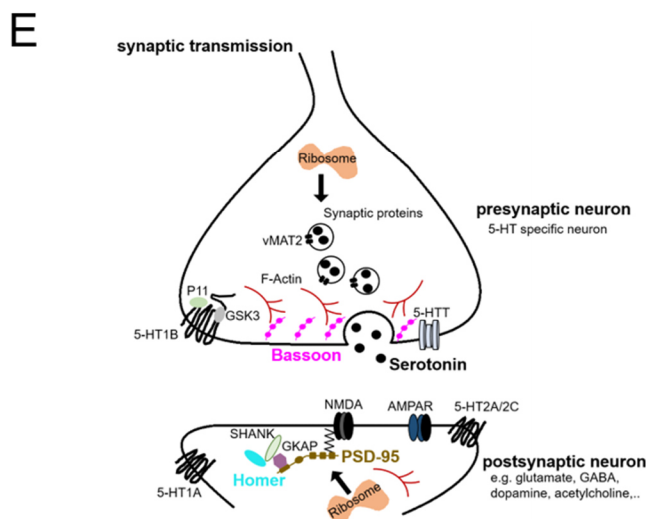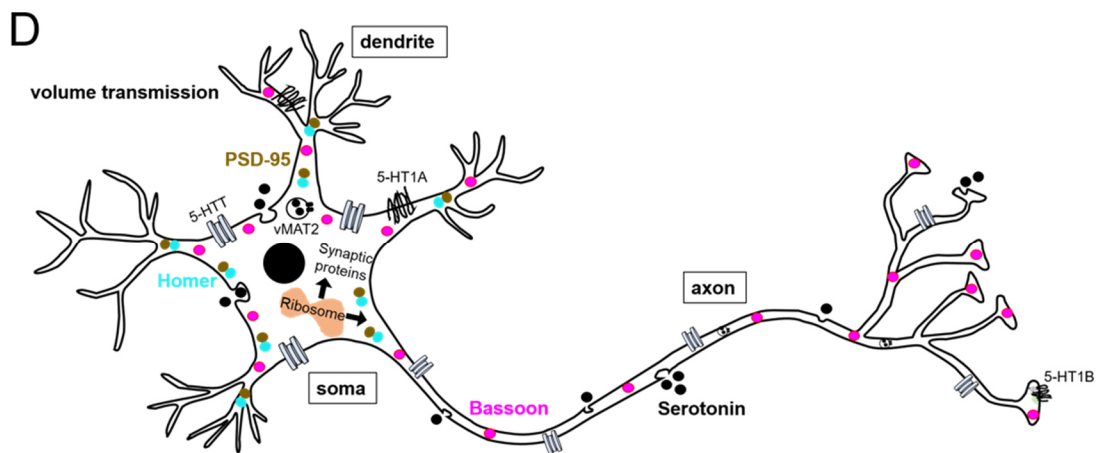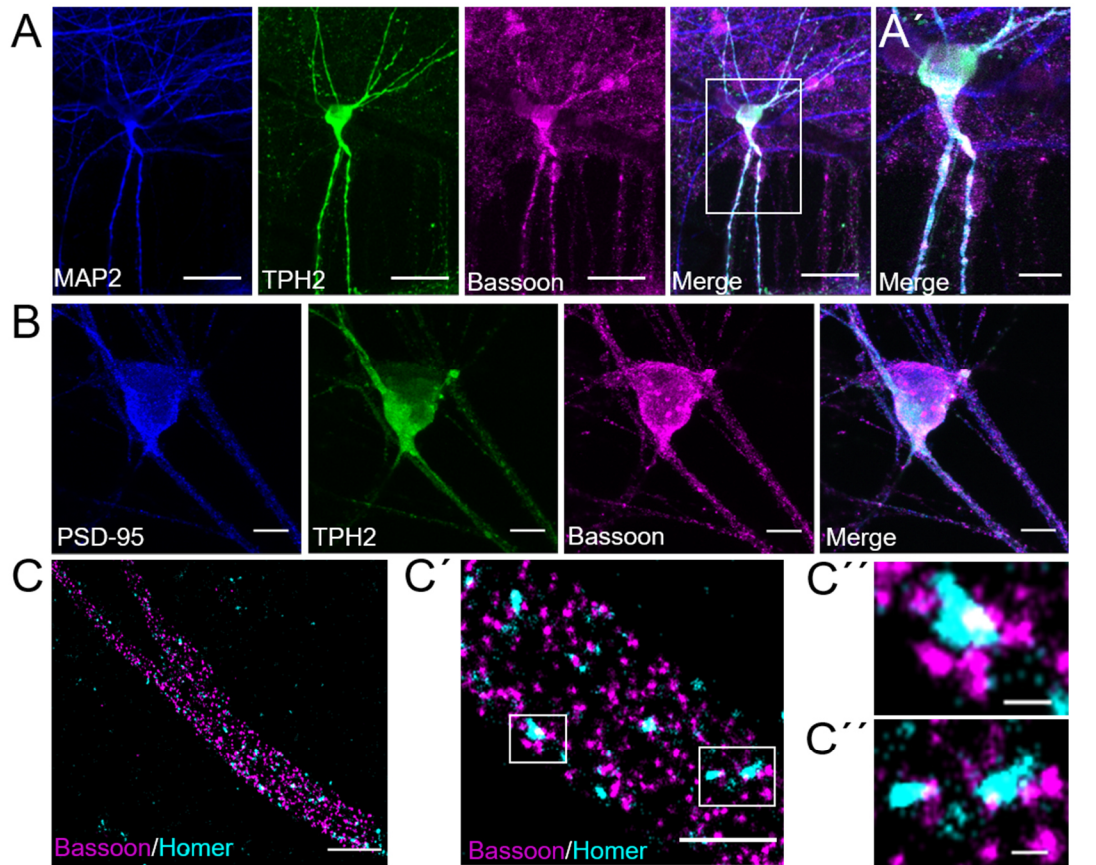
Figure 23: Protein assembly of pre- and postsynaptic markers in human iPSC-derived 5-HT specific neurons.

The use of confocal (A+B) and super-resolution (C) imaging to reveal synaptic connectivity of 5-HT specific neurons. (A) The presynaptic marker Bassoon is evenly expressed along soma and processes of TPH2+ human iPSC-derived neurons. (A´) Close-up image of (A). (B) Bassoon is localized in close proximity to the postsynaptic marker PSD-95 in dendrites and cell bodies of TPH2+ neurons. (C) dSTORM revealed a higher expression of Bassoon compared to the postsynaptic marker Homer in TPH2+ neurons. (C´) Close-up images of (C). (C´´) Example images illustrating contact points between Homer and Bassoon. Simplified schematic illustrations of Bassoon, PSD-95 and Homer expression in 5-HT release mechanisms: (D) extrasynaptic and (E) synaptic transmission. Scale bar: (A) 30 µm; (A´) 10 µm; (B) 10 µm; (C) 2 µm; (C´) 1 µm and (C´´) 150 nm.

3.2.5 Electrophysiological signature of iPSC-derived 5-HT specific neurons

Electrophysiological examination of human iPSC-derived neurons was done together with Prof. E. Wischmeyer and Dr. S. Kollert (Institute of Physiology, Molecular Electrophysiology, University of Würzburg). Single-cell patch-clamp recordings were performed to investigate the functional maturation of human iPSC-derived 5-HT specific neurons. Cultured neurons were collected from 24-well culture plates and whole-cell recordings (Hamill et al 1981) were performed weekly over a period of 6 weeks (w; 3 independent differentiations). Over the whole measurement period, voltage-gated ion currents, repetitive firing elicited by current injections, as well as spontaneous firing in neurons were observed. Voltage steps from -100 to +70 mV generated inward Na^+ and outward K^+ currents (Figure 24A), responsible for the induction of action potentials. Current injections from -120 to +120 pA elicited action potentials (Figure 24B and C). Neurons displayed two typical modes of activity: bursts with intercalated pauses or activity with constant frequency (Figure 24D). In the first 4 weeks of maturation the amplitude of the action potentials significantly increased (amplitude: w1: 61.52±5.57 mV, n=14; w2: 67.18±5.42 mV, n=16; w3: 80.67±3.98 mV, n=22; w4: 86,56±5.41 mV, n=22; w5: 87.62±3.64 mV, n=17; w6: 87.48±3.71 mV, n=5; $F_{(5,90)}$=4.538, P=0.001) (Figure 24E), while the duration of action potentials decreased (HHW: w1: 7.22±1.31 ms, n=14; w2: 7.02±1.24 ms, n=16; w3: 4.13±1.01 ms, n=22; w4: 3.09±0.3 ms, n=22; w5: 2.83±0.57 ms, n=17; w6: 2.52±0.34 ms, n=5; $F_{(5,90)}$=4.453, P=0.0011) (Figure 24F). The membrane potential did not significantly change over time (mV: w1: -48.75±1.98 mV, n=14; w2: -50±1.14 mV, n=16; w3: -54.85±2.37 mV, n=22; w4: -54.29±1.28 mV, n=22; w5: -53.88±1.52 mV, n=17; w6: -53.9±1.94 mV, n=5; $F_{(5,90)}$=1.592, P=0.1705) (Figure 24G) as well as the spike frequency (frequency: w1: 1.92±1.74 Hz, n=4; w2: 0.83±0.69 Hz, n=5; w3: 0.92±0.7 Hz, n=8; w4: 3.34±0.9 Hz, n=15; w5: 1.83±0.52 Hz, n=12; w6: 0.6±0.23 Hz, n=3; $F_{(5,41)}$= 1.447, P=0.2283) (Figure 24H).

The frequency of measured action potentials varied over time between 0.5 and 4 Hz, but always matched the criteria for 5-HT specific neuron specification and was less than 12 Hz.
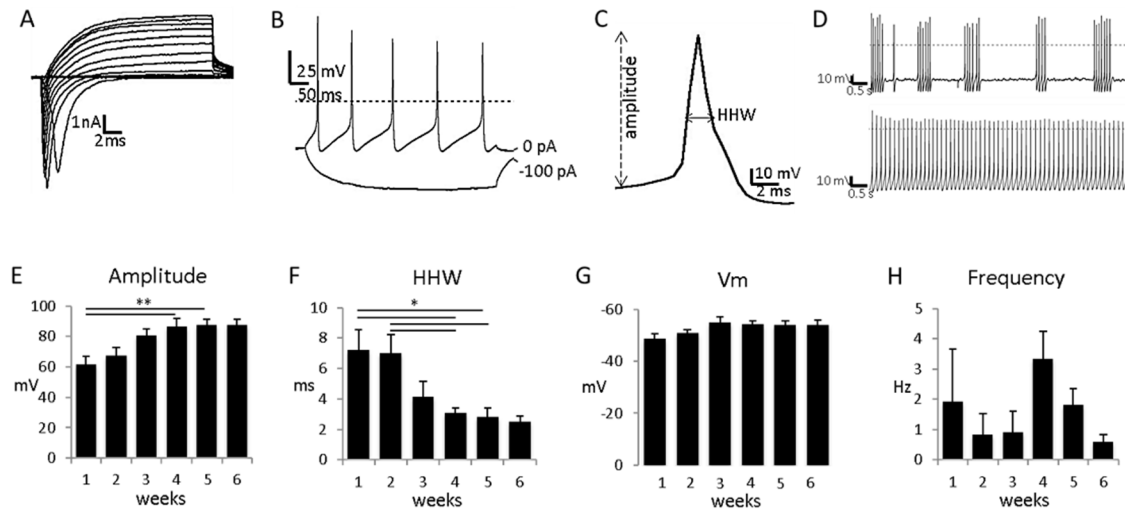

Figure 24: Electrophysiological properties of human iPSC-derived 5-HT specific neurons.
(A) Voltage-gated Na^+ and K^+ currents triggered by voltage steps from -100 to +70 mV at a holding potential of -80mV. (B) Action potentials were induced upon injection of current steps from -120 to +120 pA. Depicted are traces at -100 pA and at 0 pA with spontaneous action potentials. (C) Single action potential on an expanded time scale. Amplitude, HHW and afterhyperpolarization are indicated. (D) Neurons display two typical modes of activity: bursts with intercalated pauses (upper trace) or activity with constant frequency (lower trace). (E-H) Bar graphs of electrophysiological properties of human iPSC-derived 5-HT specific neurons over a time period of 6 weeks. (E) AP amplitude, (F) half-height width (HHW), (G) resting membrane potential and (H) AP frequency. Data is expressed as mean ± SEM. Statistical differences were found using a one-way ANOVA followed by a Newman-Keuls Multiple Comparison Test. Differences were considered to be significant when $P \leq 0.05$ (* p=0.01 to 0.05; ** p=0.001 to 0.01; *** p<0.001).

3.3 The effect of *SLC2A3* CNVs on GLUT3 expression, glucose metabolism and synapse formation

3.3.1 The effects of *SLC2A3* CNVs on GLUT3 expression

Basal *SLC2A3* expression was found to be significantly increased in human iPSCs carrying a duplication of this gene (p ≤ 0.001), while human iPSCs carrying a *SLC2A3* deletion show decreased mRNA levels of this gene, compared to control cells (p ≤ 0.01) and neurons carrying a duplication of *SLC2A3* (p ≤ 0.001) (Figure 25A). Additionally, *SLC2A3* levels were increased in human iPSC-derived neurons carrying the duplication, compared to control neurons (p ≤

0.001) (Figure 25B). However, there is no difference between control neurons and neurons carrying a deletion of this gene.
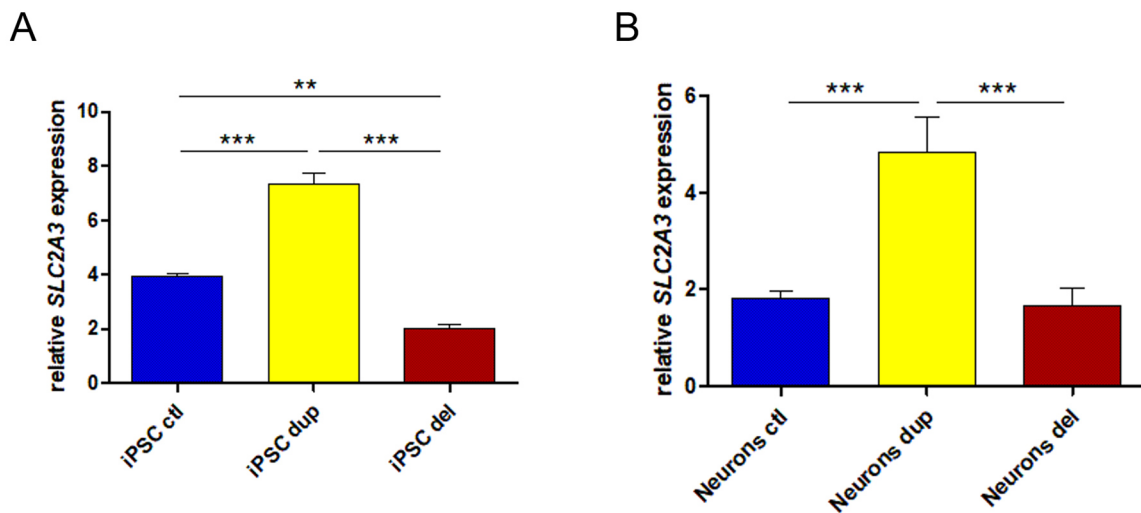

Figure 25: *SLC2A3* expression levels in human iPSCs and iPSC-derived neurons.

(A) *SLC2A3* expression is significantly increased and decreased in human iPSCs carrying a duplication or a deletion of this gene, respectively, compared to control iPSCs. (B) Neurons carrying a duplication of *SLC2A3* show higher mRNA levels compared to control neurons. However, there is no difference between control neurons and neurons carrying a deletion of this gene. Data illustrated by a column bar graph is normally distributed. Data is expressed as mean ± SEM. Statistical differences were found using one-way ANOVA, Kolmogorov–Smirnov and Bonferroni's Multiple Comparison Test (A: ctl n=5, dup n=7, del n=6; B: ctl n=10, dup n=10, del n=7).

The expression and the distribution pattern of GLUT3 under normal culture conditions was analysed in iPSCs as well as iPSC-derived neurons. We used two specific antibodies to visualize GLUT3: 1) one that binds to an intracellular domain at the C-terminus (C-GLUT3) and visualizes not only active GLUT3 incorporated into the membrane, but also internal storage of this protein as well as 2) an antibody that binds to the extracellular domain at the N-terminus of GLUT3 (N-GLUT3).

As illustrated in Figure 26, human control iPSCs and iPSCs carrying a duplication or a deletion of *SLC2A3* express N-GLUT3, which exhibits a uniform pattern along each cell of the colony.
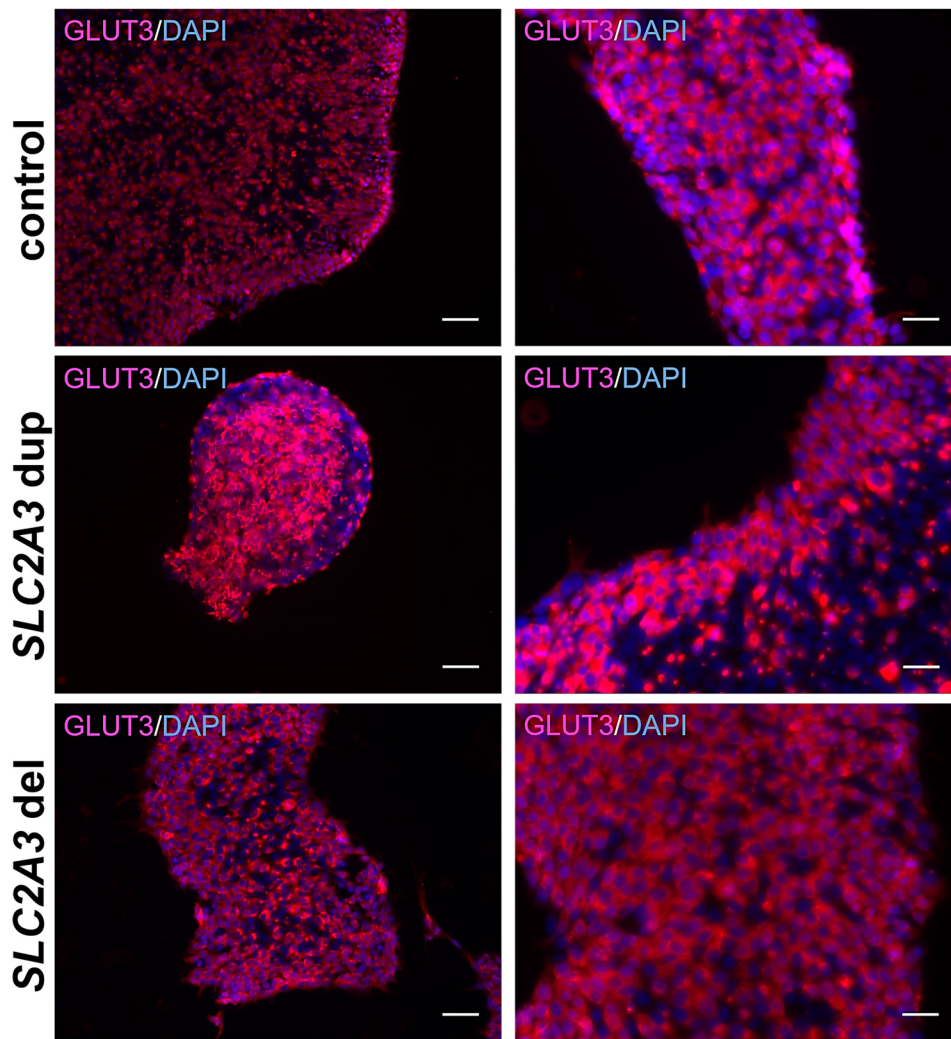
Figure 26: IF staining of the extracellular N-terminal domain of GLUT3 in human iPSCs.
Human control iPSCs as well as iPSCs carrying *SLC2A3* CNVs express GLUT3. Stem cell colonies exhibit a distribution pattern along the whole cell. Pictures were taken using epifluorescence microscopy. Scale bar: 50 µm. Cells were counterstaining with DAPI.

Since GLUT3 is known to be the neuronal glucose transporter, we next investigated the expression and distribution of C-GLUT3 (Figure 27) and N-GLUT3 (Figure 28) in ßTubIII+ neurons. Illustrated in Figure 28, human iPSC-derived neurons express C-GLUT3 evenly along their neurites and in the soma.
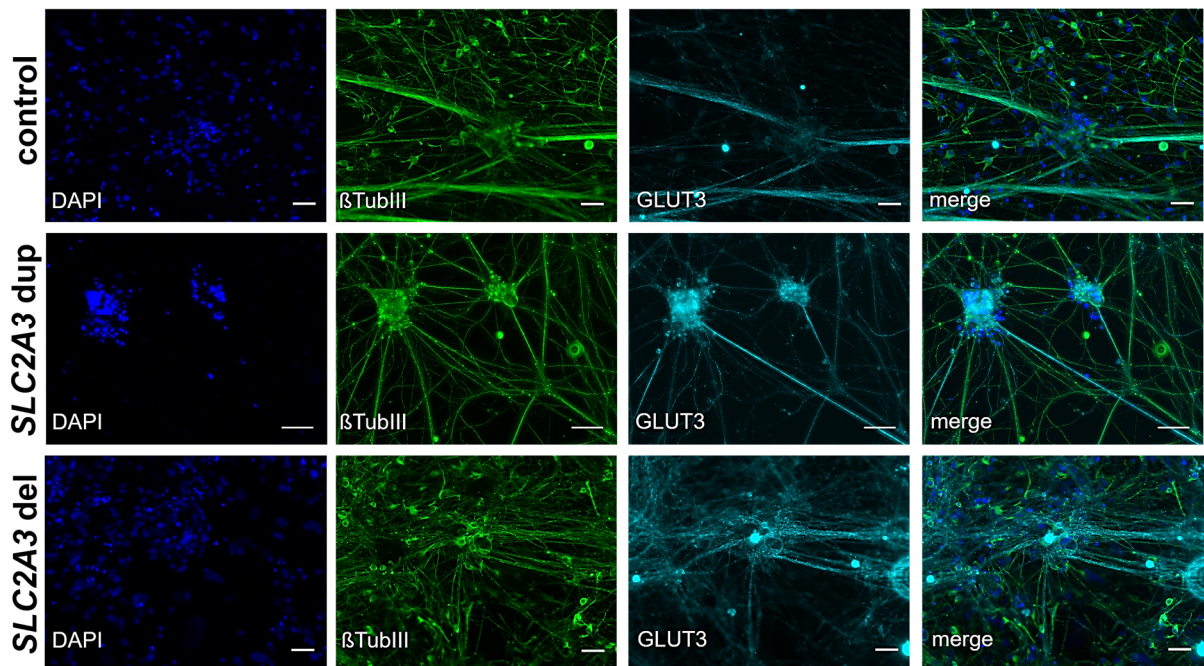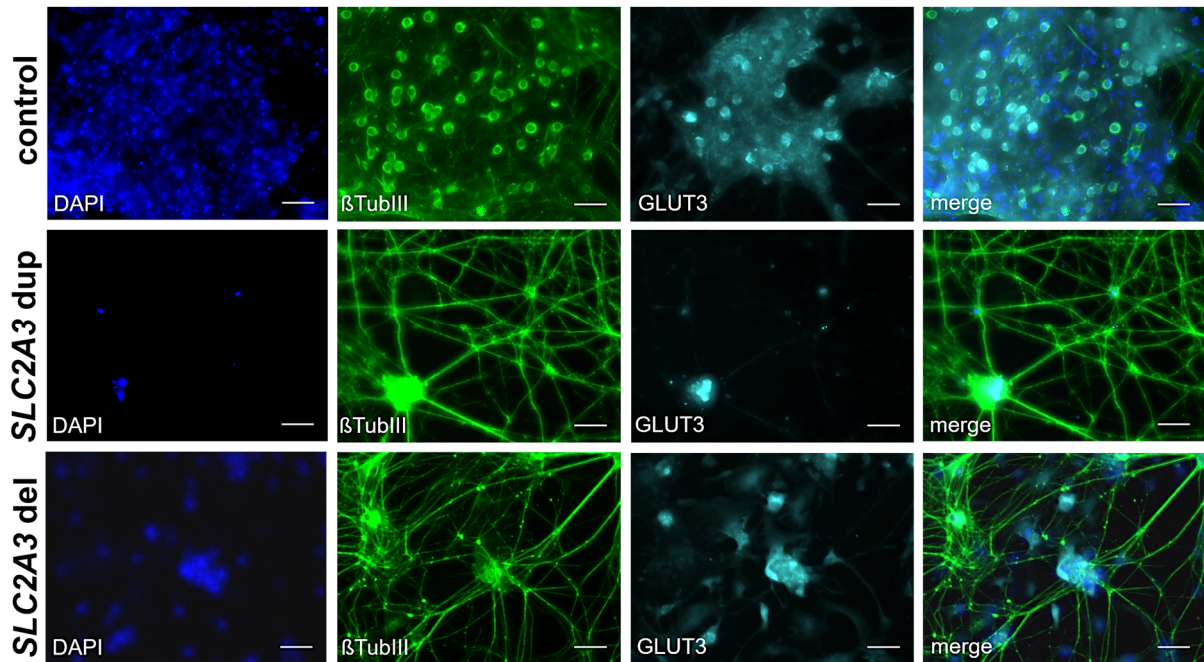
Figure 27: IF of the intracellular C-terminal domain of GLUT3 in human iPSC-derived neurons.
Human control iPSC-derived neurons as well as neurons carrying *SLC2A3* CNVs express GLUT3 along the neurites and soma. The used antibody binds intracellularly to the C-terminus of GLUT3. Pictures were taken using epifluorescence microscopy. Scale bar: 50 µm. Cells were counterstained with DAPI.

Additionally, ßTubIII+ neurons express N-GLUT3 along their neurites and in the soma as well (Figure 28). However, the expression seems to be more prominent in the cell body.
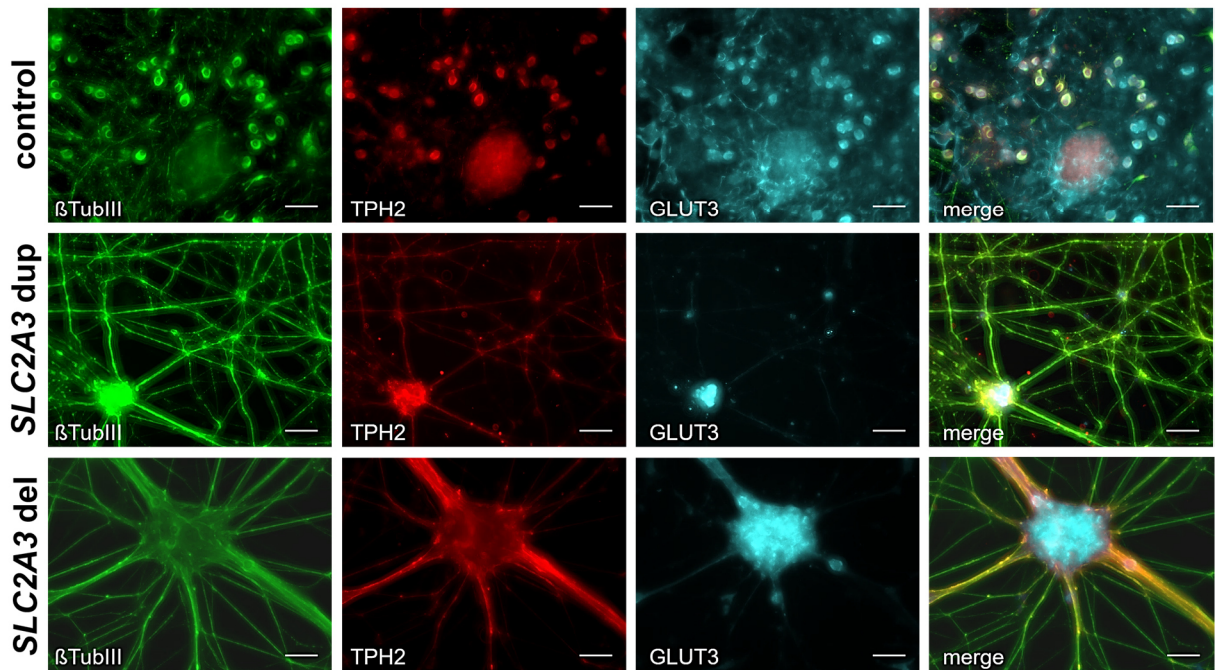
Figure 28: IF of the extracellular N-terminal domain of GLUT3 in human iPSC-derived neurons.
Human control iPSC-derived neurons as well as neurons carrying *SLC2A3* CNVs express GLUT3 along the neurites and soma with a more prominent expression in the soma. Cells were labelled using an antibody binding to the extracellular domain of GLUT3 at the N-terminal region. Pictures were taken using epifluorescence microscopy. Scale bar: 50 µm. Cells were counterstained with DAPI.

To prove that generated human iPSC-derived 5-HT specific neurons also express GLUT3, we stained cells with the N-terminal specific GLUT3 antibody. In line with the previous results, GLUT3 expression was found along neurites and in the soma (Figure 29).

Figure 29: IF of the extracellular N-terminal domain of GLUT3 in human iPSC-derived 5-HT specific neurons.

Human control iPSC-derived 5-HT specific neurons as well as 5-HT specific neurons carrying *SLC2A3* CNVs express GLUT3 along the neurites and soma with a more prominent expression in the soma. The used antibody binds extracellularly to GLUT3. Pictures were taken using epifluorescence microscopy. Scale bar: 50 µm.

To analyse if *SLC2A3* CNVs affect basal protein levels, Western blotting was performed. In a preliminary study, we tested several antibodies in several cell types in order to find the most suitable one for follow-up studies. As illustrated in Figure 30A, an antibody was used that binds to the C-terminus of GLUT3 (C-GLUT3). However, no GLUT3 signal could be observed in this Western blot. Furthermore, samples were labelled using an antibody binding to the N-terminal region of GLUT3 (Figure 30B: N-GLUT3). Finally, GLUT3 could be detected at a molecular weight of 54 kDa. Additionally, unspecific bands were observed at an approximate molecular weight of 48 kDa in fibroblasts and iPSCs. GAPDH was used as a loading control and was visualized with a size of 36 kDa in both trials.
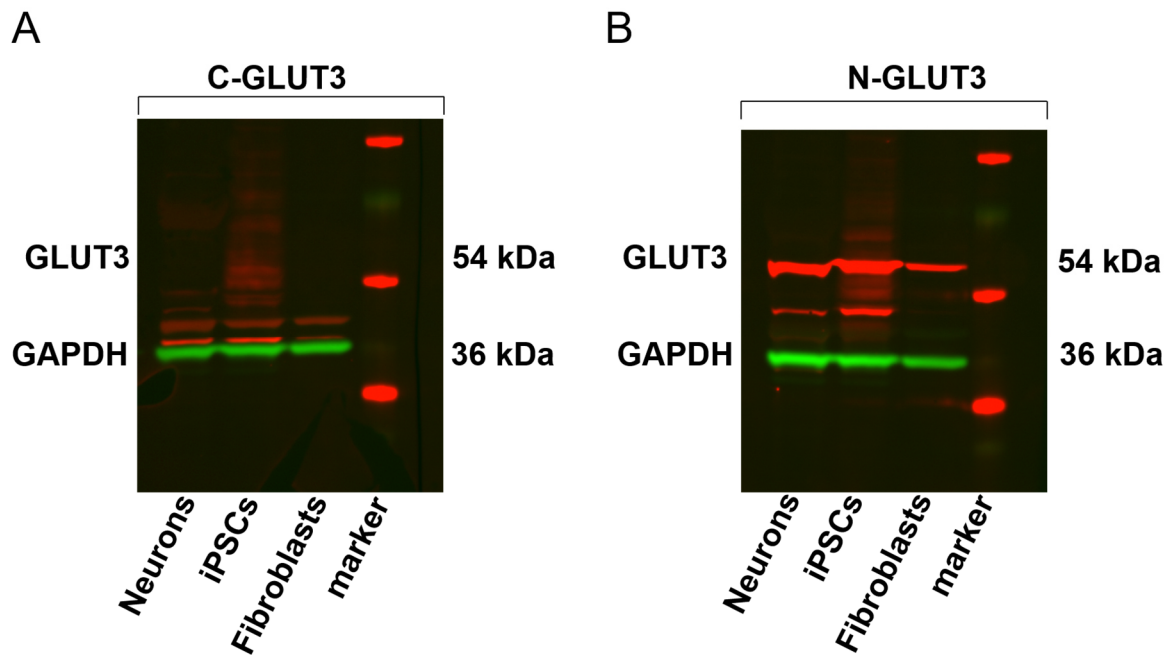
Figure 30: GLUT3 expression in different cell types using two specific antibodies illustrated by Western blot.

The expression of GLUT3 in fibroblasts, iPSCs and iPSC-derived neurons was analysed via Western blot using two GLUT3 specific antibodies. GAPDH was used as a loading control and was visualized with a size of 36 kDa in both trials. (A) The used antibody should bind to the C-terminus of GLUT3 (C-GLUT3). No signal for GLUT3 could be observed in this Western blot. (B) Samples were labelled using an antibody binding to the N-terminal region of GLUT3 (N-GLUT3). GLUT3 could be specified at a molecular weight of 54 kDa. In fibroblasts and iPSCs unspecific lanes were observed at an approximate molecular weight of 48 kDa.

Subsequent experiments were therefore performed with the antibody against N-GLUT3 (Figure 31A). We then aimed to analyse the impact of *SLC2A3* CNVs on GLUT3 expression in iPSC-derived neurons. According to Figure 31B, normalized relative protein levels of GLUT3 were decreased in differentiated neurons carrying a deletion of *SLC2A3*, compared to control neurons (p=0.0383) and neurons carrying a duplication of *SLC2A3* (p=0.0033). However, neurons carrying a duplication did not differ from control neurons (p=0.2337).
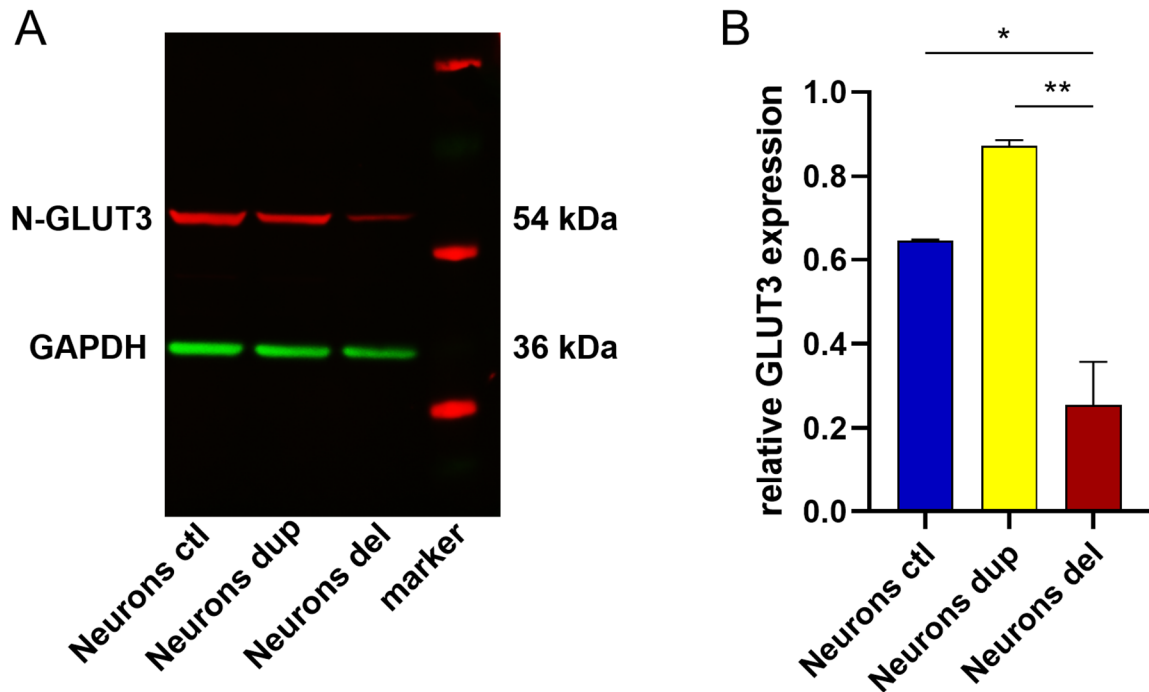
Figure 31: Decreased levels of N-GLUT3 expression in human iPSC-derived neurons.

(A) GLUT3 could be detected at a molecular weight of 54 kDa. The loading control GAPDH, with a size of 36 kDa, was found below the protein of interest. (B) The normalized relative protein level of GLUT3 was found to be decreased in differentiated neurons carrying a deletion of *SLC2A3*, compared to control neurons (p=0.0383) and neurons carrying a duplication of *SLC2A3* (p=0.0033). Data is expressed as mean ± SEM. Data is normally distributed proven by Shapiro-Wilk test. Data is expressed as mean ± SEM. Statistical differences were found using one-way ANOVA and Bonferroni's Multiple Comparison Test (Neurons ctl: n=2; Neurons dup/Neurons del: n=3). Differences were considered to be significant when P≤0.05 (* p=0.01 to 0.05; ** p=0.001 to 0.01; *** p<0.001).

To complement our finding of altered GLUT3 levels by a *SLC2A3* deletion in human iPSC-derived neurons, we used *d*STORM to precisely reveal the specific subcellular localisation of GLUT3. Measurements were conducted together with S. Wäldchen (Department of Biotechnology & Biophysics, University of Würzburg). Here, we measured the expression of GLUT3 regardless of the neuronal subtype by labelling the extracellular GLUT3 N-terminal domain. Only the protein incorporated into the membrane and thus the active form of the glucose transporter was measured. Human iPSC-derived neurons carrying a duplication of *SLC2A3* displayed a similar protein expression level of GLUT3, compared to control neurons (Figure 32). However, the deletion of *SLC2A3* lead to a decreased relative GLUT3 level, compared to control condition and cells carrying a duplication of this gene (p ≤ 0.001).
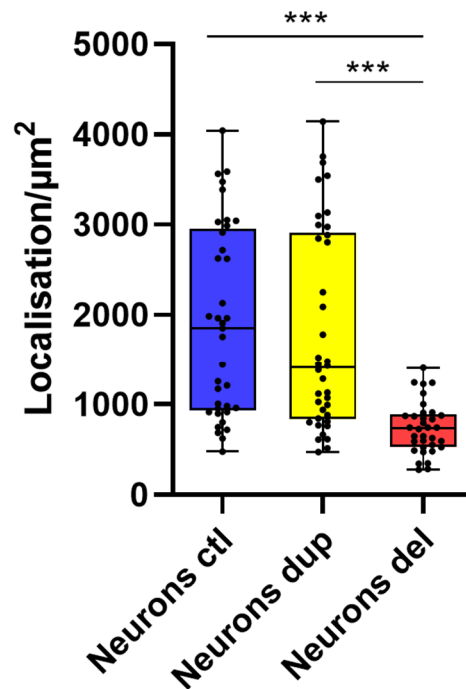
Figure 32: Relative GLUT3 protein expression is affected by a deletion of *SLC2A3* in human iPSC-derived neurons.

Localisation data of GLUT3 revealed by *d*STORM were used to calculate localisations per µm^2 for human iPSC-derived neurons carrying CNVs of *SLC2A3* and data was illustrated by a boxplot. Relative GLUT3 expression in human iPSC-derived neurons carrying a duplication of *SLC2A3* was similar to those found in control neurons and thus was not influenced by a duplication of *SLC2A3*. However, a deletion of *SLC2A3* lead to decreased relative GLUT3 levels in neurons carrying a deletion of *SLC2A3* compared to control cells and cells carrying a duplication of this gene (p ≤ 0.001). Except of "Neuron del", revealed data is not normally distributed. Data is expressed as median ± MAD. Data distribution and statistical differences were found using Kruskal-Wallis test, Kolmogorov–Smirnov and Dunn's multiple comparisons test (n=5 independent experiments). Differences were considered to be significant when P≤0.05 (* p=0.01 to 0.05; ** p=0.001 to 0.01; *** p<0.001).

3.3.2 The effects of glucose deprivation on mRNA and protein expression of human iPSC-derived neurons carrying either a duplication or a deletion of *SLC2A3*

In order to analyse the effect of glucose deprivation on GLUT3 expression, human iPSC-derived control and patient neurons were starved for 8 days (-Glc). Specifically, the impact of glucose deprivation on protein levels was examined using *d*STORM together with S. Wäldchen. However, glucose deprivation had no significant effect on GLUT3 expression in human controls as well as neurons carrying *SLC2A3* CNVs (Figure 33A and B). Since glucose deprivation is known to influence neuronal health, human iPSC-derived neurons were additionally treated with different glucose concentrations for 48 h to resemble normal (110

ng/mL), hypoglycaemic (27.5 ng/mL) and hyperglycaemic (220 ng/mL) conditions found *in vivo* and *in vitro* (Duelli et al 1999, Hou et al 2007, Lee et al 2000, Nagamatsu et al 1994, Shen et al 2009, Uehara et al 1997). Treatment with different glucose concentrations did not affect GLUT3 expression in control and patient neurons (Figure 33C).
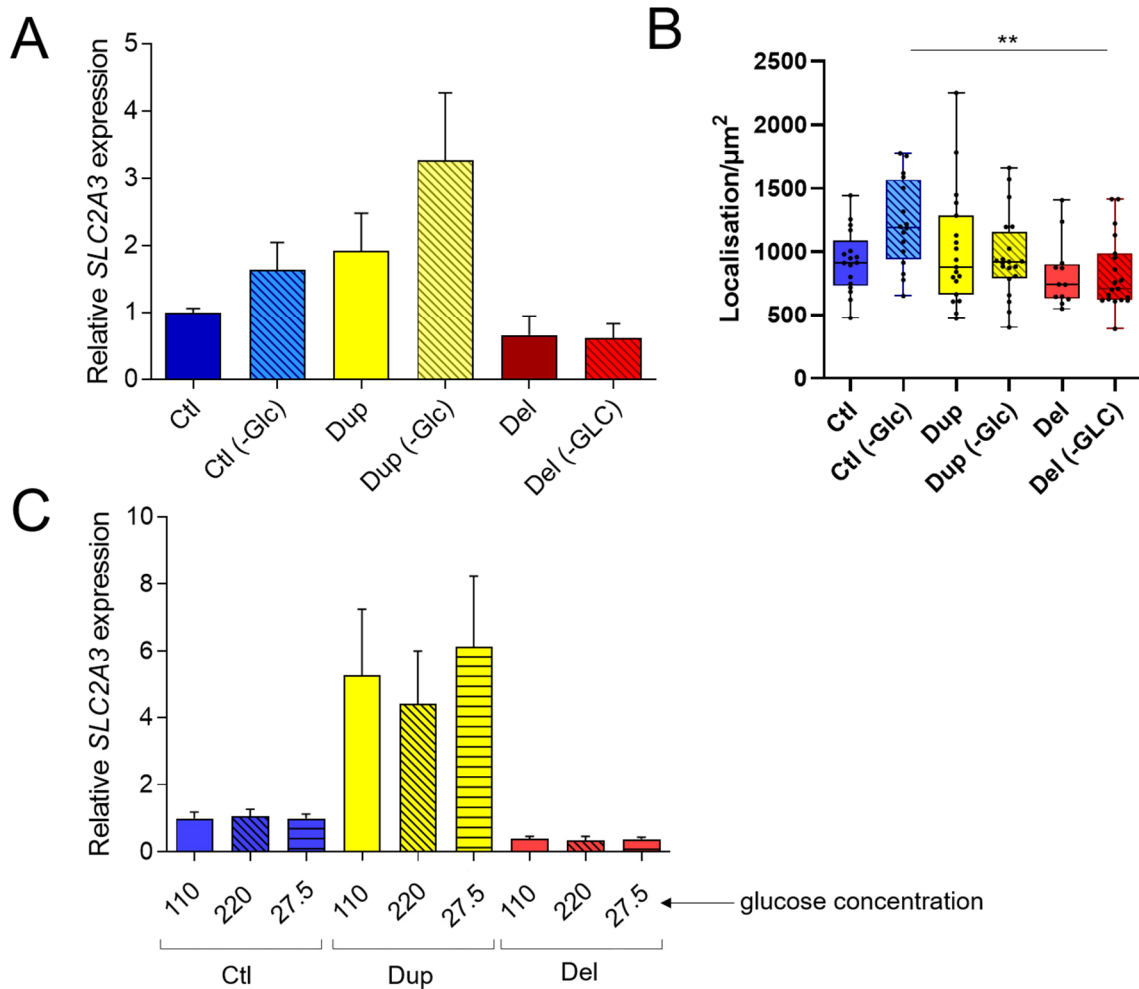

Figure 33: Glucose deprivation has no significant effect on *GLUT3* expression in human iPSC-derived controls as well as neurons carrying *SLC2A3* CNVs.

(A+B) 8 days of glucose deprivation did not affect GLUT3 in human iPSC-derived control and *SLC2A3* CNV-carrier neurons. (A) Data illustrated by a column bar graph is normally distributed and expressed as mean ± SEM. Statistical analysis was done using one-way ANOVA, Shapiro-Wilk test and Bonferroni's Multiple Comparison Test (ctl n=4, dup n=5, del n=3; B: ctl (-Glc) n=4, dup (-Glc) n=5, del (-Glc) n=3). (B) Data illustrated by a boxplot is normally distributed for all groups, expect of "Dup (-Glc)" and "Del (-Glc) and expressed as median ± MAD. Statistical analysis was done using Kruskal-Wallis test, Kolmogorov–Smirnov and Dunn's multiple comparisons test (n=3 independent experiments (C) 48 h of glucose deprivation did not affect GLUT3 expression in human iPSC-derived control and *SLC2A3* CNV-carrier neurons. Data is normally distributed, except of the group "Dup 220". Data is expressed as median ± MAD. Statistical analysis was done using Kruskal-Wallis test, Shapiro-Wilk test and Dunn's

multiple comparisons test (n=3 independent experiments). Differences were considered to be significant when P≤0.05 (* p=0.01 to 0.05; ** p=0.001 to 0.01; *** p<0.001).

3.3.3 The effects of *SLC2A3* CNVs on synapse formation in human iPSC-derived neurons

In this study, the effects of altered *SLC2A3* expression on neurodevelopmental processes, such as the assembly of synaptic proteins in neurons, were assessed. To this end, we analysed the expression of the presynaptic protein Bassoon and the postsynaptic protein Homer in human iPSC-derived neurons using *d*STORM. Measurements were conducted together with S. Wäldchen.

Specifically, localisations per μm^2 of Bassoon and Homer were calculated for human iPSC-derived neurons carrying *SLC2A3* CNVs (Figure 34). Localisation of Bassoon was calculated for neurons in general as well as 5-HT specific neurons (Figure 34A), while the localisation of Homer was just measured for total neurons in the cell culture system (Figure 34B). Regarding the localisation of Bassoon and Homer per μm^2, no difference was found in human iPSC-derived neurons as well as 5-HT specific neurons carrying a duplication or a deletion, compared to control neurons.
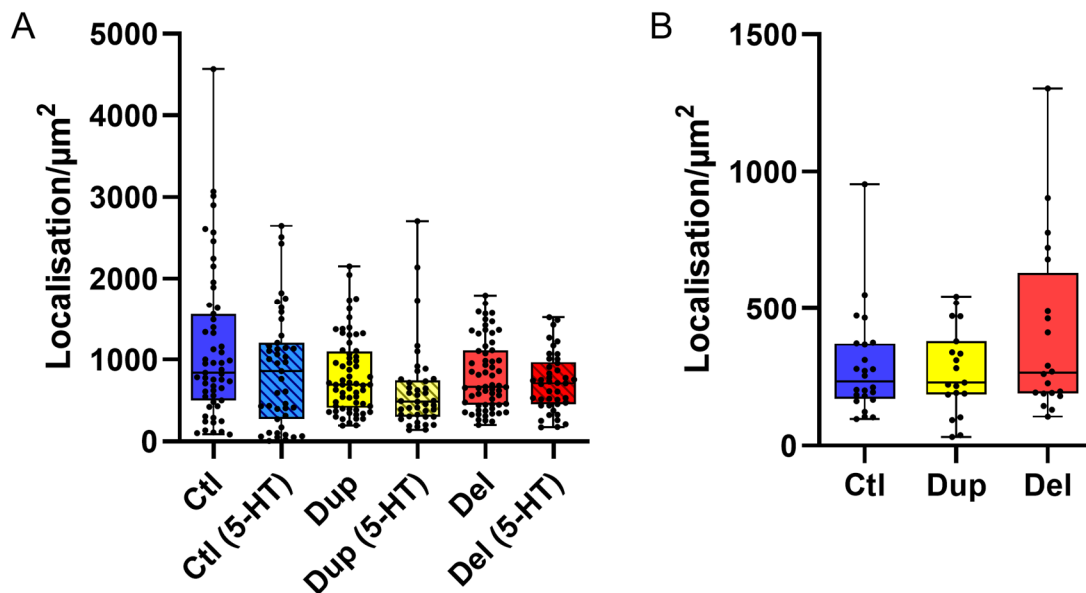

Figure 34: Relative Bassoon expression in human iPSC-derived neurons.

Localisation per μm^2 of (A) Bassoon and (B) Homer using *d*STORM. *SLC2A3* CNVs did not affect the expression of pre- and postsynaptic proteins Bassoon and Homer in human iPSC-derived neurons as well as in 5-HT specific neurons (Bassoon only). Data was illustrated by a boxplot and expressed as median ± MAD. Data distribution and

statistical analysis was done using Kruskal-Wallis test, Kolmogorov–Smirnov and Dunn's multiple comparisons test (n=4 independent experiments and n=2 for 5-HT groups).

4. Discussion

The pathogenesis of neuropsychiatric disorders is influenced by a complex interplay of environmental and genetic factors. The search of genetic risk factors underlying ADHD dysfunction has considerably advanced through several GWAS and led to the discovery of risk variants of the gene *SLC2A3*, which encodes the neuronal glucose transporter GLUT3 (Lesch et al 2011, Merker et al 2017a). In this thesis, the use of human iPSC enabled us to generate patient-derived 5-HT specific neurons, with the aim to investigate the functional consequences of disease-linked common and rare variants in human neurons of defined specification, e.g. 5-HT specific neurons. Here, we focus on the effects of CNVs on *SLC2A3* and GLUT3: particularly, we did not only analyse the effects of *SLC2A3* CNVs on basal *SLC2A3* and GLUT3 expression, but additionally the impact of those CNVs on the coping strategies of human neurons to glucose deprivation, hyper- and hypoglycaemic conditions as well as on the assembly of proteins associated to synapse formation.

Using high-end fluorescence imaging including super-resolution microscopy in combination with electrophysiological and molecular biological techniques we revealed the following major findings:

1) Human iPSCs display the characteristics of fully reprogrammed human PSCs, such as ESC-like morphology and growth behaviour, the ability to differentiate into each cell type of the human body, an unchanged karyogram and the expression of pluripotency-specific markers.

2) Human iPSCs are able to differentiate into a neuronal subtype that expresses 5-HT specific markers, exhibits the electrophysiological signature characteristic of 5-HT specific neurons and forms synapses reflected by the expression of pre- and postsynaptic proteins, such as Bassoon and Homer. Additionally, a subpopulation of CDH13+/TPH2+ cells might be indicative of dorsal raphe neurons.

3) In iPSC-derived neurons, *SLC2A3* CNVs influence the expression of GLUT3 both at the mRNA and protein level. However, this altered expression does not seem to affect coping mechanisms of neurons initiated by metabolic stress events, such as glucose deprivation, nor the assembly of proteins involved in the synaptic machinery.

4.1 Generation of human iPSC lines carrying CNVs of *SLC2A3*

An initial genome-wide screening approach for CNVs in ADHD implicated a duplication and a deletion of *SLC2A3*. This preliminary study, conducted in our laboratory, examined the effect of a *SLC2A3* duplication on mRNA and protein expression levels in Epstein–Barr virus-transformed lymphoblastoid cell lines and native peripheral blood mononuclear cell samples from duplication carriers with ADHD (Merker et al 2017a). While there was an effect seen on a mRNA level, a *SLC2A3* duplication had no effect on protein levels. However, it could not be discarded that the effect may be different in other cellular types which are more related to ADHD pathophysiology. Indeed, GLUT3 is known as the neuronal glucose transporter, and therefore there was a need for a patient-derived neuronal cell culture model. The discovery of artificially derived pluripotent stem cells by the ectopic expression of pluripotency-associated transcription factors in adult cells circumvented the difficulties of other PSC models (Takahashi et al 2007). These days, iPSCs have become a common tool to generate patient-specific cell and tissue models to reveal molecular mechanisms underlying the pathogenesis of diseases, including neurodevelopmental disorders (Halevy et al 2015, Mariani et al 2015).

In this regard, we generated human iPSCs from dermal fibroblasts of clinically diagnosed ADHD patients carrying structural variations of *SLC2A3*. The reprogramming strategy we chose was the single-stranded SeV, since it displayed an incredibly higher reprogramming efficiency, compared to our previous attempts using mRNA technology. To prove the persistence of the *SLC2A3* CNVs in our generated iPSCs, we collaborated with the company ATLAS Biolabs GmbH. This company offers a service including the Affymetrix CytoScan HD Array which presented the most relevant coverage of this specific type of structural variation. Our results confirmed that one human iPSC line carries a hemizygous CNVs of *SLC2A3* (CN=1) and one cell line a heterozygous CNV of *SLC2A3* (CN=3) at the gene locus p13.31 of chromosome 12, while one cell line shows a normal CN of 2.00 (homozygous). Thus, human iPSCs carry a gain or alternatively a loss of the *SLC2A3* gene locus with a size of 120 kbp (chr12: 8,004,411-8,124,048; hg19), where the duplicated or deleted chromosomal region comprises the complete gene locus of *SLC2A3* and the initial exons of *SLC2A14*, a paralog of *SLC2A3*. Interestingly, the findings of the structure of the duplicated chromosomal region are in line with those of the previously conducted GWAS (Lesch et al 2011, Merker et al 2017a). Therefore, reprogramming did not induce genomic alterations and no chromosomal and structural alterations were detected. We generated safe and fully reprogrammed human iPSCs that can be used to obtain any cell type of the human organism.

4.2 Establishment of a robust and reliable differentiation protocol to generate 5-HT specific neurons

The use of iPSCs as an alternative to ESCs allows the creation of donor-specific cells, therefore improving the study of complex disorders (Lu et al 2015, Mauritz et al 2008, Vadodaria et al 2015). The 5-HT system is known to be highly involved in the pathogenesis of multiple neuropsychiatric disorder; however, even if there have been several approaches to differentiate human iPSCs into dopaminergic, glutaminergic and GABAergic neurons (Intoh et al 2016, Merkle et al 2015, Sánchez-Danés et al 2012, Yang et al 2017, Yu et al 2014), little is still known about the differentiation into 5-HT specific neurons and their regional subtypes (Lu et al 2015, Vadodaria et al 2015). Therefore, the creation of new protocols as well as the expansion and refinement of already established protocols to differentiate of human iPSCs into 5-HT specific neurons is required.

Notably, the *in vitro* method developed in this thesis allows the differentiation of stem cells into 5-HT specific neurons that form synaptic connections and show the characteristic features of functional 5-HT specific neurons *in vivo*. In addition to the high percentage of 5-HT specific neurons (~42%), other neurons of various specifications, such as the catecholaminergic and GABAergic subtype, were generated. Taken together, we developed a model system reflecting the heterogeneous nature of dorsal and median raphe that is useful to examine the involvement of neuronal subtype dysfunction in patients with neurodevelopmental disorder-causing genetic variation.

4.2.1 Reproducible differentiation of human iPSCs into 5-HT specific cells – Refinement of a protocol

Lu and colleagues (2015) recently published a protocol to generate 5-HT specific neurons from human iPSCs that, however, in our attempts failed to replicate the efficiency of differentiation. We therefore adjusted the protocol to an EB formation system combined with a specific time-dependent manipulation of certain signalling pathways. Patterning of the neuroepithelia by coordinating morphogens with opposing effects along both the A-P and D-V axis generates a vast range of specific progenitors for the differentiation of divergent neural subtypes (De Robertis 2009, Harland 2000, Tao & Zhang 2016, Weinstein & Hemmati-Brivanlou 1997). Therefore, appropriate activation of WNT signalling by a specific CHIR concentration at a particular window is necessary to specify rostral hindbrain progenitor cells giving rise of 5-HT neurons (Kirkeby et al 2012a, Kriks et al 2011, Lu et al 2013, Xi et al 2012). The specific progenitor identity of our cells was distinguished by the expression of HOXA2, a marker for rostral hindbrain cells and the absence of OTX2 and HOXB1 expression which would refer to

forebrain/midbrain structures as well as the caudal division of those cells (Goridis & Rohrer 2002, Guthrie 2007). Finally, a more specific 5-HT cell program was induced by a time-dependent treatment of SHH and FGF4 (Hu et al 2009, Ye et al 1998). Exposure to increasing concentrations and duration of SHH drives the progenitors to a more ventral identity, since the D-V patterning is a dynamic process (Ribes & Briscoe 2009). A higher concentration of SHH patterns the neuroepithelia to more ventral parts, leading to progenitor cells that will differentiate into GABAergic interneurons (Nicholas et al 2013) or neuronal types with even more ventrally specification, including midbrain dopaminergic neurons (Kirkeby et al 2012b, Xi et al 2012) and hindbrain 5-HT specific neurons, when FGF4 is additionally applied after ventralization of the cells (Lu et al 2015).

Finally, these adjustments enriched the 5-HT specific neuronal population up to 42% within the overall number of neuronal cells. The reason why we continued to gain less 5-HT specific neurons compared to the previously published protocol (Lu et al 2015) might be due to the use of an EB system and the variation in size of generated aggregates. Since it is challenging to control the development of the cells within those aggregates, EBs are known to display a complex system to differentiate stem cells into specific types of cells. However, an extensive distribution is likely as this culture system includes a dynamic environment that favours further aggregation (Dang et al 2002). By using the EB system, we were able to generate a balanced neuronal culture of catecholaminergic (~40%) and 5-HT specific neurons (~42%). Of note, the interaction of neurons of catecholaminergic - specifically dopaminergic and noradrenergic specification - and 5-HT specific neurons is of relevance in the pathogenesis of neurodevelopmental conditions (Garcia et al 2019, Kapur & Remington 1996, Oades 2008) and has been examined in several animal-based studies (Daw et al 2002, Wong et al 1995). Thus, our differentiation protocol creates a model system that may be practical to further study the interaction of human catecholaminergic and 5-HT specific neurons (for review, Di Giovanni et al 2010, Monti & Jantos 2008, Niederkofler et al 2015).

4.2.2 Human iPSC-derived 5-HT specific neurons display phenotypes of both median and dorsal 5-HT specific neurons

The previously reported protocol generated a culture of high-density median raphe 5-HT specific neurons (Lu et al 2015), which arise from rostral progenitors located at rhombomeric (r) segments 2-3 (Alonso et al 2013, Bang et al 2012). We therefore examined our refined approach for subdivision into median and dorsal raphe 5-HT specific neurons. Recently, we demonstrated that CDH13 contributes to the migration of 5-HT specific neurons to distinct subregions of the raphe nuclei, preferentially the lateral wing of the dorsal raphe (Forero et al

2017) and has been associated to various neurodevelopmental disorders including ADHD (Arias-Vasquez et al 2011, Lesch et al 2008a, Neale et al 2010a, Rivero et al 2015) and ASD (Sanders et al 2011a, Sanders et al 2015). Due to the specificity of CDH13 expression and its clinical link, the expression of this protein was analysed in our 5-HT specific neurons. SIM microscopy indicates that CDH13 is highly expressed in a subset of cultured TPH2+ neurons. We conclude that differentiation generated a mixture of median and dorsal raphe 5-HT specific neurons, and we provide evidence how proteins that have been identified to influence the risk for neurodevelopmental disorders may be studied using this cell system. However, further investigation including additional markers for these various subsets of raphe nuclei is necessary.

4.2.3 5-HT specific neurons differentiated from human iPSCs show synaptic protein assembly

The early expression of markers for neuronal maturity (MAP2, Tau, NeuN) proves that our differentiation protocol enables a rapid and efficient generation of fully mature neurons. Since we yield a distinct proportion of astrocytes that are known to support neuron function, the astrocytes possibly benefit those generated neurons *in vitro* and accelerate maturation. TPH2+ neurons express Bassoon, a marker for the presynaptic active zone, as well as PSD-95 and Homer, the postsynaptic density scaffolding protein (Bresler et al 2004, Dresbach et al 2006, Tao-Cheng et al 2014). Bassoon as a marker for the active zone was therefore used to identify where human iPSC-derived 5-HT specific neurons form synapses with the property to organize transmitter release. However, we observed that Bassoon is not exclusively restricted to axon terminals as seen in hippocampal neurons, but is evenly distributed throughout the cell, and that there is a lack of coinciding pre-and postsynaptic bar structures. Interestingly, the number of synaptic connections formed by 5-HT specific neurons is small (Chazal & Ralston 1987, Moukhles et al 1997, Ridet et al 1993), while those neurons have been shown to rather release 5-HT from their soma, dendrites and axon varicosities (Colgan et al 2012, Colgan et al 2009, de Kock et al 2006, Kaushalya et al 2008, Sarkar et al 2012). This supports the assumption that our *in vitro* 5-HT specific neurons communicate through non-synaptic axonal and somatodendritic release, in addition to synaptic transmission (Adell et al 2002, De-Miguel & Trueta 2005, Lau et al 2010, Vizi et al 2004). Since volume transmission was also reported to take place in the narrow extracellular space between neurons and glia (De-Miguel et al 2015), it is possible that our generated human neurons uses this mechanism to communicate with the surrounding astrocytes.

4.2.4 Electrophysiological signature of iPSC-derived 5-HT specific neurons

Whole-cell recordings of cultured neurons performed weekly over a period of 6 weeks revealed typical ion currents, repetitive firing elicited by current injections and spontaneous firing in neurons starting already the first week of measurement. The rate of maturation and firing properties were similar within experiments and over time. Using electrophysiological properties for identifying neurons as 5-HT specific was previously discussed (Vandermaelen & Aghajanian 1983). Low rate of spontaneous action potential spikes (less than 12 Hz) with a slow, subthreshold oscillatory potential, large action potential and after hyperpolarization and long after hyperpolarization duration are characteristic features of 5-HT specific neurons (Calizo et al 2011, Scott et al 2005). Some of the applied criteria, such as input resistance or afterhyperpolarisation lead to high error rates in identifying 5-HT specific neurons as was demonstrated by Calizo and colleagues (2011). The lowest error rates were shown for action potential duration. Even if the frequency of measured action potentials varied over time in our culture, it remained between 0.5 and 4 Hz. Thus, the frequency of recorded neurons matched the criteria for 5-HT neuron specification. Over the whole time period measured spontaneous action potential firing was evident and the action potentials rose and got faster as the amplitude increased and the HHW decreased. Therefore, using HHW and frequency of action potentials provided sensitive indicators for 5-HT specific neurons, but cell types might not be distinguished by their electrophysiological properties alone.

4.3 The effect of *SLC2A3* CNVs on expression, glucose metabolism and neurodevelopmental processes

Previously, *SLC2A3* structural variations were associated with several disorders, such as Alzheimer disease (Liu et al 2008), schizophrenia (Kuzman et al 2009), ASD (Zhao et al 2010) and ADHD (Merker et al 2017a). We therefore aimed to use our established human iPSC-derived neuronal subtype model to examine the effect of CNVs of *SLC2A3* on basal expression levels, neurodevelopmental processes and the coping strategies to fluctuating glucose availability. Specifically, we decided to concentrate on 5-HT specific neurons, since their involvement in the pathogenesis of neuropsychiatric and neurodevelopmental disorders has repeatedly been shown.

4.3.1 The effects of CNVs of *SLC2A3* on mRNA and protein expression

Previous reports suggested that *SLC2A3* duplication increases *SLC2A3* mRNA expression by ~75 % in human fibroblasts (Yang et al 2009) and by 73 % in human lymphoblasts and even 220 % in human leukocytes (Merker et al 2017b). Our findings showed that a *SLC2A3*

duplication resulted in an 87 % increase of mRNA levels in human iPSCs and an 166 % increase in human iPSC-derived neurons. A *SLC2A3* deletion caused 49 % diminished mRNA expression in human iPSC, while in generated neurons this structural variation of the gene had no significant effect on the mRNA expression: an unexpected result that, however, could be explained by an error of measurement. The differentiation of human iPSCs into neurons displays a fragile development system accompanied by a variation in differentiation outcome. The distribution pattern of GLUT3 in our neuronal population was in line with previous findings revealing an expression in soma as well as fibers of human neurons (Simpson et al 2008). Studies of heterozygous Glut3$^{+/-}$ mice reported a decrease in GLUT3 expression in whole brain lysates (Schmidt et al 2008, Stuart et al 2011, Zhao et al 2010), findings in line with our results suggesting that a *SLC2A3* deletion causes a ~40 % diminished GLUT3 expression in iPSC-derived neurons. In contrast, increased *SLC2A3* mRNA levels did not come along with elevated GLUT3 levels in human neurons. However, to date, there is only one single study reporting increased protein expression in cell lines from duplication carriers (Vittori et al 2014), whereas we and others could not confirm such an effect in similar experiments (Merker et al 2017b, Simpfendorfer et al 2019). The discrepancy between mRNA and protein expression in *SLC2A3* duplication might be due to posttranscriptional or posttranslational modifications. Posttranslational downregulation, such as phosphorylation, is a common translational regulatory mechanism by which the protein biosynthesis is followed by a generally enzymatic modification of the proteins in order to form the mature product (Khy et al 2011). Here, this regulatory mechanism eliminates unnecessarily high amounts of the protein product since an excessive amount does not fulfil any assignments within the cell. Those processes may enable the organism to flexibly adapt to changes in glucose supply and demand. For instance, an increase in GLUT3 half-life was reported as a posttranslational mechanism as consequence of prolonged energy demand (Khayat et al 1998b). Of note, it is known that GLUT3 is primarily located in the plasma membrane and thus at the cell surface. In certain cell types considerable amounts of this protein were additionally found enclosed by synaptic-like vesicles (Thoidis et al 1999). For protein quantification, we used the N-GLUT3 antibody that exclusively visualized the active form of the protein being incorporated in the cell membrane. Therefore, it might be that only the protein that is actually needed is translocated to the cell membrane and the rest of GLUT3 remains stored in vesicles.

4.3.2 The effects of glucose deprivation on expression levels of human iPSC-derived neurons carrying either a duplication or a deletion of *SLC2A3*

It is likely that dysregulation of cerebral glucose metabolism during development causes structural or functional alterations in the brain. This might consequently influence the pathology

of developmental psychiatric disorders, such as ADHD (Merker et al 2017a). Dai and colleagues (2017) recently revealed metabolic changes in male glut3$^{+/-}$ mice, while the impact of lowered GLUT3 levels in humans still needs to be addressed. Here, we focused on the question, if our cells respond differently to glucose deprivation and specific hypo- and hyperglycaemic conditions, when human cells display altered basal GLUT3 levels. Specifically, previous studies formed the link between those blood glucose conditions with altered expression of GLUT3 (Duelli et al 1999, Hou et al 2007, Lee et al 2000, Nagamatsu et al 1994, Shen et al 2009, Uehara et al 1997). For instance, hypoglycaemic condition resulted in increased GLUT3 expression in rodents (Duelli et al 1999, Lee et al 2000, Nagamatsu et al 1994, Uehara et al 1997), while hypoglycaemic conditions have been reported to increase as well as a decrease GLUT3 levels (Boileau et al 1995, Hou et al 2007, Merriman-Smith et al 2003, Reagan et al 1999, Shen et al 2009). Those findings already challenged the hypothesis that surrounding glucose is regulating the expression of GLUT3. We could prove that neither glucose deprivation, nor the treatment with hypo- and hyperglycaemic conditions affected *SLC2A3* mRNA and GLUT3 expression in human neurons, independent of the CN of *SLC2A3*.

4.3.3 The effects of CNVs of *SLC2A3* on synapse formation in human iPSC-derived neurons

The establishment of synaptic connectivity and communication drives the largest energy demand of the brain (Attwell & Laughlin 2001). This fact arouses the question which role *SLC2A3* and its protein GLUT3 play in those developmental mechanisms. Therefore, several studies linked GLUT3 mRNA and protein expression with cerebral maturation in a regional and activity-dependent manner (Nehlig 1996, Nehlig & Pereira de Vasconcelos 1993) and have proven that GLUT3 expression in neurons coincides with maturation and synaptic connectivity (Vannucci et al 1998). Recently, a working group created a neural-specific conditional murine *Glut3* (*Slc2a3*) deletion to analyse the effect of a lack of GLUT3 on neurodevelopmental processes (Shin et al 2018). Those mice showed developmental defects illustrated by a reduced number of dendritic spines and a functional synaptic and cortical hyperexcitability, less brain weight and cortical thickness. On a behavioural level those mice showed reduced anxiety, spatial memories, and motor ability. These results suggest an association of altered GLUT3 expression with neurodevelopmental disorders. However, there is a need for intense examination of GLUT3 function in the human brain to clarify its role in neurodevelopmental disorder mechanisms. Until now, studies focusing on the development of neurons have identified alterations in electrophysiological activity and synapse formation in human iPSCs derived from patients compared to controls in general (Fink et al 2017). Activity-dependent neurite growth was shown to require induction of glucose metabolism and to be blocked *in vitro*

by Glut3 knockdown (Segarra-Mondejar et al 2018). Furthermore, Ferreira and colleagues (2011) revealed a direct relationship between increased synaptic activity, elevated expression of surface GLUT3, and glucose transport. However, even if GLUT3 has been linked to neurodevelopmental processes, our results suggest that lower GLUT3 levels caused by a *SLC2A3* deletion do not affect the assembly of proteins associated with synapse formation in those iPSC-derived 5-HT specific, catecholaminergic as well as GABAergic neurons.

4.4 Outlook

This thesis describes a unique way to examine candidate and risk genes that might increase the liability to neuropsychiatric disorders by the novel technique of human iPSCs and iPSC-derived neuronal subtypes. The lack of reliable and well-working differentiation protocols has been challenging in this research field and explains the need of novel differentiation procedures from human PSCs into specific cell types. We demonstrated a way to differentiate human iPSCs into a culture of median and dorsal raphe 5-HT neurons. Using this neuronal culture, however, we could not prove any effects of structural *SLC2A3* variation on neurodevelopmental processes and glucose metabolism. Interestingly, according to the astrocyte-neuron lactate shuttle (ANLS) hypothesis, astrocytes play the key role in the coupling of neuronal activity and cerebral glucose utilization, while neurons use lactate as their primary fuel (Magistretti & Pellerin 1997, Pellerin & Magistretti 2003), which challenges the role of GLUT3 as the neuronal transporter. Even if the ANLS hypothesis has already been challenged (Simpson et al 2007), it is necessary to examine glucose uptake of human iPSC-derived neurons to confirm that the previous non-significant effects of CNVs of *SLC2A3* on the cerebral metabolism are not due to the ANLS hypothesis. Since we only focused on the assembly of Homer and Bassoon in our human neurons, further examination of other proteins associated with synapse formation should be targeted in follow-up studies. Electron microscopy would additionally enable the structural visualization of a synapse to reveal any possible changes caused by an altered *SLC2A3* expression. Of note, since activity-dependent neurite growth has already been shown to be affected by altered GLUT3 expression in rats (Segarra-Mondejar et al 2018), a major interest would be the effect of structural variations of this gene on neurite outgrowth in human neurons. To conclude, it might be likely that cortical neurons, such as GABAergic neurons, may be the affected cell type, as a recent study created the connection between GLUT3 expression and neurite length in this neuronal subtype (Segarra-Mondejar et al 2018). However, the percentage of GABAergic neurons in our cell culture is extremely low and therefore a differentiation protocol resulting in a pure cortical network might reflect a suitable cell culture model for follow-up studies in this project. Finally, it should be mentioned that to date, no human study has so far associated a *SLC2A3* deletion with ADHD. Our own

control cohort includes several adults without any obvious symptoms of a neuropsychiatric disorder that, however, also carry a heterozygous *SLC2A3* deletion.

5. References

Adell A, Celada P, Abellan MT, Artigas F. 2002. Origin and functional role of the extracellular serotonin in the midbrain raphe nuclei. *Brain research. Brain research reviews* 39: 154-80

Aghajanian GK, Wang RY. 1977. Habenular and other midbrain raphe afferents demonstrated by a modified retrograde tracing technique. *Brain research* 122: 229-42

Alenina N, Klempin F. 2015. The role of serotonin in adult hippocampal neurogenesis. *Behavioural brain research* 277: 49-57

Alonso A, Merchan P, Sandoval JE, Sanchez-Arrones L, Garcia-Cazorla A, et al. 2013. Development of the serotonergic cells in murine raphe nuclei and their relations with rhombomeric domains. *Brain structure & function* 218: 1229-77

Andrade R. 1998. Regulation of membrane excitability in the central nervous system by serotonin receptor subtypes. *Annals of the New York Academy of Sciences* 861: 190-203

Andrade R, Huereca D, Lyons JG, Andrade EM, McGregor KM. 2015. 5-HT1A Receptor-Mediated Autoinhibition and the Control of Serotonergic Cell Firing. *ACS chemical neuroscience* 6: 1110-5

Arai R, Karasawa N, Geffard M, Nagatsu T, Nagatsu I. 1994. Immunohistochemical evidence that central serotonin neurons produce dopamine from exogenous L-DOPA in the rat, with reference to the involvement of aromatic L-amino acid decarboxylase. *Brain research* 667: 295-9

Araragi N, MLinar B, Baccini G, Gutknecht L, Lesch KP, Corradetti R. 2013. Conservation of 5-HT1A receptor-mediated autoinhibition of serotonin (5-HT) neurons in mice with altered 5-HT homeostasis. *Frontiers in pharmacology* 4: 97

Ardhanareeswaran K, Mariani J, Coppola G, Abyzov A, Vaccarino FM. 2017. Human induced pluripotent stem cells for modelling neurodevelopmental disorders. *Nature Reviews Neurology* 13: 265

Arias-Vasquez A, Altink ME, Rommelse NN, Slaats-Willemse DI, Buschgens CJ, et al. 2011. CDH13 is associated with working memory performance in attention deficit/hyperactivity disorder. *Genes, brain, and behavior* 10: 844-51

Arnsten AF. 2011. Catecholamine influences on dorsolateral prefrontal cortical networks. *Biological psychiatry* 69: e89-99

Attwell D, Laughlin SB. 2001. An energy budget for signaling in the grey matter of the brain. *Journal of cerebral blood flow and metabolism* 21: 1133-45

Azmitia EC. 2001. Modern views on an ancient chemical: serotonin effects on cell proliferation, maturation, and apoptosis. *Brain research bulletin* 56: 413-24

Banasr M, Hery M, Printemps R, Daszuta A. 2003. Serotonin-Induced Increases in Adult Cell Proliferation and Neurogenesis are Mediated Through Different and Common 5-HT Receptor Subtypes in the Dentate Gyrus and the Subventricular Zone. *Neuropsychopharmacology* 29: 450

Banerjee TD, Middleton F, Faraone SV. 2007. Environmental risk factors for attention-deficit hyperactivity disorder. *Acta paediatrica (Oslo, Norway : 1992)* 96: 1269-74

Bang SJ, Jensen P, Dymecki SM, Commons KG. 2012. Projections and interconnections of genetically defined serotonin neurons in mice. *The European journal of neuroscience* 35: 85-96

Barnes NM, Sharp T. 1999. A review of central 5-HT receptors and their function. *Neuropharmacology* 38: 1083-152

Barron CC, Bilan PJ, Tsakiridis T, Tsiani E. 2016. Facilitative glucose transporters: Implications for cancer detection, prognosis and treatment. *Metabolism: clinical and experimental* 65: 124-39

Berger M, Gray JA, Roth BL. 2009. The expanded biology of serotonin. *Annual review of medicine* 60: 355-66

Bernard R, Veh RW. 2012. Individual neurons in the rat lateral habenular complex project mostly to the dopaminergic ventral tegmental area or to the serotonergic raphe nuclei. *The Journal of comparative neurology* 520: 2545-58

Biederman J, Faraone SV. 2005. Attention-deficit hyperactivity disorder. *Lancet* 366: 237-48

Blier P, Steinberg S, Chaput Y, de Montigny C. 1989. Electrophysiological assessment of putative antagonists of 5-hydroxytryptamine receptors: a single-cell study in the rat dorsal raphe nucleus. *Canadian journal of physiology and pharmacology* 67: 98-105

Boileau P, Mrejen C, Girard J, Hauguel-de Mouzon S. 1995. Overexpression of GLUT3 placental glucose transporter in diabetic rats. *The Journal of clinical investigation* 96: 309-17

Borroto-Escuela DO, Agnati LF, Bechter K, Jansson A, Tarakanov AO, Fuxe K. 2015. The role of transmitter diffusion and flow versus extracellular vesicles in volume transmission in the brain neural-glial networks. *Philosophical transactions of the Royal Society of London. Series B, Biological sciences* 370

Brennand KJ, Simone A, Tran N, Gage FH. 2012. Modeling psychiatric disorders at the cellular and network levels. *Molecular Psychiatry* 17: 1239

Bresler T, Shapira M, Boeckers T, Dresbach T, Futter M, et al. 2004. Postsynaptic density assembly is fundamentally different from presynaptic active zone assembly. *The Journal of neuroscience* 24: 1507-20

Burmeister M, McInnis MG, Zollner S. 2008. Psychiatric genetics: progress amid controversy. *Nature reviews. Genetics* 9: 527-40

Bush G. 2010. Attention-deficit/hyperactivity disorder and attention networks. *Neuropsychopharmacology : official publication of the American College of Neuropsychopharmacology* 35: 278-300

Bush G. 2011. Cingulate, frontal, and parietal cortical dysfunction in attention-deficit/hyperactivity disorder. *Biological psychiatry* 69: 1160-7

Calizo LH, Akanwa A, Ma X, Pan YZ, Lemos JC, et al. 2011. Raphe serotonin neurons are not homogenous: electrophysiological, morphological and neurochemical evidence. *Neuropharmacology* 61: 524-43

Carmona S, Proal E, Hoekzema EA, Gispert JD, Picado M, et al. 2009. Ventro-striatal reductions underpin symptoms of hyperactivity and impulsivity in attention-deficit/hyperactivity disorder. *Biological psychiatry* 66: 972-7

Castellanos FX. 2009. Toward the dimensionome: parsing reward-related processing in attention-deficit/hyperactivity disorder. *Biological psychiatry* 65: 5-6

Celada P, Puig MV, Casanovas JM, Guillazo G, Artigas F. 2001. Control of dorsal raphe serotonergic neurons by the medial prefrontal cortex: Involvement of serotonin-1A, GABA(A), and glutamate receptors. *The Journal of neuroscience* 21: 9917-29

Cesar-Razquin A, Snijder B, Frappier-Brinton T, Isserlin R, Gyimesi G, et al. 2015. A Call for Systematic Research on Solute Carriers. *Cell* 162: 478-87

Chamberlain CE, Jeong J, Guo C, Allen BL, McMahon AP. 2008. Notochord-derived Shh concentrates in close association with the apically positioned basal body in neural target cells and forms a dynamic gradient during neural patterning. *Development* 135: 1097-106

Chambers SM, Fasano CA, Papapetrou EP, Tomishima M, Sadelain M, Studer L. 2009. Highly efficient neural conversion of human ES and iPS cells by dual inhibition of SMAD signaling. *Nat Biotechnol* 27: 275-80

Chazal G, Ralston HJ, 3rd. 1987. Serotonin-containing structures in the nucleus raphe dorsalis of the cat: an ultrastructural analysis of dendrites, presynaptic dendrites, and axon terminals. *The Journal of comparative neurology* 259: 317-29

Chen J, Condron BG. 2008. Branch architecture of the fly larval abdominal serotonergic neurons. *Developmental biology* 320: 30-8

Chen LQ, Hou BH, Lalonde S, Takanaga H, Hartung ML, et al. 2010. Sugar transporters for intercellular exchange and nutrition of pathogens. *Nature* 468: 527-32

Ciatto C, Bahna F, Zampieri N, VanSteenhouse HC, Katsamba PS, et al. 2010. T-cadherin structures reveal a novel adhesive binding mechanism. *Nature structural & molecular biology* 17: 339-47

Colgan LA, Cavolo SL, Commons KG, Levitan ES. 2012. Action potential-independent and pharmacologically unique vesicular serotonin release from dendrites. *The Journal of neuroscience* 32: 15737-46

Colgan LA, Putzier I, Levitan ES. 2009. Activity-dependent vesicular monoamine transporter-mediated depletion of the nucleus supports somatic release by serotonin neurons. *The Journal of neuroscience* 29: 15878-87

Colino A, Halliwell JV. 1987. Differential modulation of three separate K-conductances in hippocampal CA1 neurons by serotonin. *Nature* 328: 73-77

Dahlstroem A, Fuxe K. 1964. Evidence for the existence of monoamine-containing neurons in the central nervous system. I. Demonstration of monoamines in the cell bodies of brain stem neurons. *Acta physiologica Scandinavica. Supplementum*: Suppl 232:1-55

Dai Y, Zhao Y, Tomi M, Shin B-C, Thamotharan S, et al. 2017. Sex-Specific Life Course Changes in the Neuro-Metabolic Phenotype of Glut3 Null Heterozygous Mice: Ketogenic Diet Ameliorates Electroencephalographic Seizures and Improves Sociability. *Endocrinology* 158: 936-49

References

Dang SM, Kyba M, Perlingeiro R, Daley GQ, Zandstra PW. 2002. Efficiency of embryoid body formation and hematopoietic development from embryonic stem cells in different culture systems. *Biotechnology and bioengineering* 78: 442-53

Daw ND, Kakade S, Dayan P. 2002. Opponent interactions between serotonin and dopamine. *Neural networks : the official journal of the International Neural Network Society* 15: 603-16

De-Miguel FF, Leon-Pinzon C, Noguez P, Mendez B. 2015. Serotonin release from the neuronal cell body and its long-lasting effects on the nervous system. *Philosophical transactions of the Royal Society of London. Series B, Biological sciences* 370: 20140196

De-Miguel FF, Trueta C. 2005. Synaptic and extrasynaptic secretion of serotonin. *Cellular and molecular neurobiology* 25: 297-312

de Kock CP, Cornelisse LN, Burnashev N, Lodder JC, Timmerman AJ, et al. 2006. NMDA receptors trigger neurosecretion of 5-HT within dorsal raphe nucleus of the rat in the absence of action potential firing. *The Journal of physiology* 577: 891-905

De Robertis EM. 2009. Spemann's organizer and the self-regulation of embryonic fields. *Mech Dev* 126: 925-41

Deng D, Yan N. 2016. GLUT, SGLT, and SWEET: Structural and mechanistic investigations of the glucose transporters. *Protein Sci* 25: 546-58

Di Giovanni G, Esposito E, Di Matteo V. 2010. Role of serotonin in central dopamine dysfunction. *CNS neuroscience & therapeutics* 16: 179-94

Dresbach T, Torres V, Wittenmayer N, Altrock WD, Zamorano P, et al. 2006. Assembly of active zone precursor vesicles: obligatory trafficking of presynaptic cytomatrix proteins Bassoon and Piccolo via a trans-Golgi compartment. *The Journal of biological chemistry* 281: 6038-47

Duelli R, Staudt R, Duembgen L, Kuschinsky W. 1999. Increase in glucose transporter densities of Glut3 and decrease of glucose utilization in rat brain after one week of hypoglycemia. *Brain research* 831: 254-62

Elia J, Glessner JT, Wang K, Takahashi N, Shtir CJ, et al. 2012. Genome-wide copy number variation study associates metabotropic glutamate receptor gene networks with attention deficit hyperactivity disorder. *Nature genetics* 44: 78-84

Elsas LJ, Longo N. 1992. Glucose transporters. *Annual review of medicine* 43: 377-93

Engel M, Smidt MP, van Hooft JA. 2013. The serotonin 5-HT3 receptor: a novel neurodevelopmental target. *Frontiers in cellular neuroscience* 7: 76-76

Ericson J, Rashbass P, Schedl A, Brenner-Morton S, Kawakami A, et al. 1997. Pax6 controls progenitor cell identity and neuronal fate in response to graded Shh signaling. *Cell* 90: 169-80

Evans MJ, Kaufman MH. 1981. Establishment in culture of pluripotential cells from mouse embryos. *Nature* 292: 154-56

Faraone SV, Biederman J, Mick E. 2006. The age-dependent decline of attention deficit hyperactivity disorder: a meta-analysis of follow-up studies. *Psychological medicine* 36: 159-65

References

Fayyad J, De Graaf R, Kessler R, Alonso J, Angermeyer M, et al. 2007. Cross-national prevalence and correlates of adult attention-deficit hyperactivity disorder. *The British journal of psychiatry* 190: 402-9

Feng L, Frommer WB. 2015. Structure and function of SemiSWEET and SWEET sugar transporters. *Trends in biochemical sciences* 40: 480-6

Ferreira JM, Burnett AL, Rameau GA. 2011. Activity-dependent regulation of surface glucose transporter-3. *The Journal of neuroscience* 31: 1991-9

Fink JJ, Robinson TM, Germain ND, Sirois CL, Bolduc KA, et al. 2017. Disrupted neuronal maturation in Angelman syndrome-derived induced pluripotent stem cells. *Nature Communications* 8: 15038

Forero A, Rivero O, Wäldchen S, Ku H-P, Kiser DP, et al. 2017. Cadherin-13 Deficiency Increases Dorsal Raphe 5-HT Neuron Density and Prefrontal Cortex Innervation in the Mouse Brain. *Frontiers in Cellular Neuroscience* 11: 307

Freitas-Ferrari MC, Hallak JE, Trzesniak C, Filho AS, Machado-de-Sousa JP, et al. 2010. Neuroimaging in social anxiety disorder: a systematic review of the literature. *Progress in neuro-psychopharmacology & biological psychiatry* 34: 565-80

Fuchs PA, Henderson LP, Nicholls JG. 1982. Chemical transmission between individual Retzius and sensory neurones of the leech in culture. *The Journal of physiology* 323: 195-210

Fusaki N, Ban H, Nishiyama A, Saeki K, Hasegawa M. 2009. Efficient induction of transgene-free human pluripotent stem cells using a vector based on Sendai virus, an RNA virus that does not integrate into the host genome. *Proceedings of the Japan Academy. Series B, Physical and biological sciences* 85: 348-62

Fuxe K, Dahlstrom A, Hoistad M, Marcellino D, Jansson A, et al. 2007. From the Golgi-Cajal mapping to the transmitter-based characterization of the neuronal networks leading to two modes of brain communication: wiring and volume transmission. *Brain research reviews* 55: 17-54

Gantz SC, Levitt ES, Llamosas N, Neve KA, Williams JT. 2015. Depression of Serotonin Synaptic Transmission by the Dopamine Precursor L-DOPA. *Cell reports* 12: 944-54

Garcia LP, Witteveen JS, Middelman A, van Hulten JA, Martens GJM, et al. 2019. Perturbed Developmental Serotonin Signaling Affects Prefrontal Catecholaminergic Innervation and Cortical Integrity. *Molecular Neurobiology* 56: 1405-20

Geissler J, Lesch KP. 2011. A lifetime of attention-deficit/hyperactivity disorder: diagnostic challenges, treatment and neurobiological mechanisms. *Expert review of neurotherapeutics* 11: 1467-84

Gervasoni D, Peyron C, Rampon C, Barbagli B, Chouvet G, et al. 2000. Role and origin of the GABAergic innervation of dorsal raphe serotonergic neurons. *The Journal of neuroscience* 20: 4217-25

Gibbs EM, Calderhead DM, Holman GD, Gould GW. 1991. Phorbol ester only partially mimics the effects of insulin on glucose transport and glucose-transporter distribution in 3T3-L1 adipocytes. *The Biochemical journal* 275 (Pt 1): 145-50

Goridis C, Rohrer H. 2002. Specification of catecholaminergic and serotonergic neurons. *Nature reviews. Neuroscience* 3: 531-41

Gould GW, Thomas HM, Jess TJ, Bell GI. 1991. Expression of human glucose transporters in Xenopus oocytes: kinetic characterization and substrate specificities of the erythrocyte, liver, and brain isoforms. *Biochemistry* 30: 5139-45

Guthrie S. 2007. Patterning and axon guidance of cranial motor neurons. *Nature reviews. Neuroscience* 8: 859-71

Gutknecht L, Kriegebaum C, Waider J, Schmitt A, Lesch KP. 2009. Spatio-temporal expression of tryptophan hydroxylase isoforms in murine and human brain: convergent data from Tph2 knockout mice. *European neuropsychopharmacology* 19: 266-82

Haber RS, Weinstein SP, O'Boyle E, Morgello S. 1993. Tissue distribution of the human GLUT3 glucose transporter. *Endocrinology* 132: 2538-43

Halevy T, Czech C, Benvenisty N. 2015. Molecular Mechanisms Regulating the Defects in Fragile X Syndrome Neurons Derived from Human Pluripotent Stem Cells. *Stem Cell Reports* 4: 37-46

Hamill OP, Marty A, Neher E, Sakmann B, Sigworth FJ. 1981. Improved patch-clamp techniques for high-resolution current recording from cells and cell-free membrane patches. *Pflügers Archiv* 391: 85-100

Hannestad J, Gallezot JD, Planeta-Wilson B, Lin SF, Williams WA, et al. 2010. Clinically relevant doses of methylphenidate significantly occupy norepinephrine transporters in humans in vivo. *Biological psychiatry* 68: 854-60

Harland R. 2000. Neural induction. *Current opinion in genetics & development* 10: 357-62

Hensler JG. 2006. Serotonergic modulation of the limbic system. *Neuroscience and biobehavioral reviews* 30: 203-14

Hjorth S, Sharp T. 1991. Effect of the 5-HT1A receptor agonist 8-OH-DPAT on the release of 5-HT in dorsal and median raphe-innervated rat brain regions as measured by in vivo microdialysis. *Life sciences* 48: 1779-86

Hou WK, Xian YX, Zhang L, Lai H, Hou XG, et al. 2007. Influence of blood glucose on the expression of glucose trans-porter proteins 1 and 3 in the brain of diabetic rats. *Chinese medical journal* 120: 1704-9

Hoyer D, Hannon JP, Martin GR. 2002. Molecular, pharmacological and functional diversity of 5-HT receptors. *Pharmacology, biochemistry, and behavior* 71: 533-54

Hu BY, Du ZW, Li XJ, Ayala M, Zhang SC. 2009. Human oligodendrocytes from embryonic stem cells: conserved SHH signaling networks and divergent FGF effects. *Development* 136: 1443-52

Intoh A, Koszka K, Suzuki N, Eggan K. 2016. SLC52A3, A Brown–Vialetto–van Laere syndrome candidate gene is essential for mouse development, but dispensable for motor neuron differentiation. *Human Molecular Genetics* 25: 1814-23

Iqbal N, van Praag HM. 1995. The role of serotonin in schizophrenia. *European neuropsychopharmacology : the journal of the European College of Neuropsychopharmacology* 5 Suppl: 11-23

Jacob CP, Romanos J, Dempfle A, Heine M, Windemuth-Kieselbach C, et al. 2007. Co-morbidity of adult attention-deficit/hyperactivity disorder with focus on personality traits

and related disorders in a tertiary referral center. *European archives of psychiatry and clinical neuroscience* 257: 309-17

Jansch C, Günther K, Waider J, Ziegler GC, Forero A, et al. 2018. Generation of a human induced pluripotent stem cell (iPSC) line from a 51-year-old female with attention-deficit/hyperactivity disorder (ADHD) carrying a duplication of SLC2A3. *Stem Cell Research* 28: 136-40

Kaiser T, Feng G. 2015. Modeling psychiatric disorders for developing effective treatments. *Nature medicine* 21: 979-88

Kannari K, Tanaka H, Maeda T, Tomiyama M, Suda T, Matsunaga M. 2000. Reserpine pretreatment prevents increases in extracellular striatal dopamine following L-DOPA administration in rats with nigrostriatal denervation. *Journal of neurochemistry* 74: 263-9

Kapur S, Remington G. 1996. Serotonin-dopamine interaction and its relevance to schizophrenia. *The American journal of psychiatry* 153: 466-76

Kaushalya SK, Desai R, Arumugam S, Ghosh H, Balaji J, Maiti S. 2008. Three-photon microscopy shows that somatic release can be a quantitatively significant component of serotonergic neurotransmission in the mammalian brain. *Journal of neuroscience research* 86: 3469-80

Kayano T, Fukumoto H, Eddy RL, Fan YS, Byers MG, et al. 1988. Evidence for a family of human glucose transporter-like proteins. Sequence and gene localization of a protein expressed in fetal skeletal muscle and other tissues. *The Journal of biological chemistry* 263: 15245-8

Khayat ZA, McCall AL, Klip A. 1998a. Unique mechanism of GLUT3 glucose transporter regulation by prolonged energy demand: increased protein half-life. *The Biochemical journal* 333 (Pt 3): 713-18

Khayat ZA, McCall AL, Klip A. 1998b. Unique mechanism of GLUT3 glucose transporter regulation by prolonged energy demand: increased protein half-life. *The Biochemical journal* 333 (Pt 3): 713-8

Khy GA, Baliban RC, Floudas CA. 2011. Proteome-wide post-translational modification statistics: frequency analysis and curation of the swiss-prot database. *Scientific Reports* 1: 90

Kirkeby A, Grealish S, Wolf DA, Nelander J, Wood J, et al. 2012a. Generation of regionally specified neural progenitors and functional neurons from human embryonic stem cells under defined conditions. *Cell reports* 1: 703-14

Kirkeby A, Nelander J, Parmar M. 2012b. Generating regionalized neuronal cells from pluripotency, a step-by-step protocol. *Front Cell Neurosci* 6: 64

Kiyasova V, Gaspar P. 2011. Development of raphe serotonin neurons from specification to guidance. *The European journal of neuroscience* 34: 1553-62

Knoblich JA. 2008. Mechanisms of asymmetric stem cell division. *Cell* 132: 583-97

Kono T, Nishida M, Nishiki Y, Seki Y, Sato K, Akiba Y. 2005. Characterisation of glucose transporter (GLUT) gene expression in broiler chickens. *British poultry science* 46: 510-5

Kriks S, Shim JW, Piao J, Ganat YM, Wakeman DR, et al. 2011. Dopamine neurons derived from human ES cells efficiently engraft in animal models of Parkinson's disease. *Nature* 480: 547-51

Kroeze WK, Kristiansen K, Roth BL. 2002. Molecular biology of serotonin receptors structure and function at the molecular level. *Current topics in medicinal chemistry* 2: 507-28

Kuffler DP, Nicholls J, Drapeau P. 1987. Transmitter localization and vesicle turnover at a serotoninergic synapse between identified leech neurons in culture. *The Journal of comparative neurology* 256: 516-26

Kuzman MR, Medved V, Terzic J, Krainc D. 2009. Genome-wide expression analysis of peripheral blood identifies candidate biomarkers for schizophrenia. *Journal of psychiatric research* 43: 1073-7

Lau T, Schneidt T, Heimann F, Gundelfinger E, Schloss P. 2010. *Somatodendritic serotonin release and re-uptake in mouse embryonic stem cell-derived serotonergic neurons*. 969-78 pp.

Lauder JM. 1993. Neurotransmitters as growth regulatory signals: role of receptors and second messengers. *Trends in neurosciences* 16: 233-40

Lechin F, van der Dijs B, Hernandez-Adrian G. 2006. Dorsal raphe vs. median raphe serotonergic antagonism. Anatomical, physiological, behavioral, neuroendocrinological, neuropharmacological and clinical evidences: relevance for neuropharmacological therapy. *Progress in neuro-psychopharmacology & biological psychiatry* 30: 565-85

Lee DH, Chung MY, Lee JU, Kang DG, Paek YW. 2000. Changes of glucose transporters in the cerebral adaptation to hypoglycemia. *Diabetes research and clinical practice* 47: 15-23

Lesch KP, Selch S, Renner TJ, Jacob C, Nguyen TT, et al. 2011. Genome-wide copy number variation analysis in attention-deficit/hyperactivity disorder: association with neuropeptide Y gene dosage in an extended pedigree. *Mol Psychiatry* 16: 491-503

Lesch KP, Timmesfeld N, Renner TJ, Halperin R, Roser C, et al. 2008a. Molecular genetics of adult ADHD: converging evidence from genome-wide association and extended pedigree linkage studies. *Journal of neural transmission (Vienna, Austria : 1996)* 115: 1573-85

Lesch KP, Timmesfeld N, Renner TJ, Halperin R, Roser C, et al. 2008b. Molecular genetics of adult ADHD: converging evidence from genome-wide association and extended pedigree linkage studies. *Journal of neural transmission* 115: 1573-85

Lesch KP, Waider J. 2012. Serotonin in the modulation of neural plasticity and networks: implications for neurodevelopmental disorders. *Neuron* 76: 175-91

Li YQ, Li H, Kaneko T, Mizuno N. 2001. Morphological features and electrophysiological properties of serotonergic and non-serotonergic projection neurons in the dorsal raphe nucleus. An intracellular recording and labeling study in rat brain slices. *Brain research* 900: 110-8

Lidov HG, Molliver ME. 1982. Immunohistochemical study of the development of serotonergic neurons in the rat CNS. *Brain research bulletin* 9: 559-604

References

Lipton SA, Kater SB. 1989. Neurotransmitter regulation of neuronal outgrowth, plasticity and survival. *Trends in neurosciences* 12: 265-70

Liu Y, Liu F, Iqbal K, Grundke-Iqbal I, Gong C-X. 2008. Decreased glucose transporters correlate to abnormal hyperphosphorylation of tau in Alzheimer disease. *FEBS letters* 582: 359-64

Lowe AG, Walmsley AR. 1986. The kinetics of glucose transport in human red blood cells. *Biochimica et biophysica acta* 857: 146-54

Lu J, Liu H, Huang CT, Chen H, Du Z, et al. 2013. Generation of integration-free and region-specific neural progenitors from primate fibroblasts. *Cell reports* 3: 1580-91

Lu J, Zhong X, Liu H, Hao L, Huang CT-L, et al. 2015. Generation of serotonin neurons from human pluripotent stem cells. *Nature Biotechnology* 34: 89

Lupski JR, Belmont JW, Boerwinkle E, Gibbs RA. 2011. Clan genomics and the complex architecture of human disease. *Cell* 147: 32-43

Maejima T, Masseck OA, Mark MD, Herlitze S. 2013. Modulation of firing and synaptic transmission of serotonergic neurons by intrinsic G protein-coupled receptors and ion channels. *Front Integr Neurosci* 7: 40-40

Magistretti PJ, Pellerin L. 1997. Metabolic coupling during activation. A cellular view. *Advances in experimental medicine and biology* 413: 161-6

Mantych GJ, James DE, Chung HD, Devaskar SU. 1992. Cellular localization and characterization of Glut 3 glucose transporter isoform in human brain. *Endocrinology* 131: 1270-8

Mariani J, Coppola G, Zhang P, Abyzov A, Provini L, et al. 2015. FOXG1-Dependent Dysregulation of GABA/Glutamate Neuron Differentiation in Autism Spectrum Disorders. *Cell* 162: 375-90

Mauritz C, Schwanke K, Reppel M, Neef S, Katsirntaki K, et al. 2008. Generation of functional murine cardiac myocytes from induced pluripotent stem cells. *Circulation* 118: 507-17

Mazurier F, Gan OI, McKenzie JL, Doedens M, Dick JE. 2004. Lentivector-mediated clonal tracking reveals intrinsic heterogeneity in the human hematopoietic stem cell compartment and culture-induced stem cell impairment. *Blood* 103: 545-52

McCorvy JD, Roth BL. 2015. Structure and function of serotonin G protein-coupled receptors. *Pharmacol Ther* 150: 129-42

McDevitt RA, Neumaier JF. 2011. Regulation of dorsal raphe nucleus function by serotonin autoreceptors: a behavioral perspective. *Journal of chemical neuroanatomy* 41: 234-46

Merker S, Reif A, Ziegler GC, Weber H, Mayer U, et al. 2017a. SLC2A3 single-nucleotide polymorphism and duplication influence cognitive processing and population-specific risk for attention-deficit/hyperactivity disorder. *Journal of child psychology and psychiatry, and allied disciplines* 58: 798-809

Merkle FT, Maroof A, Wataya T, Sasai Y, Studer L, et al. 2015. Generation of neuropeptidergic hypothalamic neurons from human pluripotent stem cells. *Development* 142: 633-43

References

Merriman-Smith BR, Krushinsky A, Kistler J, Donaldson PJ. 2003. Expression patterns for glucose transporters GLUT1 and GLUT3 in the normal rat lens and in models of diabetic cataract. *Investigative ophthalmology & visual science* 44: 3458-66

Migliarini S, Pacini G, Pelosi B, Lunardi G, Pasqualetti M. 2013. Lack of brain serotonin affects postnatal development and serotonergic neuronal circuitry formation. *Mol Psychiatry* 18: 1106-18

Mikkers H, Berns A. 2003. Retroviral insertional mutagenesis: tagging cancer pathways. *Advances in cancer research* 88: 53-99

MLinar B, Montalbano A, Baccini G, Tatini F, Berlinguer Palmini R, Corradetti R. 2015. Nonexocytotic serotonin release tonically suppresses serotonergic neuron activity. *The Journal of general physiology* 145: 225-51

Monti JM, Jantos H. 2008. The roles of dopamine and serotonin, and of their receptors, in regulating sleep and waking. *Progress in brain research* 172: 625-46

Moran GR, Derecskei-Kovacs A, Hillas PJ, Fitzpatrick PF. 2000. On the Catalytic Mechanism of Tryptophan Hydroxylase. *Journal of the American Chemical Society* 122: 4535-41

Morrison SJ, Kimble J. 2006. Asymmetric and symmetric stem-cell divisions in development and cancer. *Nature* 441: 1068-74

Moukhles H, Bosler O, Bolam JP, Vallee A, Umbriaco D, et al. 1997. Quantitative and morphometric data indicate precise cellular interactions between serotonin terminals and postsynaptic targets in rat substantia nigra. *Neuroscience* 76: 1159-71

Mueckler M, Thorens B. 2013. The SLC2 (GLUT) family of membrane transporters. *Molecular aspects of medicine* 34: 121-38

Muzerelle A, Scotto-Lomassese S, Bernard JF, Soiza-Reilly M, Gaspar P. 2016. Conditional anterograde tracing reveals distinct targeting of individual serotonin cell groups (B5-B9) to the forebrain and brainstem. *Brain structure & function* 221: 535-61

Nagamatsu S, Kornhauser JM, Burant CF, Seino S, Mayo KE, Bell GI. 1992. Glucose transporter expression in brain. cDNA sequence of mouse GLUT3, the brain facilitative glucose transporter isoform, and identification of sites of expression by in situ hybridization. *The Journal of biological chemistry* 267: 467-72

Nagamatsu S, Sawa H, Inoue N, Nakamichi Y, Takeshima H, Hoshino T. 1994. Gene expression of GLUT3 glucose transporter regulated by glucose in vivo in mouse brain and in vitro in neuronal cell cultures from rat embryos. *The Biochemical journal* 300 (Pt 1): 125-31

Neale BM, Lasky-Su J, Anney R, Franke B, Zhou K, et al. 2008. Genome-wide association scan of attention deficit hyperactivity disorder. *American journal of medical genetics. Part B, Neuropsychiatric genetics : the official publication of the International Society of Psychiatric Genetics* 147B: 1337-44

Neale BM, Medland S, Ripke S, Anney RJ, Asherson P, et al. 2010a. Case-control genome-wide association study of attention-deficit/hyperactivity disorder. *Journal of the American Academy of Child and Adolescent Psychiatry* 49: 906-20

Neale BM, Medland S, Ripke S, Anney RJ, Asherson P, et al. 2010b. Case-control genome-wide association study of attention-deficit/hyperactivity disorder. *Journal of the American Academy of Child and Adolescent Psychiatry* 49: 906-20

Neely MD, Litt MJ, Tidball AM, Li GG, Aboud AA, et al. 2012. DMH1, a highly selective small molecule BMP inhibitor promotes neurogenesis of hiPSCs: comparison of PAX6 and SOX1 expression during neural induction. *ACS chemical neuroscience* 3: 482-91

Nehlig A. 1996. Respective roles of glucose and ketone bodies as substrates for cerebral energy metabolism in the suckling rat. *Developmental neuroscience* 18: 426-33

Nehlig A, Pereira de Vasconcelos A. 1993. Glucose and ketone body utilization by the brain of neonatal rats. *Progress in neurobiology* 40: 163-221

Ng KY, Chase TN, Colburn RW, Kopin IJ. 1970. L-Dopa-induced release of cerebral monoamines. *Science (New York, N.Y.)* 170: 76-7

Nicholas CR, Chen J, Tang Y, Southwell DG, Chalmers N, et al. 2013. Functional maturation of hPSC-derived forebrain interneurons requires an extended timeline and mimics human neural development. *Cell stem cell* 12: 573-86

Nichols DE, Nichols CD. 2008. Serotonin receptors. *Chemical reviews* 108: 1614-41

Niederkofler V, Asher TE, Dymecki SM. 2015. Functional Interplay between Dopaminergic and Serotonergic Neuronal Systems during Development and Adulthood. *ACS chemical neuroscience* 6: 1055-70

Nieoullon A. 2002. Dopamine and the regulation of cognition and attention. *Progress in neurobiology* 67: 53-83

Nieto Mendoza E, Hern, #xe1, ndez Echeagaray E. 2015. Dopaminergic Modulation of Striatal Inhibitory Transmission and Long-Term Plasticity. *Neural Plasticity* 2015: 15

Oades RD. 2008. Dopamine-serotonin interactions in attention-deficit hyperactivity disorder (ADHD). *Progress in brain research* 172: 543-65

Ohmine S, Dietz AB, Deeds MC, Hartjes KA, Miller DR, et al. 2011. Induced pluripotent stem cells from GMP-grade hematopoietic progenitor cells and mononuclear myeloid cells. *Stem cell research & therapy* 2: 46-46

Okaty Benjamin W, Freret Morgan E, Rood Benjamin D, Brust Rachael D, Hennessy Morgan L, et al. 2015. Multi-Scale Molecular Deconstruction of the Serotonin Neuron System. *Neuron* 88: 774-91

Okita K, Ichisaka T, Yamanaka S. 2007. Generation of germLine-competent induced pluripotent stem cells. *Nature* 448: 313-7

Pao SS, Paulsen IT, Saier MH, Jr. 1998. Major facilitator superfamily. *Microbiology and molecular biology reviews : MMBR* 62: 1-34

Paradis S, Harrar DB, Lin Y, Koon AC, Hauser JL, et al. 2007. An RNAi-based approach identifies molecules required for glutamatergic and GABAergic synapse development. *Neuron* 53: 217-32

Pavon JA, Fitzpatrick PF. 2006. Insights into the catalytic mechanisms of phenylalanine and tryptophan hydroxylase from kinetic isotope effects on aromatic hydroxylation. *Biochemistry* 45: 11030-7

Pellerin L, Magistretti PJ. 2003. Food for thought: challenging the dogmas. *Journal of cerebral blood flow and metabolism : official journal of the International Society of Cerebral Blood Flow and Metabolism* 23: 1282-6

Penington NJ, Kelly JS, Fox AP. 1993. Whole-cell recordings of inwardly rectifying K+ currents activated by 5-HT1A receptors on dorsal raphe neurones of the adult rat. *The Journal of physiology* 469: 387-405

Philippova M, Joshi MB, Kyriakakis E, Pfaff D, Erne P, Resink TJ. 2009. A guide and guard: the many faces of T-cadherin. *Cellular signalling* 21: 1035-44

Philippova MP, Bochkov VN, Stambolsky DV, Tkachuk VA, Resink TJ. 1998. T-cadherin and signal-transducing molecules co-localize in caveolin-rich membrane domains of vascular smooth muscle cells. *FEBS letters* 429: 207-10

Ranscht B, Dours-Zimmermann MT. 1991. T-cadherin, a novel cadherin cell adhesion molecule in the nervous system lacks the conserved cytoplasmic region. *Neuron* 7: 391-402

Reagan LP, Magarinos AM, Lucas LR, van Bueren A, McCall AL, McEwen BS. 1999. Regulation of GLUT-3 glucose transporter in the hippocampus of diabetic rats subjected to stress. *The American journal of physiology* 276: E879-86

Ribes V, Briscoe J. 2009. Establishing and interpreting graded Sonic Hedgehog signaling during vertebrate neural tube patterning: the role of negative feedback. *Cold Spring Harbor perspectives in biology* 1: a002014

Ridet JL, Rajaofetra N, Teilhac JR, Geffard M, Privat A. 1993. Evidence for nonsynaptic serotonergic and noradrenergic innervation of the rat dorsal horn and possible involvement of neuron-glia interactions. *Neuroscience* 52: 143-57

Rivero O, Selten MM, Sich S, Popp S, Bacmeister L, et al. 2015. Cadherin-13, a risk gene for ADHD and comorbid disorders, impacts GABAergic function in hippocampus and cognition. *Translational Psychiatry* 5: e655

Rivero O, Sich S, Popp S, Schmitt A, Franke B, Lesch KP. 2013. Impact of the ADHD-susceptibility gene CDH13 on development and function of brain networks. *European neuropsychopharmacology* 23: 492-507

Roberts KM, Fitzpatrick PF. 2013. Mechanisms of tryptophan and tyrosine hydroxylase. *IUBMB life* 65: 350-7

Roeske D, Ludwig KU, Neuhoff N, Becker J, Bartling J, et al. 2011. First genome-wide association scan on neurophysiological endophenotypes points to trans-regulation effects on SLC2A3 in dyslexic children. *Mol Psychiatry* 16: 97-107

Rumsey SC, Kwon O, Xu GW, Burant CF, Simpson I, Levine M. 1997. Glucose transporter isoforms GLUT1 and GLUT3 transport dehydroascorbic acid. *The Journal of biological chemistry* 272: 18982-9

Salatino-Oliveira A, Genro JP, Polanczyk G, Zeni C, Schmitz M, et al. 2015. Cadherin-13 gene is associated with hyperactive/impulsive symptoms in attention/deficit hyperactivity disorder. *American journal of medical genetics. Part B, Neuropsychiatric genetics :* 168b: 162-9

Sánchez-Danés A, Richaud-Patin Y, Carballo-Carbajal I, Jiménez-Delgado S, Caig C, et al. 2012. Disease-specific phenotypes in dopamine neurons from human iPS-based models of genetic and sporadic Parkinson's disease. *EMBO Molecular Medicine* 4: 380-95

Sanders SJ, Ercan-Sencicek AG, Hus V, Luo R, Murtha MT, et al. 2011a. Multiple recurrent de novo CNVs, including duplications of the 7q11.23 Williams syndrome region, are strongly associated with autism. *Neuron* 70: 863-85

Sanders SJ, Ercan-Sencicek AG, Hus V, Luo R, Murtha MT, et al. 2011b. Multiple recurrent de novo CNVs, including duplications of the 7q11.23 Williams syndrome region, are strongly associated with autism. *Neuron* 70: 863-85

Sanders SJ, He X, Willsey AJ, Ercan-Sencicek AG, Samocha KE, et al. 2015. Insights into Autism Spectrum Disorder Genomic Architecture and Biology from 71 Risk Loci. *Neuron* 87: 1215-33

Sarkar B, Das AK, Arumugam S, Kaushalya SK, Bandyopadhyay A, et al. 2012. The dynamics of somatic exocytosis in monoaminergic neurons. *Frontiers in physiology* 3: 414

Schmidt S, Richter M, Montag D, Sartorius T, Gawlik V, et al. 2008. Neuronal functions, feeding behavior, and energy balance in Slc2a3+/- mice. *American journal of physiology. Endocrinology and metabolism* 295: E1084-94

Scott MM, Wylie CJ, Lerch JK, Murphy R, Lobur K, et al. 2005. A genetic approach to access serotonin neurons for in vivo and in vitro studies. *Proceedings of the National Academy of Sciences of the United States of America* 102: 16472-77

Segarra-Mondejar M, Casellas-Diaz S, Ramiro-Pareta M, Muller-Sanchez C, Martorell-Riera A, et al. 2018. Synaptic activity-induced glycolysis facilitates membrane lipid provision and neurite outgrowth. *Embo j* 37

Segarra-Mondejar M, Casellas-Díaz S, Ramiro-Pareta M, Müller-Sánchez C, Martorell-Riera A, et al. 2018. Synaptic activity-induced glycolysis facilitates membrane lipid provision and neurite outgrowth. *The EMBO Journal*: e97368

Seki Y, Sato K, Kono T, Abe H, Akiba Y. 2003. Broiler chickens (Ross strain) lack insulin-responsive glucose transporter GLUT4 and have GLUT8 cDNA. *General and comparative endocrinology* 133: 80-7

Semina OV, Semenets TN, Zamulaeva IA, Selivanova EI, Iljina TP, et al. 2008. Dipeptide gamma-d-Glu-d-Trp (thymodepressin) inhibits migration of CD34+ cells from the bone marrow into peripheral blood during tumor growth. *Bulletin of experimental biology and medicine* 146: 96-9

Shen XH, Han YJ, Yang BC, Cui XS, Kim NH. 2009. Hyperglycemia reduces mitochondrial content and glucose transporter expression in mouse embryos developing in vitro. *The Journal of reproduction and development* 55: 534-41

Shin BC, Cepeda C, Estrada-Sanchez AM, Levine MS, Hodaei L, et al. 2018. Neural Deletion of Glucose Transporter Isoform 3 Creates Distinct Postnatal and Adult Neurobehavioral Phenotypes. *The Journal of neuroscience* 38: 9579-99

Simpfendorfer KR, Li W, Shih A, Wen H, Kothari HP, et al. 2019. Influence of genetic copy number variants of the human GLUT3 glucose transporter gene SLC2A3 on protein expression, glycolysis and rheumatoid arthritis risk: A genetic replication study. *Mol Genet Metab Rep* 19: 100470

Simpson IA, Carruthers A, Vannucci SJ. 2007. Supply and demand in cerebral energy metabolism: the role of nutrient transporters. *Journal of cerebral blood flow and metabolism* 27: 1766-91

Simpson IA, Dwyer D, Malide D, Moley KH, Travis A, Vannucci SJ. 2008. The facilitative glucose transporter GLUT3: 20 years of distinction. *American journal of physiology. Endocrinology and metabolism* 295: E242-53

Sprouse JS, Aghajanian GK. 1987. Electrophysiological responses of serotoninergic dorsal raphe neurons to 5-HT1A and 5-HT1B agonists. *Synapse* 1: 3-9

Stamford JA, Davidson C, McLaughlin DP, Hopwood SE. 2000. Control of dorsal raphe 5-HT function by multiple 5-HT(1) autoreceptors: parallel purposes or pointless plurality? *Trends in neurosciences* 23: 459-65

Stewart MH, Bosse M, Chadwick K, Menendez P, Bendall SC, Bhatia M. 2006. Clonal isolation of hESCs reveals heterogeneity within the pluripotent stem cell compartment. *Nat Methods* 3: 807-15

Stuart CA, Ross IR, Howell ME, McCurry MP, Wood TG, et al. 2011. Brain glucose transporter (Glut3) haploinsufficiency does not impair mouse brain glucose uptake. *Brain research* 1384: 15-22

Stuart CA, Wen G, Jiang J. 1999. GLUT3 protein and mRNA in autopsy muscle specimens. *Metabolism: clinical and experimental* 48: 876-80

Sullivan P, Psychiatric Genetics I. 2012. Don't give up on GWAS. *Molecular psychiatry* 17: 2-3

Swanson J, Baler RD, Volkow ND. 2011. Understanding the effects of stimulant medications on cognition in individuals with attention-deficit hyperactivity disorder: a decade of progress. *Neuropsychopharmacology* 36: 207-26

Takahashi K, Tanabe K, Ohnuki M, Narita M, Ichisaka T, et al. 2007. Induction of pluripotent stem cells from adult human fibroblasts by defined factors. *Cell* 131: 861-72

Takahashi K, Yamanaka S. 2006. Induction of pluripotent stem cells from mouse embryonic and adult fibroblast cultures by defined factors. *Cell* 126: 663-76

Tanaka H, Kannari K, Maeda T, Tomiyama M, Suda T, Matsunaga M. 1999. Role of serotonergic neurons in L-DOPA-derived extracellular dopamine in the striatum of 6-OHDA-lesioned rats. *Neuroreport* 10: 631-4

Tao-Cheng JH, Thein S, Yang Y, Reese TS, Gallant PE. 2014. Homer is concentrated at the postsynaptic density and does not redistribute after acute synaptic stimulation. *Neuroscience* 266: 80-90

Tao Y, Zhang S-C. 2016. Neural Subtype Specification from Human Pluripotent Stem Cells. *Cell stem cell* 19: 573-86

Thoidis G, Kupriyanova T, Cunningham JM, Chen P, Cadel S, et al. 1999. Glucose transporter Glut3 is targeted to secretory vesicles in neurons and PC12 cells. *The Journal of biological chemistry* 274: 14062-6

Thorens B, Mueckler M. 2010a. Glucose transporters in the 21st Century. *American journal of physiology. Endocrinology and metabolism* 298: E141-5

Thorens B, Mueckler M. 2010b. Glucose transporters in the 21st Century. *American journal of physiology. Endocrinology and metabolism* 298: E141-E45

References

Torres GE, Gainetdinov RR, Caron MG. 2003. Plasma membrane monoamine transporters: structure, regulation and function. *Nature reviews. Neuroscience* 4: 13-25

Trueta C, Kuffler DP, De-Miguel FF. 2012. Cycling of dense core vesicles involved in somatic exocytosis of serotonin by leech neurons. *Frontiers in physiology* 3: 175

Uehara Y, Nipper V, McCall AL. 1997. Chronic insulin hypoglycemia induces GLUT-3 protein in rat brain neurons. *The American journal of physiology* 272: E716-9

Vadodaria KC, Mertens J, Paquola A, Bardy C, Li X, et al. 2015. Generation of functional human serotonergic neurons from fibroblasts. *Molecular Psychiatry* 21: 49

Vandermaelen CP, Aghajanian GK. 1983. Electrophysiological and pharmacological characterization of serotonergic dorsal raphe neurons recorded extracellularly and intracellularly in rat brain slices. *Brain research* 289: 109-19

Vannucci SJ, Clark RR, Koehler-Stec E, Li K, Smith CB, et al. 1998. Glucose transporter expression in brain: relationship to cerebral glucose utilization. *Developmental neuroscience* 20: 369-79

Varga V, Losonczy A, Zemelman BV, Borhegyi Z, Nyiri G, et al. 2009. Fast synaptic subcortical control of hippocampal circuits. *Science (New York, N.Y.)* 326: 449-53

Vergo S, Johansen JL, Leist M, Lotharius J. 2007. Vesicular monoamine transporter 2 regulates the sensitivity of rat dopaminergic neurons to disturbed cytosolic dopamine levels. *Brain research* 1185: 18-32

Vitalis T, Parnavelas JG. 2003. The role of serotonin in early cortical development. *Developmental neuroscience* 25: 245-56

Vittori A, Breda C, Repici M, Orth M, Roos RA, et al. 2014. Copy-number variation of the neuronal glucose transporter gene SLC2A3 and age of onset in Huntington's disease. *Hum Mol Genet* 23: 3129-37

Vizi ES, Kiss JP, Lendvai B. 2004. Nonsynaptic communication in the central nervous system. *Neurochemistry International* 45: 443-51

Walther DJ, Bader M. 2003. A unique central tryptophan hydroxylase isoform. *Biochemical pharmacology* 66: 1673-80

Walther DJ, Peter JU, Bashammakh S, Hortnagl H, Voits M, et al. 2003. Synthesis of serotonin by a second tryptophan hydroxylase isoform. *Science* 299: 76

Warren L, Manos PD, Ahfeldt T, Loh YH, Li H, et al. 2010. Highly efficient reprogramming to pluripotency and directed differentiation of human cells with synthetic modified mRNA. *Cell stem cell* 7: 618-30

Weinstein DC, Hemmati-Brivanlou A. 1997. Neural induction in Xenopus laevis: evidence for the default model. *Current opinion in neurobiology* 7: 7-12

Williams NM, Franke B, Mick E, Anney RJ, Freitag CM, et al. 2012. Genome-wide analysis of copy number variants in attention deficit hyperactivity disorder: the role of rare variants and duplications at 15q13.3. *The American journal of psychiatry* 169: 195-204

Wong PT, Feng H, Teo WL. 1995. Interaction of the dopaminergic and serotonergic systems in the rat striatum: effects of selective antagonists and uptake inhibitors. *Neuroscience research* 23: 115-9

Wood IS, Hunter L, Trayhurn P. 2003. Expression of Class III facilitative glucose transporter genes (GLUT-10 and GLUT-12) in mouse and human adipose tissues. *Biochemical and biophysical research communications* 308: 43-9

Wright EM. 2013. Glucose transport families SLC5 and SLC50. *Molecular aspects of medicine* 34: 183-96

Wright EM, Loo DD, Hirayama BA. 2011. Biology of human sodium glucose transporters. *Physiological reviews* 91: 733-94

Wu X, Freeze HH. 2002. GLUT14, a duplicon of GLUT3, is specifically expressed in testis as alternative splice forms. *Genomics* 80: 553-7

Xi J, Liu Y, Liu H, Chen H, Emborg ME, Zhang SC. 2012. Specification of midbrain dopamine neurons from primate pluripotent stem cells. *Stem cells* 30: 1655-63

Yan N. 2015. Structural Biology of the Major Facilitator Superfamily Transporters. *Annual review of biophysics* 44: 257-83

Yang N, Chanda S, Marro S, Ng Y-H, Janas JA, et al. 2017. Generation of pure GABAergic neurons by transcription factor programming. *Nature Methods* 14: 621

Yang S, Wang K, Gregory B, Berrettini W, Wang LS, et al. 2009. Genomic landscape of a three-generation pedigree segregating affective disorder. *PloS one* 4: e4474

Ye W, Shimamura K, Rubenstein JL, Hynes MA, Rosenthal A. 1998. FGF and Shh signals control dopaminergic and serotonergic cell fate in the anterior neural plate. *Cell* 93: 755-66

Yohn CN, Gergues MM, Samuels BA. 2017. The role of 5-HT receptors in depression. *Molecular Brain* 10: 28

Yu Diana X, Di Giorgio Francesco P, Yao J, Marchetto Maria C, Brennand K, et al. 2014. Modeling Hippocampal Neurogenesis Using Human Pluripotent Stem Cells. *Stem Cell Reports* 2: 295-310

Zhang SC, Wernig M, Duncan ID, Brustle O, Thomson JA. 2001. In vitro differentiation of transplantable neural precursors from human embryonic stem cells. *Nat Biotechnol* 19: 1129-33

Zhang Z-w. 2003. Serotonin Induces Tonic Firing in Layer V Pyramidal Neurons of Rat Prefrontal Cortex during Postnatal Development. *The Journal of Neuroscience* 23: 3373-84

Zhao Y, Fung C, Shin D, Shin BC, Thamotharan S, et al. 2010. Neuronal glucose transporter isoform 3 deficient mice demonstrate features of autism spectrum disorders. *Mol Psychiatry* 15: 286-99

6. Appendix

6.1 List of Abbreviations

AADC	L-amino acid decarboxylase
aADHD	adult attention-deficit/hyperactivity disorder
Ach	acetylcholine
ADHD	attention-deficit/hyperactivity disorder
AFP	alpha-1- fetoprotein
ANLS	astrocyte-neuron lactate shuttle
A-P	anterior-posterior
ASD	autism spectrum disorder
B1-B9	raphe nuclei 1-9
BDNF	brain-derived neurotrophic factor
BMPs	bone morphogenetic proteins
BSA	bovine serum albumin
CA	California
cADHD	child attention-deficit/hyperactivity disorder
cAMP	cyclic adenosine monophosphate
CCD camera	charge-coupled device camera
CDH13	cadherin-13
CDH13+	cadherin-13 overexpressing
cDNA	complementary desoxyribonucleic acid
C-GLUT3	C-terminal domain GLUT3
CHIR	CHIR99021
c-MYC	avian myelocytomatosis viral oncogene homolog
CN	copy number state
CNS	central nervous system
CNV	copy-number variant
CRE	cAMP response element

CREB	CRE-binding protein
Ct	threshold cycle
C-terminal domain	carboxyl-terminal domain
Cq	quantification cycle
DA	dopamine
DAPI	4', 6-diamidino-2-phenylindole
DMEM	Dulbecco`s modified Eagle´s Medium
DNA	deoxyribonucleic acid
dNTPs	desoxyribonucleotide triphosphates
DPBS	Dulbecco's Phosphate-Buffered Saline
DR	dorsal raphe
dSTORM	Direct stochastic optical reconstruction microscopy
dT	oligo deoxythymidine
D-V	dorso-ventral
EBs	embryoid bodies
ECL	enhanced chemiluminescence
EDTA	ethylenediaminetetraacetic acid
EEG	electroencephalography
eGFP	enhanced green fluorescent protein
EGTA	ethylene-bis(oxyethylenenitrilo) tetraacetate
EHS	Engelbreth-Holm-Swarm
ESCs	embryonic stem cells
FBS	foetal bovine serum
FGFs	fibroblast growth factors
fMRI	functional magnetic resonance imaging
FOXA2	forkhead box A2
GABA	gamma-Aminobutyric acid
GABA+	gamma-Aminobutyric acid-positive
GAD1	Glutamate decarboxylase 1 gene
GATA2	GATA-binding factor 2

GDNF	glial cell-derived neurotrophic factor
GIRK	G protein-coupled inwardly rectifying potassium channels
GLUT3	glucose transporter-3
GLUT3+	Glucose transporter-3-positive
glut3+/−	heterozygous for glut3
GPCR	G-protein coupled receptor
GSK-3-ß	glycogen synthase kinase 3β
GTG-banding	Giemsa banding
GWAS	genome-wide association study
h	hour(s)
HHW	half-height width
HOXA2	Homeobox protein Hox-A2
HRP	horseradish peroxidise
Hz	hertz
IA	Iowa
IF	immunofluorescence
iPSCs	induced pluripotent stem cells
kbp	kilobase pair
k_{cat}	turnover number
kDa	kilodalton
Klf4	kruppel-like factor 4
Km	Michaelis constant
LAM	laminin
LDN	LDN-193189
L-DOPA	L-3,4-dihydroxyphenylalanine
LDS	lithium dodecyl sulfate
LOH	loss-of-heterozygosity
MA	Massachusetts
MAO-A	monoamine oxidase A
MAP2	microtubule-associated protein 2

mb	megabases
MD	Maryland
Mg2+	magnesium
MEFs	mouse embryonic fibroblasts
MFS	major facilitator superfamily
min	minute(s)
MMLV	Moloney Murine Leukemia Virus
MN	Minnesota
MO	Missouri
MR	median raphe
mRNA	messenger ribonucleic acid
ms	millisecond
mV	millivolt
NA	noradrenalin
NEAA	MEM non-essential amino acid solution
NeuN	neuronal nuclear protein
ng	nanogram
NGF	nerve growth factor
N-GLUT3	N-GLUT3
NHDFs	Normal Human Dermal Fibroblasts
NJ	New Jersey
NKX6.1	homeobox protein Nkx-6.1
N-terminal domain	amino-terminal domain
NPC	Neural progenitor cell
NY	New York
Oct4	octamer-binding transcription factor 4
OD	optical density
OTX2	orthodenticle homeobox 2
PA	Pennsylvania
PAX6	paired box protein-6

PBS	phosphate buffered saline
PBS-T	phosphate buffered saline-tween
PCBs	polychlorinated biphenyls
PD	Parkinson's disease
PET	positron emission tomography
PFA	paraformaldehyde
PFC	prefrontal cortex
PO	polyornithine
PSC	pluripotent stem cells
PSD	postsynaptic density
qRT-PCR	quantitative real time PCR
RA	retinoic acid
RI	ROCK inhibitor
RIPA buffer	Radio-Immunoprecipitation Assay buffer
RNA	ribonucleic acid
RNase	RNA-dependent DNA polymerase with ribonuclease
ROCK	Rho-associated protein kinase
RT	reverse transcriptase
s	second(s)
SB	SB432543
SDC	medium supplemented with SB+DMH-1+CHIR
SDS-PAGE	sodium dodecyl sulfate polyacrylamide gel electrophoresis
SeV	Sendai virus
SGLTs	sodium-driven glucose symporters
SHH	sonic hedgehog
SIM	structured illumination microscopy
SLC2A3	solute carrier family 2, facilitated glucose transporter member 3
SMA	alpha-smooth muscle actin
SN	substantia nigra
SNP	single nucleotide polymorphism

Sox2	SRY-box 2
SPECT	single photon emission computed tomography
SRY	sex determining region Y
TBS	tris buffered saline
TBS-T	tris buffered saline-tween
TE buffer	tris-EDTA buffer
TGF-ß	transforming growth factor beta
TH	tyrosine hydroxylase
TH+	tyrosine hydroxylase-positiv
TM	transmembrane domains
TPH	tryptophan hydroxylase
TPH2	tryptophan hydroxylase-2
TPH2+	TPH2-positive
TPH2-	TPH2-negative
UV	ultraviolet
VA	Virginia
vMAT2	vesicular monoamine transporter
VT	Vermont
WA	Washington
WI	Wisconsin
w1-6	week 1-6
5-HT	serotonin
5-HT1-7	serotonin specific receptors
5-HTP	L-tryptophan to 5-hydroxy-L-tryptophan
5-HTT	serotonin transporter
β-ME	β-mercaptoethanol
ßTubIII	beta-Tubulin III
ßTubIII+	beta-Tubulin III-positive
ΔRn	delta normalized reporter
-Glc	8 days of glucose deprivation

6.2 List of Figures

6.3 List of Tables

6.4 Publication list

Jansch, C., A. Forero, S. Kollert, S. Wäldchen, E. Svirin, J. Waider, G. C. Ziegler, F. Edenhofer, M. Sauer, E. Wischmeyer and K.-P. Lesch (2019). Serotonin-specific neurons differentiated from human iPSCs form distinct subtypes with synaptic protein assembly. submitted

Corominas, J., M. Klein, T. Zayats, O. Rivero, G. C. Ziegler, M. Pauper, K. Neveling, G. Poelmans, **C. Jansch**, E. Svirin, J. Geissler, H. Weber, A. Reif, A. Arias Vasquez, T. E. Galesloot, L. Kiemeney, J. K. Buitelaar, J. A. Ramos-Quiroga, B. Cormand, M. Ribases, K. Hveem, M. E. Gabrielsen, P. Hoffmann, S. Cichon, J. Haavik, S. Johansson, C. P. Jacob, M. Romanos, B. Franke and K. P. Lesch (2018). Identification of ADHD risk genes in extended pedigrees by combining linkage analysis and whole-exome sequencing. Mol Psychiatry.

Forero, A., O. Rivero, S. Wäldchen, H.-P. Ku, D. P. Kiser, Y. Gärtner, L. S. Pennington, J. Waider, P. Gaspar, **C. Jansch**, F. Edenhofer, T. J. Resink, R. Blum, M. Sauer and K.-P. Lesch (2017). "Cadherin-13 Deficiency Increases Dorsal Raphe 5-HT Neuron Density and Prefrontal Cortex Innervation in the Mouse Brain." Frontiers in Cellular Neuroscience **11**: 307.

Jansch, C., K. Günther, J. Waider, G. C. Ziegler, A. Forero, S. Kollert, E. Svirin, D. Pühringer, C. K. Kwok, R. Ullmann, A. Maierhofer, J. Flunkert, T. Haaf, F. Edenhofer and K.-P. Lesch (2018). Generation of a human induced pluripotent stem cell (iPSC) line from a 51-year-old female with attention-deficit/hyperactivity disorder (ADHD) carrying a duplication of SLC2A3. Stem Cell Research **28**: 136-140.

Merker, S., A. Reif, G. C. Ziegler, H. Weber, U. Mayer, A. C. Ehlis, A. Conzelmann, S. Johansson, C. Muller-Reible, I. Nanda, T. Haaf, R. Ullmann, M. Romanos, A. J. Fallgatter, P. Pauli, T. Strekalova, **C. Jansch**, A. A. Vasquez, J. Haavik, M. Ribases, J. A. Ramos-Quiroga, J. K. Buitelaar, B. Franke and K. P. Lesch (2017). SLC2A3 single-nucleotide polymorphism and duplication influence cognitive processing and population-specific risk for attention-deficit/hyperactivity disorder. J Child Psychol Psychiatry **58**: 798-809.

Reber, S. O., P. H. Siebler, N. C. Donner, J. T. Morton, D. G. Smith, J. M. Kopelman, K. R. Lowe, K. J. Wheeler, J. H. Fox, J. E. Hassell, Jr., B. N. Greenwood, **C. Jansch**, A. Lechner, D. Schmidt, N. Uschold-Schmidt, A. M. Fuchsl, D. Langgartner, F. R. Walker, M. W. Hale, G. Lopez Perez, W. Van Treuren, A. Gonzalez, A. L. Halweg-Edwards, M. Fleshner, C. L. Raison, G. A. Rook, S. D. Peddada, R. Knight and C. A. Lowry (2016). Immunization with a heat-killed preparation of the environmental bacterium Mycobacterium vaccae promotes stress resilience in mice. Proc Natl Acad Sci U S A **113**: E3130-3139.

6.5 Curriculum Vitae

Personal Details

Name	Charline Jansch
Date of Birth	18.12.1987
Place of Birth	Neuss

Work Experience

09/2014 – 07/2019

Division of Molecular Psychiatry, University Hospital of Würzburg, Würzburg

- Research Scientist, Ph.D. student

- Supervisor: Prof. Dr. med. Klaus-Peter Lesch

- Establishment of hiPSC-based technologies in the Laboratory of Translational Neuroscience and development of a robust and reliable differentiation protocol for the generation of hiPSC-derived neuronal subtypes

- Independent planning and conductance of experiments in the field of stem cell research and molecular biology

- Usage of high-resolution microscopy (SIM, *d*STORM) and electrophysiology to complement hiPSC-based differentiation procedure

- Supervision and training of students and competent guidance of technical assistants

12/2013 - 04/2014

Department of Psychiatry, Psychosomatics and Psychotherapy, University Hospital of Würzburg, Würzburg

- Research Assistant

- Supervisor: Prof. Dr. med. Andreas Reif

- Genotyping studies via polymerase chain reaction (PCR)

03/2012

Department of Integrative Physiology and Center for Neuroscience, University of Colorado, Boulder

- Professional Research Assistant

- Supervisor: Dr. Chris Lowry, PhD

- Taking a lead role in conducting analysis of active/reactive emotional coping behaviour in the M. vaccae/chronic subordinate colony study

- Moderating a tutorial to train co-workers in these methods: "chronic subordinate colony housing (CSC) as an adequate and reliable mouse model of chronic psychosocial stress"

- Participating in weekly lab meetings

- Carrying out other duties, as specified by the PI

Education

Ph.D. study | 2014 – 2019 | University of Würzburg

- Graduate School of Life Science (GSLS)
- Neurobiology and stem cell research
- Supervisor: Prof. Dr. med. Klaus-Peter Lesch
- Thesis title: "Human induced pluripotent stem cells as a unique tool to clarify the role of *SLC2A3* copy number variants in attention-deficit/hyperactivity disorder."
- Degree: Dr. rer. nat.

Master of Science (M.Sc.) | 2012 - 2014 | University of Würzburg

- Neurobiology and human genetics
- Supervisor: Prof. Dr. med. Klaus-Peter Lesch
- "Downstream targets of Cadherin-13 in neuronal cell culture models"
- Degree: Master of Science (M.SC.) Biology

Bachelor of Science (B.SC.) | 2008 - 2011 | University of Regensburg

- Basics of life science research
- Supervisor: Prof. Dr. rer. nat. Stefan O. Reber
- "Effects of Mycobacterium vaccae immunization on CSC-induced anxiety and HPA axis changes."
- Degree: Bachelor of Science (B.SC.) Biology

Abitur | 2000 - 2007 | Descartes-Gymnasium Neuburg/Donau

General qualification for university entrance

Scholarships

Graduate School of Life Science (GSLS) Travel Fellowship

For the 11th FENS Forum of Neuroscience 2018 in Berlin, Germany

J-1 VISA: Research Scholar

Visiting scholar at the University of Colorado at Boulder (Professional Research Assistant)

Further Qualifications

Good scientific practice – *Dr. S. Schröder-Köhne – 2 hour Workshop*

- Basic principles of responsible conduct of research
- Categories of research misconduct
- National and international regulations and guidelines
- Institutions and procedures dealing with misconduct

Project management – *Dr. D. Bittner – 8 hour workshop*

- Definition project/project management
- Project structure and structural elements

- Time and resource planning
- Monitoring and controlling projects

Scientific image processing & analysis – *Dr. Brocher – 16 hour Workshop*

- Basics in microscopy and imaging
- Correct image adjustments
- Manual and automatic counting of features
- Quantitative image analysis – length, area, volume, surface, intensity

Open access and copyright in sciences – *Christian Schmauch – 4 hour Workshop*

- How to make your own articles visible
- How to use repositories for publishing your article and thesis
- How to avoid violations of the copyright

Statistical data analysis with SPSS – *Daniela Keller – 27 hour Workshop*

- Basics about descriptive statistics
- Parametric and non-parametric tests for comparing means
- Required sample sizes and insight into the design of experiments
- Parametric and non-parametric tests

Poster design – *Barry Drees – 7 hour Workshop*

- Fundamental concepts of how to prepare a poster to communicate to a broad audience
- Strengths and weaknesses of posters
- Need for visual impact and simplicity of message that is central to a good poster

Conferences

13th Göttingen Meeting of the German Neuroscience Society

Göttingen, Germany, 2019

11th FENS Forum of Neuroscience

Berlin, Germany, 2018

Würzburg Center of Mental Health Science Conference

Würzburg, Germany, 2017

ERA-NET NEURON Mid-Term Symposium

Riga, Latvia, 2017

Jahreskongress der Deutschen Gesellschaft für Biologische Psychiatrie

Würzburg, Germany, 2016

10th FENS Forum of Neuroscience

Copenhagen, Denmark, 2016

EUREKA! Symposium

Würzburg, Germany, 2015

Key Skills

Language

- German (Mother tongue)

- English (fluent in spoken and written)

- French (basic knowledge)

Techniques

- Cell culture laboratory; S2-safety level laboratory

- Human induced pluripotent stem cells (hiPSCs)

- Microfluidic devices (Microfluidic Chips)

- Microelectrode arrays (MEAs)

- Cell culture and molecular biological techniques

Software

- Microsoft Office

- SPSS

- GraphPad Prism

- ImageJ

Personal Skills

- Project planning and performing

- Protocol establishment & problem solving

- Teamwork

Neuburg an der Donau, November 18th, 2019

_____

Signature (Charline Jansch)

6.6 Acknowledgement

Affidavit

I hereby confirm that my thesis entitled "Effects of *SLC2A3* copy number variants on neurodevelopment and glucose metabolism in ADHD patient-specific neurons" is the result of my own work. I did not receive any help or support from commercial consultants. All sources and / or materials applied are listed and specified in the thesis.

Furthermore, I confirm that this thesis has not yet been submitted as part of another examination process neither in identical nor in similar form.

Place, Date   Signature

Eidesstaatliche Erklärung

Hiermit erkläre ich an Eides statt, die Dissertation " Effekte der *SLC2A3* Kopienzahlvarianten auf Neuroentwicklung und Glukosemetabolismus in ADHS Patienten-spezifischen Neuronen" eigenständig, d.h. insbesondere selbstständig und ohne Hilfe eines kommerziellen Promotionsberaters, angefertigt und keine anderen als die von mir angegebenen Quellen als Hilfsmittel verwendet zu haben.

Ort, Datum   Unterschrift